Justus-Liebig-Universität Gießen

Micelle-Templated Carbon Coatings and Their Applications for Catalysis

Dissertation

zur Erlangung des akademischen Grades
„doctor rerum naturalium"
(Dr. rer. nat.)

eingereicht an der
Naturwissenschaftlichen Fakultät
Justus-Liebig-Universität Gießen

Von

Laemthong Chuenchom

Gießen, im Mai 2013

"Imagination is more important than knowledge."

Albert Einstein

Dedicated to my father

Dean / Dekan

Reviewer / Gutachter Prof. Dr. Bernd Michael Smarsly

Reviewer / Gutachter Prof. Dr. Arne Thomas

Submitted / Eingereicht:

Declaration/ Erlärung

The present thesis was prepared at the Justus Liebig University of Giessen and the Technical University of Berlin (TU Berlin) under the supervision and guidance of Prof. Dr. Bernd Michael Smarsly and Dr.-Ing. Ralph Krähnert.

I declare:
The present thesis was prepared by myself and without illicit help from others. Any citations being included literally or by adaptation from the literature or personal communication, have been marked appropriately. The principles of best practice in academia, as documented in the respective charter of the Justus Liebig University of Giessen have been applied in all investigations constituting this thesis.

Die vorliegende Arbeit wurden in an der Justus-Liebig-Universität Gießen und der Technical Universität Berlin bei Prof. Dr. Bernd Michael Smarsly und Dr.-Ing. Ralph Krähnert durchgeführt.

Ich erkläre:
Ich habe die vorgelegte Dissertation selbständig und ohne unerlaubte fremde Hilfe und nur mit den Hilfen angefertigt, die ich in der Dissertation angegeben habe. Alle Textstellen, die wörtlich oder sinngemäß aus veröffentlichten Schriften entnommen sind, und alle Angaben, die auf mündlichen Auskünften beruhen, sind als solche kenntlich gemacht. Bei den von mir durchgeführten und in der Dissertation erwähnten Untersuchungen habe ich die Grundsätze guter wissenschaftlicher Praxis eingehalten, wie sie in der „Satzung der Justus-Liebig-Universität Gießen zur Sicherung guter wissenschaftlicher Praxis“ niedergelegt sind.

Gießen, den 9. Mai 2013

_____

Laemthong Chuenchom

Acknowledgments

The present thesis has been performed in the Institute of Chemistry, the Technical University of Berlin (TU Berlin) and the Institute of Physical Chemistry, Justus Liebig University of Giessen.

I would like to express my sincere appreciation to all the people who have been involved in and contributed to the success of this work.

Prof. Dr. Bernd Smarsly is acknowledged for the opportunity to work in Giessen as a PhD student in his research group and his fruitful discussions, support and encouragement.

My special thanks go to Dr.-Ing. Ralph Krähnert for the opportunity to do my PhD in his research group at TU Berlin and for the excellent supervision. Without his guidance, support, and patience, I would have not been able to finish my PhD.

I particularly appreciate the assistance he has offered in both results-based planning of new experiments and scientific writing. I am also grateful to him for his proofreading of my thesis.

I wish to express grateful thanks to the colleagues at TU Berlin, Dr. Erik Ortel, Benjamin Paul, Björn Eckhardt, Denis Bernsmeier, Michael Bernicke, Frau Kornelia Weh for their friendship, support, fruitful scientific discussions, plenty of beautiful SEM and TEM images and help with other measurements. The support from all of them has mainly led to the success of this thesis. I am also grateful to them for their proofreading and correction of my thesis.

Furthermore, I would like at the Federal Ministry of Education and Research, Germany (Nanofutur program / DEPOKAT [FKZ 03X5517]) for the financial support. The Department of Chemistry, Prince of Songkla University, Thailand is gratefully acknowledged for providing a scholarship and allowing me to pursuit my PhD study in Germany.

Many thanks go to my colleagues in Giessen, Dr. Rainer Ostermann, Dr. Sebastien Sallard, Dr. Takeshi Hara, Dr. Simone Mascotto, Dr. Jan Haetage, Dr. Till von Graberg, Dr. Christian Suchomski, Dr. Philipp Adelhelm, Dr. Torsten Brezesinski, Kristin Brezesinski, Christoph Weidmann, Claas Wessel, Michael Schröder, Daniela Stoeckel, Christian Reitz, Matthias Böhm, Kristin Faber, Rüdiger Ellinghaus, Martin von der Lehr, Junpei Yue, Julia Migenda, Frau Gwyneth Schulz, Kristin Tropp, and the others whose names are not mentioned here for their friendship, plenty of fun times, scientific discussions and support. Their friendship has made a very enjoyable atmosphere for me during the time in Giessen.

I gratefully thank Frau Anika Berhardt for elemental analysis, Frau Antonie Pospiech for help with FT-IR measurements, Phisan Katekomol (AK Arne Thomas, TU Berlin) for performing TGA analysis.

Special thanks go to my “Thai” friends and Thai community both in Berlin and in Giessen/Frankfurt. All of them have made the life in Germany be like a home.

I am especially thankful to my girlfriend, Waralee Watcharin, for her understanding, infinite patience, and moral support.

Finally, I would like to thank my parents and my brother for their understanding, support, and encouragement both in bad times and in good times.

Abstract

The aim of this thesis was to develop synthesis methods for catalytically active carbon coatings with controlled pore structure. The synthesis strategy is based on evaporation-induced self-assembly (EISA) and soft-templating principles using resorcinol-formaldehyde (RF) as a carbon precursor and amphiphilic block-copolymers as structure-directing soft-templates. The main goal was to obtain a desirable 3D pore morphology on different substrates. Hence, synthesis procedures for bulk mesoporous carbon powders prepared under acidic conditions were refined and adapted to surface coatings. The synthesis yielded porous crack-free carbon films with pore sizes depending on the employed pore template. Films templated with F127 possessed a contracted 3D cubic mesostructure (*Im3m*) with pores of about 8 nm width and 4 to 6 nm height. The film thickness (measured after carbonization at 600°C) could be increased up to about 820 nm by increasing the withdrawal speed of dip-coating while retaining the mesostructure. The films templated with F127 possess high surface areas up to 520 m^2/cm^3 (BET) and pore volumes up to 0.45 cm^3/cm^3.

Templating with different polymers (PIB-PEO 3000 as well as 10k-PB polymers) resulted in increased pore diameters up to 20 nm (measured in the direction parallel to the substrate). Also here, an increase in withdrawal speed of dip-coating increased the film thickness up to 640 nm. However, thicker films templated with PIB-PEO 3000 exhibited a reduced degree of mesopore order.

In order to synthesize mesoporous carbon films containing catalytically active metal particles the synthesis procedure was extended to incorporate also appropriate Pd and Pt precursors. The synthesis employing F127 as a template yielded high quality, uniform mesoporous carbon coatings containing either Pd or Pt particles. Pd loading as high as 3 wt% were successfully reached. The Pd/C films carbonized at 600°C possess a contracted *Im3m* mesopore structure with uniform pore sizes of ~8 nm in the direction parallel to the substrate and ~6 nm in the direction perpendicular to the substrate. A thickness of ~400 nm, a surface area of 587 m^2/cm^3 (BET) and well-distributed Pd particles with a uniform size of ~15 nm were obtained.

The synthesis procedure for mesoporous Pd/C catalyst films was then adapted to coat also steel plates, which are typically used as substrates in a catalytic reactor. The facile and reproducible synthesis of these catalyst coatings allowed for up scaling up to 25 steel plates with identical features for both mesopore structure and Pd particles. The Pd-containing mesoporous carbon coatings on the steel plates were tested as catalysts for gas-phase hydrogenation of 1,3-butadiene. The Pd/C catalyst coatings proved to be highly active and selective with conversions of up to 80% at a reaction temperature of 80°C and high selectivity to butenes of up to ~95%.

Zusammenfassung

Das Ziel dieser Arbeit war es Synthesemethoden für katalytisch aktive Kohlenstoffbeschichtungen mit kontrollierter Porenstruktur zu entwickeln. Die Synthesestrategie basiert auf der verdampfungsinduzierten Selbstorganisation (engl. evaporation-induced self-assembly, EISA) mit einer Resorcin-Formaldehydverbindung als Kohlenstoffquelle und amphiphilen Blockcopolymeren als strukturdirigierende Template. Der Schwerpunkt dieser Arbeit war es eine dreidimensionale Porenstruktur mit vernetzten Poren auf verschiedenen Substraten zu erhalten. Dazu wurde eine Synthesevorschrift für mesoporösen Kohlenstoff, synthetisiert in Pulverform, unter sauren Bedingungen adaptiert und weiterentwickelt. Es wurden poröse, rissfreien C-Filme erhalten mit Porengrößen, die abhänging vom verwendeten Templat waren. Mit Pluronic F127 templatierte Filme besaßen eine kontrahierte kubische 3D-Mesostruktur (*Im3m*) mit Poren von 8 nm Breite parallel und 4 bis 6 nm Höhe normal zum Substrat. Die Schichtdicke (gemessen nach der Karbonisierung bei 600 °C) konnte bei schnellem Herausziehen des Substrates auf bis zu 820 nm erhöht werden, unter Beibehaltung der Mesostruktur. Die F127-templatierten Filme zeigten eine BET-Oberfläche von bis zu 520 m^2/cm^3 und ein Porenvolumen bis zu 0.45 cm^3/cm^3.

Die templatierte Porengröße (parallel zum Substrat) konnte auf etwa 20 nm erhöht werden durch Verwendung verschiedener Polymere (PIB-PEO 3000 und 10k-PB Polymeren).Auch hier konnte bei Wahl einer hohen Ziegeschwindigkeit eine Filmdicke von bis zu 640 nm realisiert werden. Jedoch verringert sich der Grad der Porenordnung mit ansteigender Schichtdicke.

Um mesoporöse C-Filme mit katalytisch aktiven Metallpartikeln zu erzeugen, wurden Pd- oder Pt-Vorläufer in die Syntheseprozedur integriert. Eine Synthese mit F127 als Porentemplat führte zu einheitlichen mesoporösen Kohlenstoffschichten, die Pd- bzw. Pt-Partikeln enthielten. Eine Pd-Beladung von bis zu drei Gewichtsprozenten konnte erreicht werden. Die Filme besaßen eine kontrahierte *Im3m* Porenstruktur mit einer einheitlichen Porengröße von etwa 8 nm parallel und etwa 6 nm normal zum Substrat. Die Schichtdicke betrug etwa 400 nm und die BET Oberfläche etwa 587 m^2/cm^3. Die homogen in der Schicht verteilten Pd-Partikeln besaßen eine gleichmäßige Größe von ungefähr 15 nm.

Pd-haltige mesoporöse C-Filme wurden auch auf Stahlsubstraten abgeschieden und diese Platten als Katalysatoren in einem Reaktor verwendet. Die einfache und reproduzierbare Synthesemethode ermöglichte ein Up-Scaling auf bis zu 25 Stahlplatten mit gleicher Mesoporenstruktur und Pd-Partikelgröße.Die Pd-haltigen mesoporösen C-Schichten auf Stahlsubstraten wurden in der Hydrierungsreaktion von 1,3-Butadien in der Gasphase katalytisch getestet. Die Katalysatoren zeigten eine hohe Aktivität mit Umsätzen bis zu 80% bei einer Reaktionstemperatur von 80°C sowie eine hohe Selektivität zu Butenen von bis zu 95%.

Contents

Chapter 1
Motivation and aims

1.1 General relevance of carbon materials

Carbon is one of the most versatile elements and can have several kinds of allotropes. Figure 1.1 shows different allotropes of carbon materials. The crystalline allotropes most commonly found are diamond and graphite. Every carbon atom in diamond possesses sp^3 hybridisation and is tretrahedral coordinated. In contrast, in graphite, each carbon atom is bonded to the other three though sp^2 hybridisation, forming a layered, planar structure of a hexagonal lattice. Besides those allotropes, other crystalline carbon structures include fullerenes, single and multi-walled carbon nanotubes (CNTs), and graphene. They exhibit unprecedented physico-chemical properties. In addition to all the crystalline allotropes, amorphous carbons are another class, and are polycrystalline materials with no-long range crystalline order. Examples of amorphous carbons are activated carbons, glassy carbons, carbon black, soot, and chars.

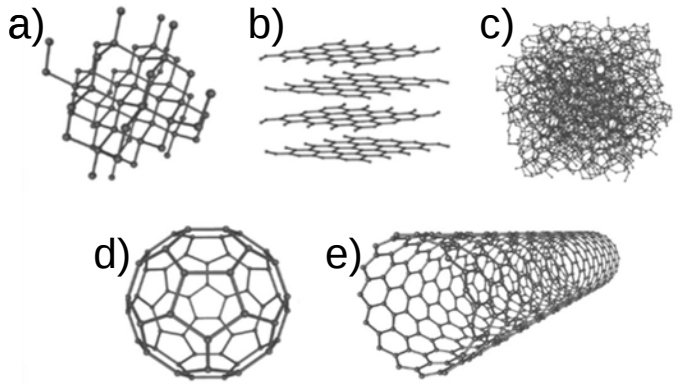

Figure 1.1. Different allotropes of carbon materials: a) diamond, b) graphite, c) amorphous carbon, d) C_{60} fullerene, e) carbon nanotube. [1]

Plenty of carbon materials in various macroscopic forms, ranging from powders, fibers, and foams exist in our daily lives due to their various essential applications related to environmental protection, energy storage, catalysis, biological issues, chromatography. From the point of view of materials chemistry, novel synthesis strategies and fundamental understanding of their properties are necessarily desired to improve the performance of carbon materials.

The majority of carbon materials for such aforementioned applications are in general synthesized though heat treatment of carbon atom-rich organic precursors. The process is

called "carbonisation". The precursors undergo thermal decomposition, so called "pyrolysis", under an inert atmosphere. This leads to elimination of volatile compounds including heteroatoms and make the precursors become rich in the carbon content. Upon an increase in carbonisation temperature, the condensation reaction takes place, and the aromatic units localise and grow, leading to formation of microcrystallites, as illustrated in Figure 1.2. This approach is normally employed to synthesize amorphous carbons, while the more crystalline carbon materials are produced through more sophisticated procedures, for example laser ablation, electro-arc discharge or chemical vapour deposition (CVD).

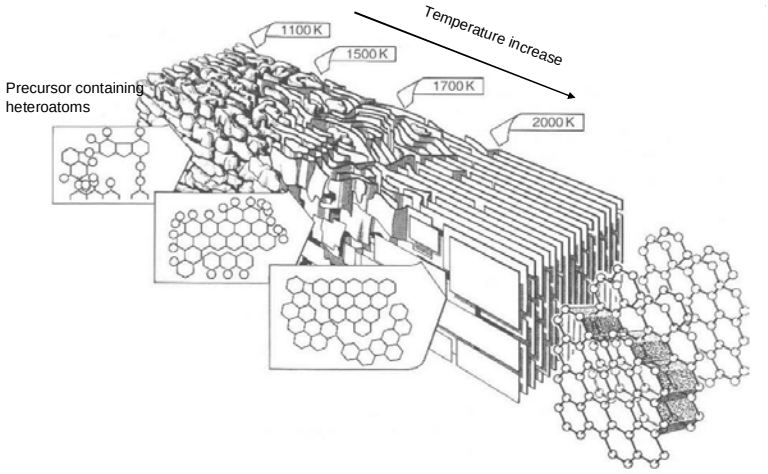

Figure 1.2. Illustration of structural changes in the carbon microstructure upon carbonisation.[2]

1.2 Carbon materials for catalysis

Carbon materials have been widely used as catalytic supports in heterogeneous catalysis, in particular for noble metal catalysts for various organic reactions. Carbon supports possess desirable properties, such as their chemical inertness, stability in the absence of molecular oxygen against high or low pH, good mechanical stability, and high surface area.
Various types of carbon materials, including carbon nanotubes (CNTs), carbon nanofibers (CNFs), activated carbons, and carbon aerogels (CAs) have been employed as catalyst supports.[3-6] Among them, in particular, porous carbons (activated carbons and carbon aerogels) are most commonly used for this application. With respect to IUPAC identification, porous carbons can be classified according to their pore diameter as microporous (size < 2 nm), mesoporous (2-50 nm), and macroporous (> 50 nm) carbons.

Activated carbon prepared by either chemical or physical activation is the most commonly applied material as support in catalysis due to its facile preparation, high surface area and pore volume, low cost and the possibility of large-scale processing. However, activated carbon features a locally inhomogeneous structure and usually possesses a wide distribution of pore sizes, ranging from micropores (size < 2 nm) to macropores (> 50 nm).[7] Moreover, the

abundant presence of micropores often limits mass transfer and pore accessibility in applications in catalysis. This feature normally leads to non-uniform distribution of metal active sites, which impairs their applications and fails to establish the relationship between pore texture/metal size of the catalysts with catalytic performance.

From catalysis point of view, when the rapid diffusion of larger molecules to the internal surface of porous carbon is required, materials possessing controllable pore dimensions in the size range of mesopores (2-50 nm) are desirable. This kind of pores provides advantages in terms of mass transfer and efficient utility of the internal surface, so that the active species can be accessible.[8, 9]
Besides the mesopore architectures, size and dispersion of the active particles on the carbon supports have an effect on catalytic functions. If the catalyst particles are uniformly and highly dispersed within the mesopore systems, very high conversion and selectivity can be achieved.[6]

Although significant progress in the synthesis of mesoporous carbons with well-defined mesopore structures has been achieved through both hard-[10, 11] and soft-templating strategies,[12-14] most of them are in the form of powder. In fact, from the point of view of catalysis, mesoporous carbons in the form of film coatings would be attractive catalyst-support materials when coated on walls of chemical reactors. However, the successful synthesis of such mesoporous carbon coatings still poses several challenges concerning the synthesis procedures, quality of the carbon coatings, and control over the pore morphology.

In fact, coating of porous carbon materials on substrates has largely been performed by depositing powder carbon materials, which requires an additional binder. This results in a time-consuming synthesis procedure. In addition, no control over pore structure and the blockage of the pore system by the binder are often obtained.[15-17]

Concerning the challenges stated above, this thesis focuses mainly on a rational synthesis approach to ordered mesoporous carbon coatings (or films) based on the soft-templating strategy by employing amphiphilic block-copolymers as structural directing templates whose micelles act as mesopore formation agents.
This approach based on the micelle templating concept has proved to be an efficient way of producing well-defined mesoporous metal oxides.[18, 19] However, only few reports on mesoporous carbon coatings through this approach have been addressed so far.[20-27]

1.3 Thesis objectives and outline

The main objective of this thesis was to develop a facile synthesis procedure for the preparation of mesoporous carbons in the film morphology with desirable and well-defined mesopore structure. Afterwards, the well-developed method was extended to incorporate in-situ nanoparticles that act as active species in such carbon coatings for the first time, rendering the carbon films active for catalytic applications.

Chapter 2 of the thesis will address the state of the art and principles of the synthesis of mesoporous carbons via the soft-templating in relation to relevant literature. Specific aspects of the synthesis in form of film morphology, as well as a general concept for the model reaction presented in this thesis are also provided.

Chapter 3 provides detailed synthesis routes for the materials obtained in this thesis. Characterisation methods and the catalytic testing are also given in this chapter.

In Chapter 4, a developed soft-templating approach is presented to synthesize mesoporous carbons in the film morphology with a desirable mesopore structure. The synthesis is based on the organic-organic self-assembly formed though the evaporation-induced self-assembly (EISA) with recorcinol-formaldehyde (RF) as a carbon precursor and amphiphilic block-copolymers as templates. By utilising different kinds of block-copolymer templates, the possibility of tuning mesopore size can be achieved. Furthermore, the opportunity to adjust the film thickness, while keeping the mesopore structure is shown for the materials templated with F127 polymer, posing the possibility for the catalytic use. The effect of carbonisation temperature on mesopore structure and pore size is also highlighted.

In Chapter 5, the successful synthesis presented in Chapter 4 is further extended in order to prepare the practical catalyst films containing Pd and Pt particles. Changes in the mesopore structure and particle dispersion are investigated. Based on a model reaction system, the gas-phase hydrogenation of 1,3-butadiene, the catalytic tests on selected Pd-containing mesoporous carbon film coatings are performed, and high performance of the catalysts discussed.

Chapter 2
State of the art and principles

In this chapter, the principles relevant to the current research in the field of synthesis of templated mesoporous carbons and catalyst materials based on the mesoporous carbons are described. Section 2.1 will first present a general overview of the synthesis of porous carbon materials. Section 2.2 describes the principles of synthesis of templated mesoporous carbons based on the soft templating strategies. Sections 2.1 and 2.2 have recently been published as a review article.[28] Section 2.3 gives a concept of shaping soft-templated mesoporous carbons into the form of films as well as in situ modification with metal species during the film formation. The last section 2.4 will provide principles of catalysis of hydrogenation of 1,3-butadiene, which has been used as a model system for studies of catalytic performance for the Pd-containing mesoporous carbon films prepared in this thesis.

2.1. Classical synthesis of porous carbon materials

The synthesis of porous carbon materials with high surface area can be achieved by various methods, for instance by catalytic activation of carbon precursors,[3, 4] carbonization of polymer blends containing thermally decomposable components,[29] as well as the carbonization of resorcinol-formaldehyde aerogels.[5] However, carbon materials derived from these syntheses often possess a broad pore size distribution, ranging from micro- to macropores. To obtain materials with narrow and controlled pore size distributions, especially in the mesopore range, one suitable strategy is the replication of a rigid template material which already possesses controlled mesoporosity, the method so-called "hard-templating". Using this "hard-templating" approach and mesoporous silica as the template, Ryoo et al. [30, 31] as well as Heyon et al.[32] pioneered the synthesis of ordered mesoporous carbons (OMCs). Since then, hard templating has been further improved using a variety of mesoporous oxides as described in different reviews,[8, 10-12, 31-36] but it also inherits severe drawbacks. In particular, the necessity of removing the inorganic template employing hazardous chemicals such as HF or NaOH is a drawback in industrial applications. Moreover, facile control over the pore size and structure of the classical hard-templated OMCs is obstructed by the fact that the carbon pore system represents the inverse structure of the template porosity, e.g. the wall thickness of the mesoporous oxide determines the pore size of the carbon material. Although demonstrated recently for titania, independent control of the wall thickness remains challenging for many templating oxides.[37] In contrast, direct soft templating of the carbon material can provide an alternative facile way to control its mesopore structure and to avoid the chemicals employed for removal of hard templates.

Similar to the self-assembly observed during the synthesis of ordered mesoporous metal oxides, soft-templating of mesoporous carbon materials involves the cooperative assembly of structure-directing agents able to form lyotropic phases with suitable organic carbon precursors. Since the first successful synthesis of ordered mesoporous carbons by soft-templating with micelles of amphiphilic block-copolymers reported by Dai and co-workers in 2004,[38] rapid progress in this field has been reviewed by different authors.[12, 13, 36, 39]
More recently, the soft-templating approach has been extended to synthesize macropores in hierarchical meso-macroporous carbon without the help of any inorganic templating material (e.g. SiO_2).[40-43] Thus, soft-templating of meso- and macropores using only organic species can now provide access routes towards chemically pure carbon with controlled hierarchical porosity.

2.2 Principles of soft-templating of mesoporous carbon using amphiphilic block-copolymers

Similar to metal oxides, mesoporous carbon materials with ordered mesoporosity and narrow pore size distribution can be synthesized using a nanocasting approach that employs micelles of amphiphilic block copolymers as templates. The most common copolymers are poly(ethylene oxide)-*b*-poly(propylene oxide)-*b*-poly(ethylene oxide) triblock copolymers (PEO-*b*-PPO-*b*-PEO) from the Pluronic family,[44-46] polystyrene-*b*-poly(4-vinylpiridine)(PS-*b*-P4VP)[38] or polystyrene-*b*-poly(ethylene oxide) (PS-*b*-PEO).[47] Typically applied carbon precursors are small clusters of phenol/formaldehyde, or so-called "resol" (a soluble low-molecular weight polymer (M_w = 500-5000 g/mol) derived from acid-catalyzed or base-catalyzed polymerization of a mixture of phenol and formaldehyde),[14, 46-48] so-called "RF resin" (recorcinol-formalydehyde)[38] and "PF resin" phloroglucinol-formaldehyde.[44] Typical synthesis procedures involve the mixing of a solvent (such as ethanol, water, THF, or mixtures of them), precursor (e.g. a resin of low molecular weight containing OH groups), and template (e.g. tri-block copolymers of the type PEO-*b*-PPO-*b*-PEO). This mixture assembles into an ordered mesophase. The mesophase is stabilized via thermal or catalytic crosslinking. Finally, the template is removed, e.g. by thermal treatment, which results in a porous carbonaceous material. The thermal treatment also induces a compaction of the material, which leads to a shrinkage of the pore system. The shrinkage occurs either isotropically (powders) or uni-axial (films on a substrate), where uniaxial shrinkage perpendicular to the substrate results in elliptical deformation of the pore shape.[49] The described synthesis approach provides access to mesoporous carbons with pore sizes ranging from 3 - 30 nm,[14, 38, 48] and with surface areas between 280[14] and 1510 m^2/g.[47]

2.2.1 Key issues for the successful synthesis

The synthesis of mesoporous carbons via micelle templating imposes a number of requirements on the chemical and physical material behaviour of the synthesis ingredients. In order to derive micelle-templated mesoporous carbon (1), the structure-directing polymer must provide a driving force for micelle formation, and strong interactions between the precursor and one of the blocks in the templating block-copolymer, such as e.g. hydrogen-bonding between PEO-chains in the template and OH-groups in the precursor resin, is required to prevent macrophase separation. Furthermore, (2) the precursor should be able to cross-link in order to stabilize the framework of the forming pore system. Finally, (3) the cross-linked precursor should possess a higher thermal stability than the template in order to facilitate a thermal template removal without collapse of the pore structure. The listed conditions are discussed in more detail below.

Condition 1: interactions between templates and precursors

In order to form a mesostructured phase from a structure-directing agent and precursor, a driving force must exist for microphase separation. The driving force for micelle formation and self-assembly of the structure directing agent, usually a block co-polymer, is based on the constituent blocks of the polymer possessing different affinities to the precursor resin, where one block interacts more strongly (e.g. through hydrogen bonding) with the precursor resins than the other block.

This can be achieved by selecting carbon precursors containing a large number of hydroxyl groups (-OH),[13, 38, 44] which can strongly interact with the polar parts of structure-directing block copolymers. Furthermore, precursor aggregates should be small enough to enable assembly around micelles.

The most commonly employed mechanism for self-assembly is the I^0S^0 mechanism, where I represents -OH or -NH moieties of the carbon precursors and S represents hydrophilic blocks of block-copolymers, respectively.[50, 51] This mechanism relies on hydrogen bonding between template polymer blocks and precursor resin.[13, 45, 52] Such H-bonding resembles the formation mechanism of mesostructured oxides proposed as modulation of the hybrid interface mechanism (MHI).[50, 53] In general, the I^0S^0 mechanism involves both the neutral polymer blocks and precursor molecules in the absence of electrostatic interactions. Dai et al., however, recently reported that under highly acidic conditions the self-assembly of polymeric precursors can also be driven by $I^+X^-S^+$ mechanism; where X represents counterions (Cl^- in this case), along with the normal I^0S^0 mechanism.[54] The acidic conditions induce protonation of phenol molecules (or their derivatives) and of cross-linked phenols. Moreover, the EO blocks of the Pluronic block copolymers are also protonated. Using Cl^- as a mediator, coulombic interactions can then facilitate the $I^+X^-S^+$ mechanism and enable the self-assembly of surfactant−polymer nanocomposites.[54] Very recently, Goldfarb et al. reported on formation mechanism of a cubic mesoporous carbon monolith synthesized using the resol and F127 as a precursor and template through the evaporation-induced self-assembly (EISA) process using electron paramagnetic resonance (EPR).[55] The investigation demonstrated that during evaporation, a resol-pluronic composite is formed through strong H-bonds between

hydroxyl groups of the resol and oxygens of the PEO block, with the resol penetrating all the way to the PPO-PEO interface. During thermopolymerisation step, the PPO-PEO regions are segregated more strongly, while the polymerising resol is driven out to the outer PEO corona, resulting in an ordered composite with a resol-free PPO core.

Condition 2: ability of precursors to cross-link

In order to provide a sufficiently stable and rigid framework that withstands template removal, which is typically carried out at temperatures between 350[14, 48] and 1800 °C,[54] carbon precursors must undergo a stabilisation process prior to the template removal. This stabilisation can be achieved by "thermal curing" in either base-catalysed or acid-catalysed condensation of the typically employed precursor combination of resol or phenol and formaldehyde.[13, 54] In cases where precursor molecules lack 3D interconnecting sites, such as linear novolac resins, insufficient cross-linking results in unstable frameworks, which are prone to pore collapse upon carbonisation.[56, 57]

Condition 3: different thermal stability between precursors and templates

Removal of the template is a key step for obtaining mesoporous carbon structures. Template removal is usually realized by thermal treatment ("carbonisation") under inert gas atmosphere that relies on the difference in thermal stability between the template and the carbon precursors. According to thermogravimetric analysis (TGA) under inert atmosphere (N_2 or Ar), notable weight losses of approximately 97.5, 98.8, and 96.8% are observed in the temperature range of 300−400 °C for pure copolymers F127, P123, and F108, respectively,[14] while PS-*b*-P4VP starts to decompose at 328 °C and finishes at 430 °C with only negligible residue (0.7 wt%).[38] Common resins (resol, resorcinol/formaldehyde) release under inert atmosphere only small molecules at such temperatures, i.e. water, H_2, CO_2, but retain the crosslinked precursor framework.[12]

Employing inert atmosphere (N_2, Ar) prevents combustion of the carbon precursor. Besides being stable enough to withstand template removal, the precursors must also be able to transform into a carbon matrix during subsequent treatments at higher temperatures. In general, properties such as electrical conductivity, adsorption and catalytic functionality largely depend on the extent to which the carbonized material is transformed into graphite.

Temperatures reported for thermal treatment range from 350[14, 48] to 2600 °C.[54] In general, a temperature of at least 600 °C is required to completely carbonise the precursor matrix, hence materials treated at lower temperatures do not possess a fully carbonized framework.[14] Unfortunately, excessive temperatures induce a collapse of the carbons mesopores. Hence, a complete conversion of the mesoporous carbon framework has not been reported so far.

A critical view on the carbon microstructure

With respect to the carbonization of such resins, it is important to discuss the impact of the heat treatment on the microstructure of carbonaceous materials with sp^2 carbon as the predominant hybridization. In numerous publications, the terms "graphitization" and "graphitic carbon" are used for the aforementioned resin-derived carbons, which is, however, not applicable to the materials presented. Strictly speaking, "graphitic carbon" is a well-

defined terminus: The use of the term graphitic carbon is justified if three-dimensional hexagonal crystalline long-range order can be detected in the material by diffraction methods, independent of the volume fraction and the homogeneity of distribution of such crystalline domains. Otherwise, the term "non-graphitic carbon" should be used.[58] Thus, "non-graphitic carbon" is the correct terminus to describe sp^2 carbon materials showing diffuse reflections in XRD experiments without the presence of (*hkl*) reflections. This corresponds to graphene stacks without 3D correlation between the stacked graphenes. The quite diffuse reflections observed in X-ray scattering of template carbons results from the significant degree of disorder and the small size of the graphene stacks.[59] Hence, a classification of resin-based carbons as "graphitic" is obsolete, unless 3D long-range order can be shown by XRD experiments; such XRD patterns, to the best of our knowledge, are not observed for soft template carbons, taking into account that "graphitization" usually occurs at temperatures above ca. 2200 °C, where the mesostructure usually breaks down.[54] The microstructure of such "non-graphitic" carbons and the evaluation by appropriate X-ray scattering approaches is described in literature.[15, 59, 60]

2.2.2 Typical examples for the synthesis of micelle-templated mesoporous carbon

Different synthesis routes allow the preparation of mesoporous carbons with different pore structures such as two-dimensional hexagonal (*p6mm*), three-dimensional bicontinuous (*Ia3d*), or body-centered cubic (*Im3m*). In 2004, Dai and co-workers established the synthesis of crack-free highly ordered hexagonal mesoporous carbon films via soft-templating using PS-*b*-P4VP as a template, resorcinol as carbon precursors, and formaldehyde to induce polymerisation of the resorcinol molecules.[38]

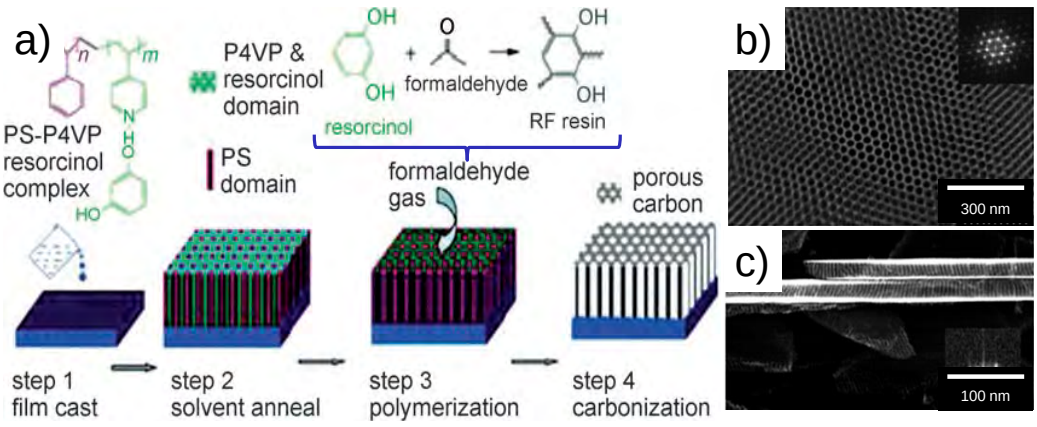

Figure 2.1. Synthesis of mesoporous carbon templated with micelles of PS-*b*-P4VP as reported by Dai et al.[38] a) schematic representation of the synthesis process: Step 1: film casting of PS-*b*-P4VP/resorcinol supramolecular assembly on Si wafer. Step 2: Microphase separation during solvent annealing at 80 °C in DMF/benzene vapour. Resorcinol organizes between the P4VP domains. Step 3: polymerisation of resorcinol exposing the film to formaldehyde gas. Step 4: Pyrolysis in N_2 resulting in arrays of hexagonally arranged carbon channels. b) SEM image after carbonisation at 800 °C (top view). c) SEM image in cross section, showing pore channels perpendicular to the substrate surface and the thickness of around 9 nm.[38]

The reported synthesis procedure is illustrated in Figure 2.1a. It involves formation of the molecular assembly, film casting, control of the solvent evaporation, polymerisation of the resorcinol located in between P4VP regions using gaseous formaldehyde, and finally thermal treatment at 800 °C to remove the polymer template and form a carbon matrix. SEM images of the resulting material are depicted in Figure 2.1b and c, showing thin films (~100 nm) completely penetrated by a hexagonal pore arrangement.

Ikkala et al. reported the formation of ordered mesoporous polymers utilizing also PS-*b*-P4VP, but a different precursor, phenolic resin. Pore structures were varied between worm-like, spherical and lamellar structures adjusting the ratio of phenolic resin to amount of template. Samples in the shape of films with the thicknesses up to about 100 micrometers were synthesized. However, calcination was performed only at 420 °C, a temperature which is sufficient for template removal, but not for carbonization.[57, 61]

Due to pricing and availability, the template polymer PS-*b*-P4VS is not suitable for a large-scale synthesis. Tanaka et al. demonstrated that also the common and cheap Pluronic triblock copolymer PEO-*b*-PPO-*b*-PEO can template mesoporous carbon.[62] They employed Pluronic F127 as template, resorcinol-formaldehyde "RF" as carbon precursor, and triethyl orthoacetate (EOA) as co-precursor. EOA served two purposes; it increased the carbon content of the final material and significantly enhanced the ordering of the porous structures. As shown in Figure 2.2, films with hexagonally ordered pores arranged parallel to the substrate were obtained after spin coating of the solutions, curing at 90 °C and subsequent carbonisation at temperatures ranging from 400 to 800 °C.

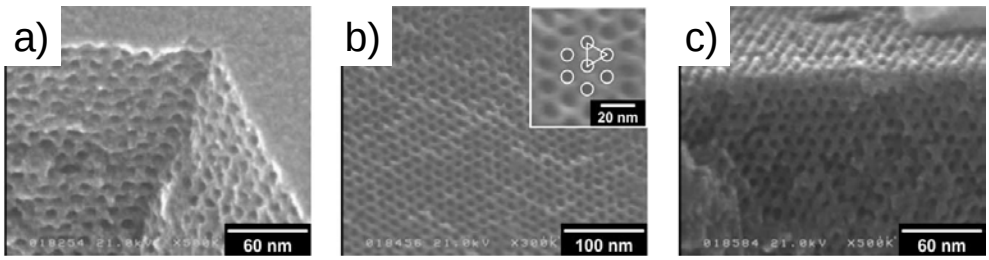

Figure 2.2. Mesoporous carbon synthesized by Tanaka et al. [62] from mixtures of resorcinol-formaldehyde, triethyl orthoacetate and Pluronic F127. SEM images of the carbon materials after calcination at temperatures of a) 400 °C, b) 600 °C and c) 800 °C.[62]

Zhao et al. demonstrated that also other polymers from the Pluronic family act as templates in the synthesis of mesoporous carbons from resol[13] i.e. F127,[14, 48] F108[14] as well as P123.[45, 48] The formed pore structure can be tuned by variation of the fraction of the hydrophobic block, either via the PEO content of the block copolymer or via changing the resol-to-template ratio in the solution. The resulting increase in curvature at the micelle interface in the composite provides the incentive for mesophase transition from lamellar (*La*) towards bicontinuous (*Ia3d*), hexagonal (*p6mm)*, and cubic globular (*Im3m)*, as illustrated in Figure 2.3.

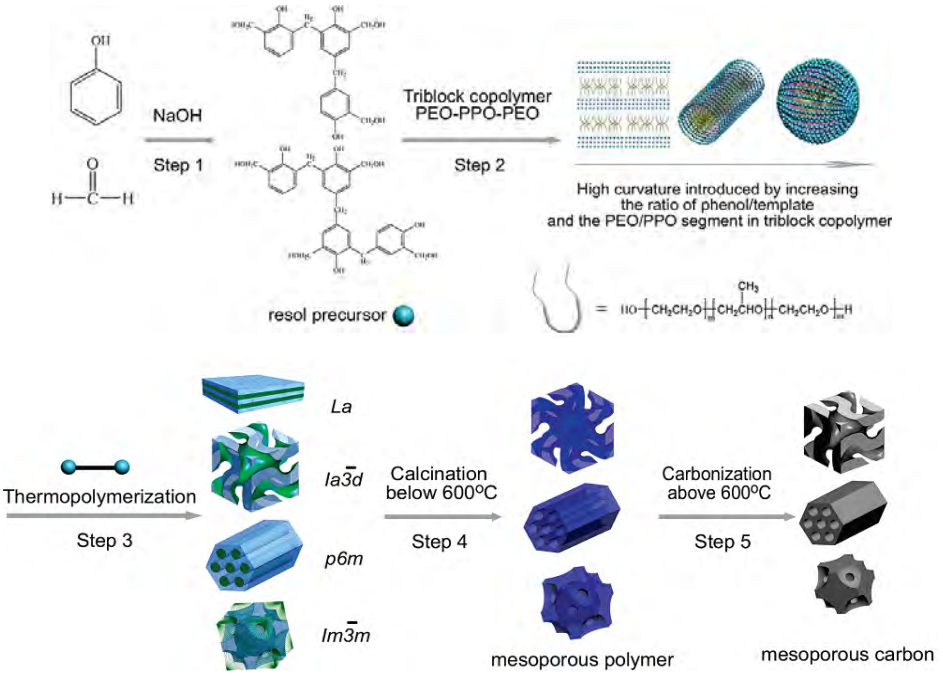

Figure 2.3. Schematic illustration of the preparation of ordered mesoporous polymer resins and carbon frameworks using resol as a carbon precursor as reported by Zhao et al. [14] The obtained pore structure can be controlled in step 2 by the composition and concentration of the template polymer.[14]

2.2.3. Control over pore morphology, pore size and approaches to obtain large mesopores

2.2.3.1 Templating with conventional Pluronic polymers

Significant effort has been dedicated to elucidating factors that control morphology and pore size of mesoporous carbons templated, including different templates such as Pluronic F127 and P123 and different carbon precursors. Besides the ratio between the amounts of precursor and template also various other synthesis parameters affect the final pore morphology of mesoporous carbons as reported recently.[63-71] Tanaka et al.[64] demonstrated the importance of the solution composition: carbon powders were synthesized from resorcinol-phloroglucinol/formaldehyde and F127 dissolved in different amounts of ethanol and water. A three dimensional wormhole-like mesostructure was formed with EtOH/water ratios in the range of 0.5 to 1.25. When the molar ratio was increased to 2.5, a hexagonal *p6mm* structure was obtained. This observation was explained by the fact that ethanol swells the hydrophobic cores of F127 micelles and interacts with both, PPO and PEO segments, due to its polar characteristics. Hence, ethanol molecules are located at the hydrophilic-hydrophobic interface, which results in a decreased interfacial curvature and in consequence induces a transition between different phases of the micelle-templated pore system as a function of water and ethanol content. Long et al. synthesized mesoporous carbons using resorcinol-furfural oligomers as precursor and F127 as template.[63] They reported that at the same ratio between amounts of precursor and template an increase in the degree of polymerization of the precursor resin induced a mesophase transition from *Im3m* to *p6mm* and then to a disordered

phase. The degree of polymerisation was adjusted using different reaction times of precursor crosslinking. The observed phase transition was attributed to the lower thermodynamic driving force of oligomers to mix with PEO segments. In a similar study, Hayashi et al. recently reported that also the pore diameter of soft-templated mesoporous carbons changes with polymerization time.[72] They used resorcinol-formaldehyde, triethylorthoacetate (EOA) and F127 as a precursor, co-precursor and template, respectively, under acidic conditions. Extending polymerisation time while keeping other parameters constant, they enlarged pore sizes from 7 to 12.5 nm. The increase in pore size was rationalized by expansion of the micelle core of F127 due to higher water content that was incorporated into the micelle core.
The mesostructure of mesoporous carbons can also be adjusted using mixtures of different template molecules, based on the mixtures of commercially available triblock copolymers and reverse triblock copolymers (PPO-*b*-PEO-*b*-PPO). This approach has been illustrated by Qian et al.[71] They used resol as a carbon precursor and ethanol as a solvent in combination with different mixtures of Pluronic type polymers of regular (e.g. F127: PEO_{100}-*b*-PPO_{70}-*b*-PEO_{100}) as well as inverse structure (PPO_{19}-*b*-PEO_{33}-*b*-PPO_{19}). A simple estimation of the molar ratio of hydrophilic and hydrophobic section was proposed to predict the final mesostructure of the resulting mesoporous carbons. By changing the molar ratio of F127 to PEO_{19}-*b*-PEO_{33}-*b*-PPO_{19}, two different phases were obtained, i.e. *p6mm* and *Im3m*.

2.2.3.2 Towards bigger mesopore size with larger polymers and swelling agents

Size and connectivity of pores are important criteria for many practical applications. Different Pluronic polymers can template cubic pore systems with pore diameters between 3 nm[14, 45, 73] and 7 nm.[46, 74] Using high-molecular-weight PS-*b*-P4VP as template and resorcinol/formaldehyde as precursor, Dai et al. synthesized mesoporous carbon films possessing larger pores of around 33 nm in diameter, yet pores were hexagonally arranged parallel to substrate, i.e. not well interconnected.[38] To accomplish the synthesis of carbon materials with large mesopores also in cubic pore systems, two different approaches have been pursued: increasing the size of template molecules to generate larger micelles, and swelling of the micelles by addition of an additional swelling agent.
Zhao et al. employed high-molecular-weight PS-*b*-PEO polymers with various sizes of the PS block.[47, 75] The templates PS-*b*-PEO were synthesized through atom transfer radical polymerisation. By controlling the polymerisation time, polymers with different PS block lengths were obtained. Average molecular weights of the polymers amounted to 17900, 29700, and 37200, corresponding to approximate molecular compositions of PS_{120}-*b*-PEO_{125}, PS_{230}-*b*-PEO_{125} and PS_{305}-*b*-PEO_{125}, respectively. Mesoporous carbon films were then synthesized using the template polymers in combination with THF as a solvent and resol as a carbon precursor. SAXS and TEM analysis indicated formation of mesostructured carbon of fcc type with a space group *Fm3m*. Mesopores templated by PS_{120}-*b*-PEO_{125}, PS_{230}-*b*-PEO_{125} and PS_{305}-*b*-PEO_{125} measured 11.9, 22.7 and 33.3 nm in diameter and featured cell parameters of 33.0, 46.5 and 54.2 nm, respectively. A SEM image of the carbon with pores templated with PS_{230}-*b*-PEO_{125} is shown in Figure 2.4a.

Besides two-component block-copolymers of AB type (e.g. PS-*b*-PEO) and ABA (e.g. PEO-*b*-PPO-*b*-PEO) type also triblock-copolymers of ABC type have been developed, featuring not only higher molecular weights, but also graded functionality along the molecule chains. Zhao et al. synthesized an amphiphilic ABC-type triblock copolymer (PEO_{125}-*b*-$PMMA_{100}$-*b*-PS_{138}) with gradient hydrophilicity using ATRP method. The polymer templates highly ordered mesoporous carbons with pore diameters up to 20 nm using resol as carbon precursor and THF as a solvent.[76] The carbon films obtained via evaporation-induced self-assembly (EISA) featured a face-centered cubic (FCC) closed-packed mesostructure (space group *Fm3m*) (see Figure 2.4b). Yet, the tailored synthesis of one ABC-type polymer for each pore size requires significant effort.

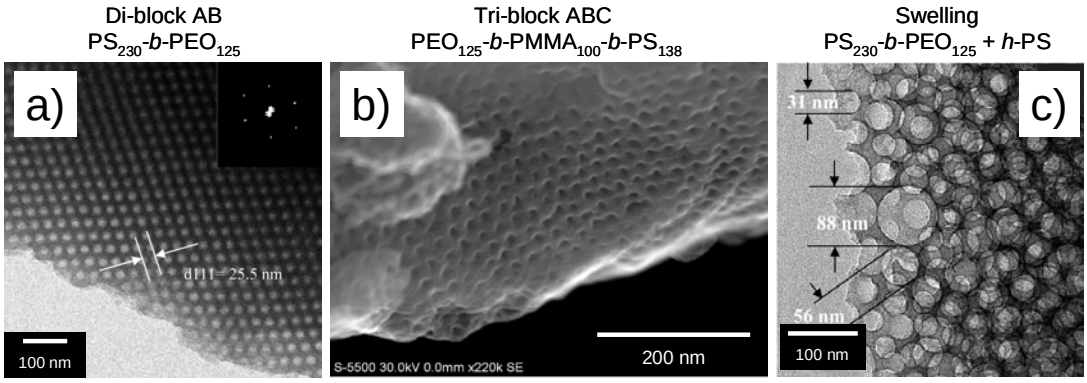

Figure 2.4. Carbon materials with large mesopores derived by different approaches: a) TEM image of mesoporous carbon templated by Zhao et al. [47] with di-block copolymer PS_{230}-*b*-PEO_{125} after carbonisation in N_2 at 800 °C. b) SEM image of mesoporous carbon templated by Schüth and Zhao et al.[76] using ABC type triblock PEO_{125}-*b*-$PMMA_{100}$-*b*-PS_{138} after carbonisation in N_2 at 1200 °C. c) TEM image of an ultra-large mesopore carbon prepared by Zhao et al. [77] adding 30 wt% of pore-swelling agent *h*-PS to solutions containing micelles of PS_{230}-*b*-PEO_{125} as template. Sample was carbonised in N_2 at 800 °C.

In contrast, changing the size of a micelle by swelling its core with a swelling agent as reported e.g. for the synthesis of mesoporous silica[51, 78-81] is a more facile and flexible method of pore size tuning. Zhao et al. synthesized ultra-large-pore ordered mesoporous carbons employing a diblock-copolymer PS_{230}-*b*-PEO_{125} as template and low-molecular-weight homopolystyrene (M_n of 5100 g/mol, *h*-PS_{49}) as "pore expander" using resol as carbon precursor and THF as solvent.[77] EISA was employed for film casting. Samples were carbonised in flowing N_2 at 800 °C. When the amount of swelling agent *h*-PS was varied between 0 and 20 wt% relative to PS-*b*-PEO content, mesoporous carbons with highly ordered face-centre cubic mesostructure (space group *Fm3m*) were obtained. Pore size was tuned in the range of 23 to 37 nm, corresponding cell parameters amounted to 46 to 58 nm. However, with increasing amount of *h*-PS the wall thickness decreased from 9.9 down to 3.6 nm. Moreover, a further increase in *h*-PS content resulted in larger pore sizes up to 90 nm, but also in multimodal pore size distributions and the formation of a foam-like disordered porous structure (Figure 2.4c).

Mechanistically, the increase in pore size upon *h*-PS addition has been explained by a continuous solubilizing process. Whereas the PEO block of PS-*b*-PEO interacts with the resol resin, the PS block forms the micelle core. Due to its small size and hydrophobic nature the swelling agent *h*-PS is soluble in the micelle core and increases the core size. In contrast, excessive amount of *h*-PS added to the system cannot be homogeneously accommodated in the micelle cores, resulting in simultaneous microphase and macrophase separation and the formation of a worm-like disordered mesostructure. Hence, excessive swelling of micelles to generate ultra-large mesopores gradually compromises order and homogeneity of the templated pore system.

2.2.4. Roles of the carbon precursors, solvents and catalysts

The choice of precursor is critical to the formation of mesoporous carbons. Precursor molecules typically employed in the resin formation that precedes the synthesis of soft-templated mesoporous carbons are shown in Figure 2.5, i.e. phenol, resorcinol and phloroglucinol. Chemical crosslinking of these molecules, often with formaldehyde acting as linker, forms the oligomers that co-assemble with the templates micelles. Due to a high degree of crosslinking that can be obtained by a simple thermal treatment around 100 °C, resol is the most common choice of precursor resin. The resol precursor resin consists of low molecular-weight clusters of phenol units that are linked mainly through methylene groups. It is produced by acid-catalyzed or base-catalyzed polymerization of phenol and formaldehyde employing a molar formaldehyde-to-phenol ratio greater than one. After neutralization, the hydroxyl groups of resol facilitate hydrogen bonding with hydrophilic chains of block copolymers inducing the desired microphase separation.[13, 48, 55, 74, 76, 82]

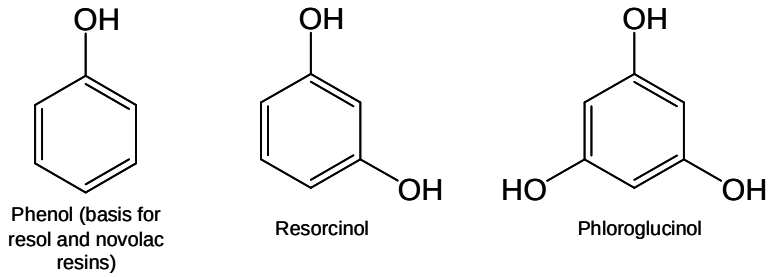

Figure 2.5. Chemical structures of precursor molecules that are commonly used in the preparation of the precursor resin used for soft-templating of mesoporous carbon materials.

Novolac is also a phenol-formaldehyde resin, but synthesized at a formaldehyde-to-phenol ratio less than one. Since a molar ratio of formaldehyde to phenol of one enables every phenol to be linked via methylene bridges, in theory one single crosslinked molecule results. Thus, Novolac resins are less suitable than resol resins to generate a framework that withstands thermal template removal due to their lower degree of cross-linking.[61, 73]

Other precursor resins that have been employed for the synthesis of mesoporous carbon are based on either resorcinol or phloroglucinol. The structural similarity to phenol evident from Figure 2.5 implies similarities also in chemistry and polymerization behaviour, but gradual differences in terms of interaction strength with the template polymer and the degree of crosslinking. Dai et al. reported that phloroglucinol (1,3,5-trihydroxybenzene) interacts more strongly than phenol/formaldehyde or resorcinol/formaldehyde complexes with Pluronic templates due to the fact that it can form triple hydrogen bonds with the PEO blocks of F127.[44] The proposed mechanism of interaction between phloroglucinol and Pluronic-type templates is illustrated in Figure 2.6. Moreover, phloroglucinol was reported to polymerize more rapidly than either resorcinol or phenol (about 40 min vs. 1 and 2 to 3 weeks, respectively, for mixtures with formaldehyde, ethanol, water, F127 and 0.01 M HCl). In addition, the structure of mesoporous carbon obtained under similar synthesis conditions (curing at 100 °C, carbonization at 850 °C under nitrogen atmosphere), but with the different precursors, differed significantly.[44] Whereas carbons based on phloroglucinol possessed a highly ordered 2D hexagonal system (*p6mm*), resorcinol and phenol only resulted in poorly structured microporous carbons. Hence, the OH content of the precursor molecule as well as the formaldehyde content in the resin are variables that can be used to adjust the self-assembly behaviour and thermal stability of the structured mesophase.

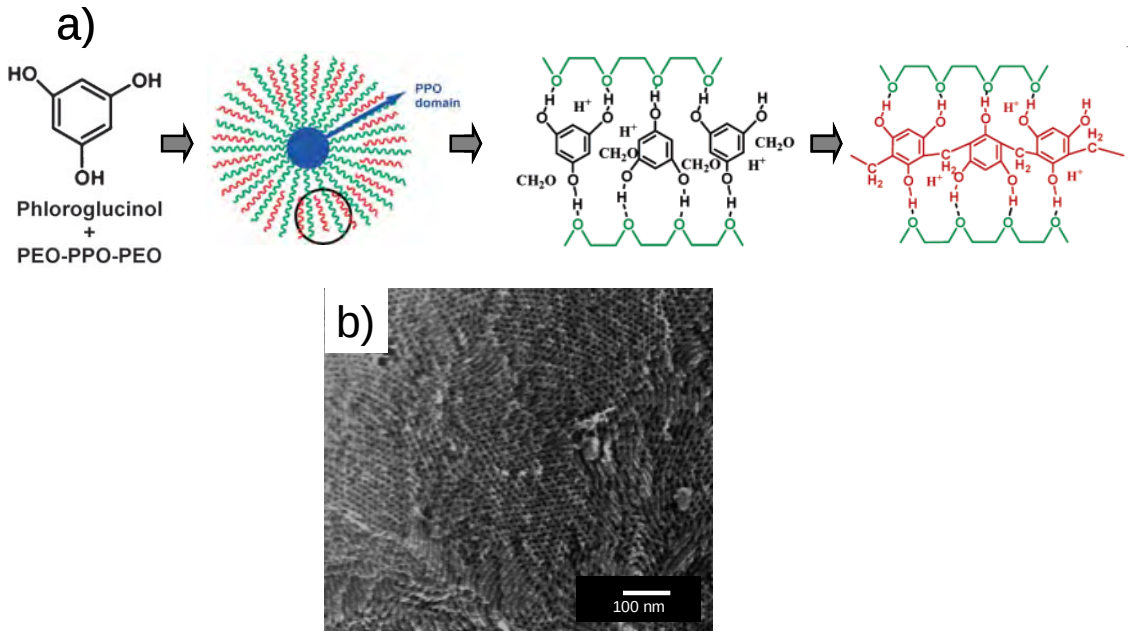

Figure 2.6. Synthesis of mesoporous carbon from alternative precursor, phloroglucinol as reported by Dai and co-workers.[44] a) schematic illustration of polymerization of phloroglucinol and formaldehyde and its interaction with PPO block of micelles of the template polymer. b) SEM image of the mesoporous carbon obtained by templating with F127 and calcination at 850 °C.[44]

The synthesis approaches described so far employ organic solvents such as ethanol, THF, or their mixtures with water. In contrast, Lu and Schüth et al. reported the synthesis of mesoporous carbons in aqueous phase under mild conditions.[83] In the synthesis procedure, crosslinking of the precursor resin resorcinol/formaldehyde was catalyzed by an amino acid

(glutamic acid) whereas Pluronic F127 served as a structure-directing agent. Phase separation occurred within 10 h at 60 °C, which was accelerated at higher reaction temperatures. After further aging at 90 °C for 48 h the obtained precipitate, a glass-like bright red solid, was converted into mesoporous carbon by carbonisation under an argon atmosphere at a temperature up to 850 °C.

The idea of using halogen-free cross-linking catalysts was further pursued by the same group.[84, 85] N-containing catalysts, namely 1, 6-diaminohexane (DAH)[84] and lysine,[85] were used in a synthesis that involved resorcinol and formaldehyde as a carbon precursor and F127 as a template. Using either catalyst in the polymerisation of resorcinol and formaldehyde resulted in rapid gelation within 15 min at 90 °C. The polymer monoliths thus obtained were dried and then carbonised at 800-850 °C under nitrogen, which yielded crack-free mesoporous carbon monoliths. More interestingly, the synthesis resulted in a nitrogen-containing framework of the carbon monoliths, where the nitrogen contained in the DAH or lysine catalysts was incorporated into the final carbon structure. Since only hydrocarbon molecules are present in the reaction systems, i.e. no metal or halogenide ions, the resulting carbons were of superior purity, which is beneficial to sensitive applications.

Mesoporous carbon materials can be also synthesized using renewable materials such as sugars as precursor.[86, 87] Antonietti et al. recently reported the synthesis of ordered mesoporous carbons through a sugar-based direct hydrothermal carbonisation (HTC)/soft-templating approach.[86] D-Fructose functioned as a carbon precursor whereas Pluronic F127 acted as pore template during the synthesis under hydrothermal conditions at 130 °C. Water was employed as a solvent. The mesostructured solid resulting from the hydrothermal carbonisation was further carbonised by thermal treatment at 550 °C to obtain higher carbon content. The proposed templating mechanism involves H-bonding of D-Fructose to the template PEO moiety under hydrothermal conditions.

2.3. Specific aspects of synthesis of mesoporous carbons in the film morphology

Herein, the aspects concerning shaping soft-templated mesoporous carbons into the form of films are highlighted.

As discussed above, the mechanism involving the evaporation-induced self-assembly (EISA) process has been successfully employed to prepare ordered mesoporous carbons in the form of powder.[14] In principle and similar to systems involving metal oxides,[19, 88, 89] a homogeneous solution containing both a carbon precursor and a polymer template used as a structure directing agent is prepared in a volatile solvent. Due to the stability and nonvalatility of the carbon precursor, the gradual evaporation of the solvent progressively increases the concentration of the polymer template, which results in the formation of micelles, and drives the organisation of precursor-polymer composite in the form of liquid-crystalline mesophase. The composite is subsequently thermopolymerised to further crosslink the precursor and lock

in place the polymer template, finally followed by the carbonisation step to remove the template and convert the precursor into carbon matrix, leaving the templated mesopores behind.

.

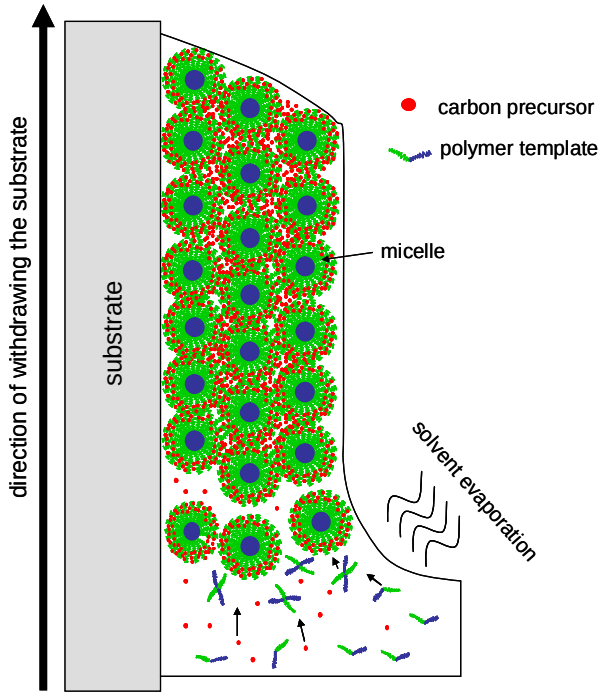

Figure 2.7. Schematic representation of the EISA process during dip coating. The substrate is pulled at a defined speed out of the dip-coating solution, the solvent silmutaneously evaporates, resulting in the formation of the precursor-template composite. Micelles of the polymer rearrange and are surrounded by the carbon precursor.

In this thesis, the dip-coating technique has been utilised to deposit the mesophase. By dipping the substrate with a homogeneous solution containing a precursor and template under controlled conditions (withdrawal speed, temperature, and relative humidity), a homogeneous film is obtained, followed by themopolymerisation at ca. 100°C and carbonisation at higher temperatures under an inert atmosphere. Figure 2.7 schematically represents the EISA process for the synthesis of the mesoporous carbon film using the dip-coating technique

Compared to powder materials prepared though EISA, the synthesis of mesoporous carbon films faces additional challenges. During template removal and conversion of the precursor into a carbon matrix, anisotropic shrinkage of the films takes place. The films only contract uniaxially perpendicular to the substrate surface (Z direction or out-of-plane) due to the fixed dimensions in the other two directions (XY direction or in-plane). As a result of this, the initial structure is strongly distorted.[20, 23-27, 49] If the contraction is too high, collapse of the mesopore structure occurs. Since the distortion can lead to structural changes, or even to the collapse of the templated pores, Chapter 4 of this thesis also focuses on the structural information obtained by the investigation of the films using various characterisation techniques, in order to prove the quality of the mesoporous carbon film materials synthesized in this work.

2.3.1 Synthesis of supported catalysts with carbon as support: towards in situ modification with metal species during film formation

To prepare catalysts based on metal or metal oxide particles on carbon supports, various kinds of carbon materials have been used. As stated above, due to their unformed mesopore size, mesoporous carbons provide advantages over the ones without controlled pore morphology and size. Therefore, mesoporous carbons synthesized through either hard- or soft-templating strategy have been used as catalyst supports for different kinds of metal/metal oxide active particles and catalytic reactions; for example Fe_2O_3 for the Fishcer-Tropsch synthesis,[90] Ir for the catalytic decomposition of N_2H_4,[91] Pd for oxidation of alcohols to aldehydes,[92] MnO for the wet oxidation of phenol,[93] Pd for the Heck coupling reaction of chlorobenzene and styrene, and the Ullmann coupling reaction of chlorobenzene,[94] Ru for the selective hydrogenation of cinnamaldehyde,[95] Ag for the catalytic reduction of 4-nitrophenol,[96] Pt for the electrocatalytic oxygen reduction reaction (ORR).[97] However, most of the catalysts supported on such ordered mesoporous carbons have been synthesized through the time-consuming impregnation method, followed by catalyst activation. In contrast, introduction of the the metal component directly during the synthesis of mesoporous carbons could offer unique advantages, escpecially in terms of commecial interest and large scale production. Similar to the RF-based carbon aerogel systems,[5] in fact, metal component can readily be incorporated into a mixture of a carbon precursor and a polymer soft-template.[91, 95, 98-103]
The successful synthesis of these metal/metal oxide particles in such soft-templated mesoporous carbon is attributable to the strong interactions of the metal species with the oxygen functionalities of the carbon precursor via coordination, resulting in good dispersion of the metal species. Depending on the nature of the metal species as well as the carbonisation conditions, either metallic[91, 95, 104] or metal oxide particles[90, 93, 105] could be obtained and embedded inside the carbon matrix.

In the EISA process, such strong interactions proceed while the solvent evaporates. This results in a higher concentration of the polymer template and the formation of a well-ordered mesostructure, while the metal species are well distributed in the carbon precursor matrix. After thermopolymerisation to further crosslink the precursor matrix, subsequent carbonisation converts the precursor matrix into carbon, removes the template, and at the same time results in the formation of metal/metal oxide particles. One of the challenges in incorporating metal species in to the soft-templated mesoporous carbons is that their presence possibly disturbs the self-assembly process, thereby influencing the final ordering of the mesopore structure. Therefore, effective control over the synthesis is necessary.

For in situ incorporation of metal species into mesoporous carbon films, the EISA process can be readily applied to coating on substrates. This facile approach has not been so far reported in the literature. Based on the in situ incorporation of the metal species during the self-assembly, Chapter 5 of the thesis presents the successful synthesis of Pd and Pt-containing ordered mesoporous films with a desirable well-defined mesopore structure by extending the established method for the synthesis of mesoporous carbon films presented in Chapter 4. The

resulting Pd-containing mesoporous carbon films have been also tested in a catalytic reactor and provide the high performance of gas-phase 1,3-butadiene hydrogenation for the first time.

2.4. Catalysis of hydrogenation of 1,3-butadiene

1,3-butadiene (or so-called only as butadiene) is a simple conjugated diene with a chemical formula C_4H_6. 1,3-butadiene is a by-product of the stream cracking of petroleum in the production of unsaturated hydrocarbons.[106-109] 1,3-butadiene is found as a contaminant in different chemical feed stream processes. In certain cases, its presence should be avoided. For example, in the production of polybutene, which is widely used as plasticizers for high-molecular weight polymers, from 1-butene, traces of 1,3-butadiene must be selectively converted into 1-butene. Further hydrogenation into *n*-butane should be prevented in order to avoid a loss of quality of the polymer.[106] Another example is in alkylation processes used to produce high-octane gasoline from butanes and butenes. In these processes, 1,3-butadiene is a contaminant and could lead to an increase in the content of undesired heavy alkylation gas oil;[107, 110] therefore, it must be converted into butenes. In this type of conversion, the suppression of 1-butene to 2-butene is unnecessary since 2-butene can produce gasoline of even higher octane number than 1-butene. For above reasons, the hydrogenation of 1,3-butadiene has attracted much attention.

The butadiene hydrogenation is frequently catalyzed by heterogeneous palladium-based catalysts.[111-113] The reaction can take place in the gas or liquid phase. In this thesis, the gas-phase reactions are considered. Figure 2.8 shows schematically possible reaction pathways. The hydrogenation of 1,3-butadiene results in a subsequent reaction with the isomeric intermediates of 1-butene, *trans*-2-butene, *cis*-2-butene and *n*-butane as a product of total hydrogenation.

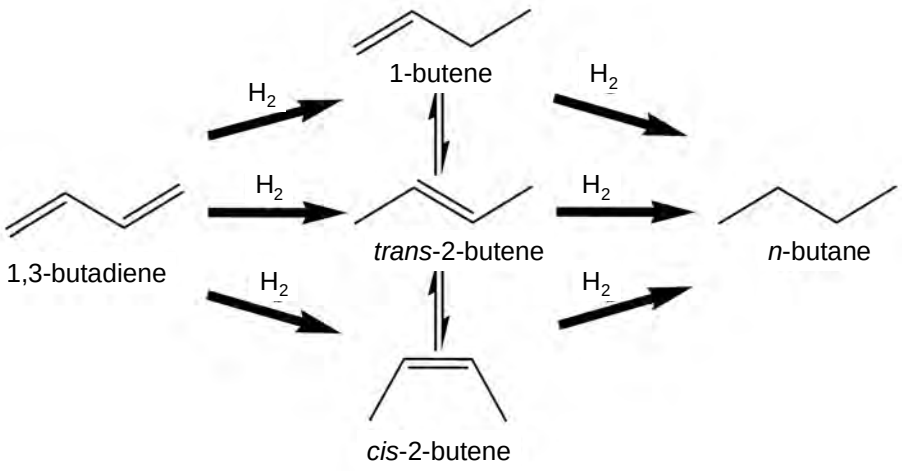

Figure 2.8. Schematic representation of the reaction pathways in the hydrogenation of 1,3-butadiene. [111]

To describe the reaction, various mechanisms have been proposed. According Silvestre-Albero et al., it is only one possible mechanism where 1,3-butadiene molecules are adsorbed on the (111) and (110) planes of Pd in the first step.[112] A hydrogen atom is then added to one of the two double bonds, leading to the formation of 1-butenyl or 2-butenyl. 2-butenyl is further hydrogenated via a 1,2-addition to 1-butene or a 1,4-addition to 2-butene (*trans*- and *cis*-). As the adsorption enthalpy of 1,3-butadiene (-138 kJ/mol) is significantly higher than the adsorption enthalpies of the butene isomers (-56 kJ/mol to -75 kJ/mol), the main species adsorbed on the Pd is 1,3-butadiene. Consequently, there is a selective hydrogenation of 1,3-butadiene to butenes.[113] Only when a low concentration of 1,3-butadiene is present, butene is hydrogenated to *n*-butane.

In the present work, the 1,3-butadiene hydrogenation is used as a model reaction to test the catalytic properties of Pd-containing mesoporous carbon catalysts. In general, with such a model reaction, the effects of synthesis parameters on activity, selectivity, diffusion properties and stability of a supported catalyst can be examined.

Chapter 3
Experimental

This chapter provides detailed synthesis routes to mesoporous carbon films (section 3.2), including catalyst films containing Pt and Pd particles (section 3.3). The chemicals, materials, routes to the synthesis of the polymer templates and substrate pre-treatment method used in this thesis are provided (section 3.1). The analytical methods used to characterise the synthesized materials are briefly described (section 3.4).
Based on a model reaction of the gas-phase hydrogenation of butadiene, the templated mesoporous catalysts were selected to investigate catalytic performance for this reaction. Therefore, the set-up of the reactor and catalytic testing are also presented (section 3.5).

3.1 Chemicals and materials

3.1.1 Precursors and solvents

Resorcinol and formaldehyde (37 wt% in water) used as a carbon precursor were purchased from Sigma-Aldrich. MilliQ water was used for all synthesis procedures. Ethanol (EtOH, >99.9%, absolute) and tetrahydrofuran (THF, >99.9%, absolute) were purchased from VWR. 3.0 M hydrochloric acid (HCl) was prepared from 12 M HCl and used as a catalyst in preparation of carbon precursor solutions. Platinum nitrate ($Pt(NO_3)_2$, 98%), and Palladium(II)acetylacetonate ($Pd(C_5H_7O_2)_2$ or $Pd(acac)_2$, 98%) were purchased from Alfa Aesar, and served as precursors for Pt and Pd nanoparticles, respectively. All the purchased chemicals were used without further purification.

3.1.2 Templates

F127
A triblock copolymer, Pluronic F127 (PEO_{106}-*b*-PPO_{70}-*b*-PEO_{106}, M_w = 12600) was purchased from Sigma-Aldrich.

PIB-PEO 3000
$CH_3C(CH_3)_2(CH_2C(CH_3)_2)_{53.5}CH_2C(CH_3)_2C_6H_4O(CH_2CH_2O)_{45}H$ polymer (referred to as PIB-PEO 3000) was synthesised as reported by von Graberg et al.[114] PIB phenol 3000 (377 g, 126 mmol) and potassium tert-butylate (1.60 g, 14.3 mmol) were placed in a 1-liter flask, and the remaining water was removed by distillation at 100 °C under reduced pressure for 3 h in a rotary evaporator. The reaction mixture was placed in a 2-liter autoclave and purged three

times with nitrogen at 100 °C. Then, ethylene oxide (252 g, 5.72 mol) was added in portions at 120 °C and the mixture was allowed to postreact overnight. PIB-PEO 3000 (541 g, 86%) was observed as a colorless rubberlike solid. The molecular weight and its distribution were determined by size exclusion chromatography (SEC) using tetrahydrofuran as eluent and PSS SDV columns as solid phase. The weight-averaged and number-averaged molecular masses were M_w = 7050 g/mol and M_n = 5620 g/mol, respectively (M_w/M_n = 1.25). Its chemical structure is shown in Figure 3.1a.

10k-PB

Poly(ethyleneoxide)-*b*-poly(1,2-butadiene-*co*-1,4-butadiene)-*b*-poly(ethyleneoxide) containing 18700 g/mol PEO and 10000 g/mol PB), PEO_{213}-*b*-PB_{184}-*b*-PEO_{213} (referred to as 10k-PB) was purchased from PSM GmbH. The polymer was synthesized as reported in a previous publication by Ortel et al.[37] First, 23 g of the PB polymer (Krasol, Sartomer) was dissolved in 250 mL THF. Then, an equimolar amount of phosphazene base t-BuP_4 (1 M solution in hexane, Fluka) was added to the solution using a syringe. The solution was cooled to -30 °C, and the required amount of EO was cryo-distilled into the reactor. The reaction mixture was stirred and slowly heated to 20 °C. After the heat of the polymerization reaction had been released, the reactor was heated to 50 °C and stirred for two days under a dry argon atmosphere. Thereafter, the polymerisation was quenched with acetic acid and the crude product was precipitated into cold acetone (-30 °C). The polymer was redissolved in distilled water and washed with an acidic cation exchanger (Dowex 50WX8-400). The polymer solution was precipitated again into cold acetone and dried under vacuum. The 10k-PB possesses a polydispersity index (PDI) of 1.19. Its chemical structure is shown in Figure 3.1b.

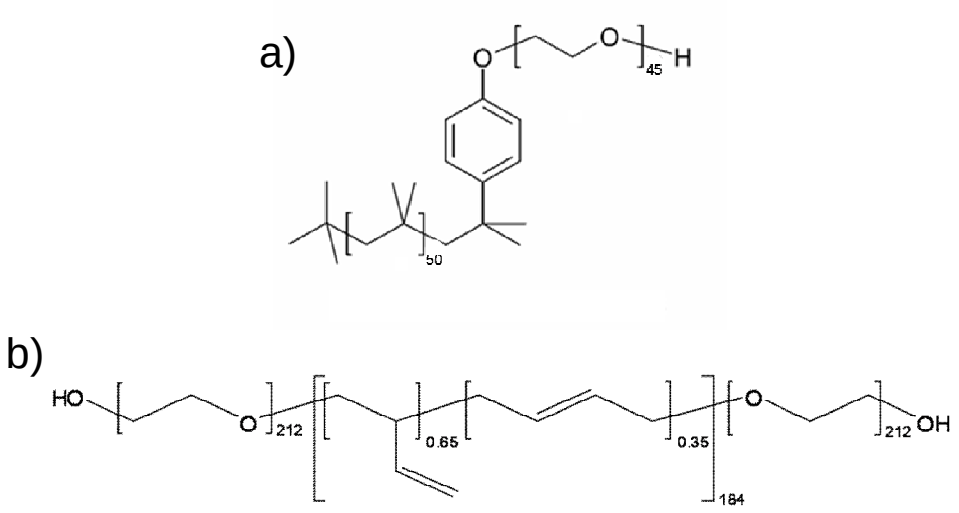

Figure 3.1. Molecular structures of a) PIB-PEO 3000 and b) PEO_{213}-*b*-PB_{184}-*b*-PEO_{213} polymers (10k-PB) used as big-pore templates in this thesis

3.1.3 Substrate pre-treatment

Si-wafer substrates were cleaned with ethanol and calcined in air (2 h, 600 °C) prior to film deposition. Stainless steel was employed as substrates when catalyst films were used to investigate catalytic performance in butadiene hydrogenation reaction, as well as to check integrity of pore morphology of mesoporous carbon films compared to those coated on Si wafers. Coupons of stainless steel with three different thicknesses (0.5, 0.25 and 0.1 mm) (material number 1.4301, AISI 304, X5CrNi18-10) cut to 30 x 27 mm dimensions in width were used as substrates. The coupons were grinded for 2 min with 180-grit sandpaper to remove the undefined oxide layer. Afterwards, the coupons were washed with soap in hot water, rinsed in a large amount of deionised water, further cleaned with acetone, ultrasonicated in EtOH, and finally dried at room temperature. To passivate the steel surface, the washed and dried coupons were calcined in air at 600 °C for 2 h to yield 'grinded and pre-calcined steel plates' prior to dip-coating.[115]

3.2 Synthesis of mesoporous carbon films

In general, the synthesis of templated porous films starts with the preparation of a coating solution. In the method developed in this thesis, the 'precipitating-redissolving' process was employed to prepared a homogeneous dip-coating solution.[54, 116, 117] The synthesis was performed based on the interactions of a carbon precursor and a block-copolymer as a template in a EtOH/H_2O mixture under highly acidic conditions, similar to the synthesis reported by Dai et al.[54]

Employing this system, resorcinol (R) and formaldehyde (F) polymerise in an EtOH/H_2O mixture under acidic conditions. The mixture was subsequently left standing for a certain period of time, which afterwards resulted in a two-layer system, which was composed of a precipitated white turbid polymer-rich lower layer, and a transparent EtOH/H_2O upper phase. The polymer resin composite containing the polymerised carbon precursor and the template was obtained by discarding the upper phase (EtOH/H_2O mixture). The precipitated resin composite was then redissolved in a good volatile solvent, which in our case was THF. The dissolution of the composite in THF results in a homogeneous solution, which was employed for the dip-coating process. Subsequently, the dip-coating process on substrates was performed using the coating solution with a dip-coating instrument (id LAB) (Figure 3.2) under controlled conditions of temperature and relative humidity (%RH).

Figure 3.2. Dip-coating instrument from id LAB.

After the dip-coating, the coated film was left to evaporate the solvent until there were no visible changes in color on the film in a controlled environment. Subsequently, the dried coated film was subjected to thermopolymerisation of the polymer-rich phase at 100 °C to harden the film. Then, the film was pyrolysed at higher temperatures under an inert atmosphere of N_2 to remove the template and convert the resin into a carbon matrix.

3.2.1 Synthesis of mesoporous carbon films using F127 as a template

In a typical synthesis of the coating solution, 1.1 g of resorcinol was mixed with 0.3 g of F127 in 4.5 mL of EtOH and the mixture of both was dissolved until a clear solution was obtained. Afterwards, 4.5 mL of 3M HCl was added. The mixture was stirred for a minute. Then, 1.3 g of formaldehyde (37% in water) was added into the above solution, and the mixture was kept undisturbed. After ~ 4 min, the solution became turbid. 10 min after the addition of the formaldehyde solution, a white precipitate that was a mixture of the precursor and polymer template rich phase was separated from the mixture by centrifugation at 3500 rpm for 5 min and the top-layer solution containing a majority of EtOH and H_2O was discarded. After that, the white precipitate was immediately dissolved in 5 mL of THF to obtain a clear light yellow solution .The solution was used for dip-coating. The dip-coating process was performed on either Si wafers or grinded and pre-calcined steel plates at a chosen withdrawal speed in a controlled environment. After the dip-coating, the coated films were heat-treated at 100 °C for 24 h, followed by carbonisation of the films at higher temperatures under a nitrogen atmosphere. The conditions for the dip-coating and carbonisation for the films are summarised in Table 3.1.

Table 3.1. Conditions for the dip-coating and carbonisation for the films templated with F127

Material template/withdrawal speed/ carbonisation temperature	**F127/spd60/400**	**F127/spd60/600**	**F127/spd60/800**	**F127/spd60/400**	**F127/spd300/400**[b]	**F127/spd300/600**[b]	**F127/spd300/800**[b]
Coating parameters							
Temperature	25 °C,	25 °C,	25 °C,	25 °C,	25 °C,	25 °C,	25 °C,
Relative humidity	30 %RH	30 %RH	30 %RH	30 %RH	30 %RH	30 %RH	30 %RH
withdrawal speed of dip-coating[a]	60 mm/min	60 mm/min	60 mm/min	150 mm/min	300 mm/min	300 mm/min	300 mm/min
[a]*Carbonisation under N_2 atmosphere*							
heating ramp	1 °C/min	1 °C/min	1 °C/min	1 °C/min	1 °C/min	1 °C/min	1 °C/min
temperature, holding time	400 °C, 3 h	600 °C, 3 h	800 °C, 3 h	600 °C, 3 h	400 °C, 3 h	600 °C, 3 h	800 °C, 3 h

[a] All the dip-coated materials were then subject to thermal treatment at 100 °C for 24 h before carbonisation
[b] The materials were also used for N_2 sorption analysis

3.2.2 Synthesis of mesoporous carbon films using PIB-PEO 3000 as a template

The synthetic procedure for the coating solution based on PIB-PEO 3000 was similar to that using F127, except for the ratio of the resorcinol to the template and the centrifugation speed. In a typical preparation, 1.1 g of resorcinol was mixed with 165 mg of PIB-PEO 3000 in 4.5 mL of EtOH and the mixture of both was dissolved until a clear solution was obtained. Subsequently, 4.5 mL of 3M HCl was added. The mixture was stirred for a minute until a clear solution was obtained. Then, 1.3 g of formaldehyde (37% in water) was added into the above solution. After ~ 4 min, the solution became turbid. 10 min after the addition of the formaldehyde solution, the white precipitate, which was a mixture of the cross-linked precursor and polymer template rich phase, was separated from the mixture by centrifugation at 8500 rpm for 5 min. The top-layer solvent-rich phase was discarded. After that, the white precipitate was dissolved in 5 ml THF to obtain a clear light yellow solution .The solution was used for dip-coating. The dip-coating process was performed on either Si wafers or grinded and pre-calcined steel plates at a chosen withdrawal speed in a controlled environment. After the dip-coating, the coated films were the subjected to the same heat-treatment and carbonisation as for the films templated with F127. The conditions for the dip-coating and carbonisation for the films are summarised in Table 3.2.

Table 3.2. Conditions for the dip-coating and carbonisation for the films templated with PIB-PEO 3000

Material template/ withdrawal speed/carbonisation temperature	**PIB-PEO 3000/ spd60/600**	**PIB-PEO 3000/ spd150/600**	**PIB-PEO 3000/ spd300/600**	**PIB-PEO 3000/ spd600/400**[b]	**PIB-PEO 3000/ spd600/600**[b]	**PIB-PEO 3000/ spd600/800**[b]
Coating parameters						
temperature	25 °C,	25 °C,	25 °C,	25 °C,	25 °C,	25 °C,
relative humidity	20 %RH	20 %RH	20 %RH	20 %RH	20 %RH	20 %RH
withdrawal speed of dip-coating[a]	60 mm/min	150 mm/min	300 mm/min	600 mm/min	600 mm/min	600 mm/min
Carbonisation under N_2 atmosphere						
heating ramp	1 °C/min	1 °C/min	1 °C/min	1 °C/min	1 °C/min	1 °C/min
temperature, holding time	600 °C, 3 h	600 °C, 3 h	600 °C, 3 h	400 °C, 3 h	600 °C, 3 h	800 °C, 3 h

[a] All the dip-coated materials were then subject to thermal treatment at 100 °C for 24 h before carbonisation
[b] The materials were also used for N_2 sorption analysis

3.2.3 Synthesis of mesoporous carbon films using 10k-PB as a template

In general, the synthetic procedure for the coating solution based on 10k-PB polymer (PEO_{213}-*b*-PB_{184}-*b*-PEO_{213}) was similar to that using F127 and PIB-PEO 3000, except for the ratio of resorcinol to the template, the period that white precipitate occurred, the amount of solvents and catalyst, and the centrifugation speed. In a typical preparation, 1.1 g of resorcinol was mixed with 110 mg of 10k-PB in 7 mL of EtOH and the mixture of both was dissolved until a clear solution was obtained. Subsequently, 3 mL of 3M HCl was added. The mixture was stirred for a minute until a clear solution was obtained. Then, 1.3 g of formaldehyde (37% in water) was added into the above solution. After ~ 30 min, the solution became turbid. 40 min after the addition of the formaldehyde solution, the white precipitate, which was a mixture of the cross-linked precursor and polymer template rich phase, was separated from the mixture by centrifugation at 8500 rpm for 5 min. The top-layer solvent-rich phrase was discarded. After that, the white precipitate was dissolved in 5 ml THF to obtain a clear light yellow solution .The solution was used for dip-coating. The dip-coating process was performed on Si-wafers at a withdrawal speed of 600 mm/min and at 30% RH. After the dip-coating, the coated films were then subject to the same heat-treatment at 100 °C for 24 h and carbonisation at 600°C for 3 h. A heating ramp to 600 °C was 1 °C/min.

3.3 Synthesis of mesoporous catalyst films containing Pd or Pt particles using F127 as a template

Typically, the procedures of making mesoporous catalyst films are similar to those for the pristine mesoporous carbon films as described in section 3.2, except that the solutions of noble metal precursors are, in parallel, dissolved in THF, and mixed with the RF/polymer

template composite. This method results in in situ incorporation of the metal precursors into the matrix of the polymer composite.

3.3.1 Synthesis of Pd-containing mesoporous carbon catalyst films using F127 as a template and $Pd(acac)_2$ as Pd particle source

In a typical synthesis of the coating solution, 1.1 g of resorcinol was mixed with 0.3 g of F127 in 4.5 ml of EtOH and the mixture of both was dissolved until a clear solution was obtained. Afterwards, 4.5 mL of 3M HCl was added. The mixture was stirred for a minute. Then, 1.3 g of formaldehyde (37%) was added into the above solution. After ~ 4 min, the solution became turbid. 10 min after the addition of the formaldehyde solution, a white precipitate that was a mixture of the precursor and polymer template rich phase was separated from the mixture by centrifugation at 3500 rpm for 5 min and the top-layer solution containing a majority of EtOH and H_2O discarded. Subsequently, the white precipitate was dissolved in a solution of $Pd(acac)_2$ (16 mg, for 0.5% Pd, or 31.5 mg for 1% Pd with respect to the carbon content in resorcinol and formaldehyde (wt%)) in 5 mL of THF without sonication to obtain a clear orange solution .The resulting solution was used for dip-coating. For the catalyst films employed for the testing in butadiene hydrogenation, the films were coated on several grinded and pre-calcined steel plates using the same coating solution. After the dip-coating, the coated films were subject to the same heat-treatment and carbonisation as described above for the mesoporous carbon films without noble metal. The conditions for the dip-coating and carbonisation for the films are summarised in Table 3.3.

Table 3.3. Conditions for the dip-coating and carbonisation for the films templated with F127 and using $Pd(acac)_2$ as Pd particle source

Material name[a]	0.5%Pd/C-600	1%Pd/C-400	1%Pd/C-600[c]	1%Pd/C-800
amount of $Pd(acac)_2$	16 mg	31.5 mg	31.5 mg	31.5 mg
Coating parameters				
temperature	25 °C,	25 °C,	25 °C,	25 °C,
relative humidity	30 %RH	30 %RH	30 %RH	30 %RH
withdrawal speed of dip-coating[b]	60 mm/min	60 mm/min	60 mm/min	60 mm/min
Carbonisation under N_2 atmosphere				
heating ramp	1 °C/min	1 °C/min	1 °C/min	1 °C/min
temperature, holding time	600 °C, 3 h	400 °C, 3 h	600 °C, 3 h	800 °C, 3 h

[a] All the resulting materials were templated using F127

[b] All the dip-coated materials were then subject to thermal treatment at 100 °C for 24 h before carbonisation

[c] The materials were also prepared on grinded and pre-calcined steel plates, subsequently used in the reactor

3.3.2 Synthesis of Pt-containing mesoporous carbon catalyst films using F127 as a template and $Pt(NO_3)_2$ as Pt particle source

The method for preparation of the coating solution containing Pt particle source was performed in a similar way to that for Pd-containing mesoporous carbon films. In a typical synthesis of the coating solution, 1.1 g of resorcinol was mixed with 0.3 g of F127 in 4.5 ml of EtOH and the mixture of both was dissolved until the clear solution was obtained. Afterwards, 4.5 mL of 3M HCl was added. The mixture was stirred for a minute. Then, 1.3 g of formaldehyde (37%) was added into the above solution. After ~ 4 min, the solution became turbid. 10 min after the addition of the formaldehyde solution, a white precipitate that was a mixture of the precursor and polymer template rich phase was separated from the mixture by centrifugation at 3500 rpm for 5 min and the top-layer solution containing a majority of EtOH and H_2O discarded. Subsequently, the white precipitate was dissolved in a solution of ($Pt(NO_3)_2$ (9 mg, for 0.5% Pt, or 18 mg for 1% Pt with respect to the carbon content in resorcinol and formaldehyde (wt%)) in 5 mL of THF to obtain a clear orange solution .The resulting solution was used for dip-coating. The dip-coating process was performed on either Si-wafers at a chosen withdrawal speed in a controlled environment. For the catalyst films employed for the testing in butadiene hydrogenation, the films were coated on several grinded and pre-calcined steel plates using the same coating solution. After the dip-coating, the coated films were subject to the same heat-treatment and carbonisation as described above for the mesoporous carbon films without noble particles. The conditions for the dip-coating and carbonisation for the films are summarised in Table 3.4.

Table 3.4. Conditions for the dip-coating and carbonisation for the films templated with F127 and using ($Pt(NO_3)_2$ as Pt particle source

Material name[a]	1%Pt/C-400	1%Pt/C-600	1%Pt/C-800
amount of $Pt(NO_3)_2$	18 mg	18 mg	18 mg
Coating parameters			
temperature	25 °C,	25 °C,	25 °C,
relative humidity	30 %RH	30 %RH	30 %RH
withdrawal speed of dip-coating[b]	60 mm/min	60 mm/min	60 mm/min
Carbonisation under N_2 atmosphere			
heating ramp	1 °C/min	1 °C/min	1 °C/min
temperature, holding time	400 °C, 3 h	600 °C, 3 h	800 °C, 3 h

[a] All the resulting materials were templated using F127
[b] All the dip-coated materials were then subject to thermal treatment at 100 °C for 24 h before carbonisation

3.4 Characterisation

Scanning electron microscopy (SEM)

SEM images were collected on a JEOL 7401F scanning electron microscope operated between 4.0 and 10.0 kV. To determine film thicknesses, pore morphology in cross-section area, samples coated on silicon wafers were split into two pieces and imaged at the cross-section. Image J program, version 1.39u (http://rsbweb.nih.gov/ij), was employed to determine the pore diameter, film thickness, size of Pt and Pd particles and to obtain fast Fourier transform (FFT) images from the SEM images.

Transmission electron microscopy (TEM)

To further investigate the mesostructure of the films and Pt and Pd particles, TEM images were recorded on a FEI Tecnai G² 20 S-TWIN operated at 200 kV, as well as a Zeiss EM Omega 812 X at an acceleration voltage of 120 kV on fragments of film samples scraped off the substrates and deposited on carbon-coated copper grids.

Two-dimensional small-angle X-Ray scattering technique (2D-SAXS)

2D-SAXS patterns were collected at HASYLAB B1 beamline at DESY (Hamburg, Germany) with a PILATUS 1M detector at a sample to detector distance of 3589 mm and calibrated energy of 16 keV. The patterns were recorded in transmission mode with the incoming X-ray beam positioned at β = 90 and 20° relative to the substrate surface. The SAXS data were processed employing the computer program FIT2D. The modulus of the scattering vector q is defined in terms of the scattering angle θ and the wavelength λ of the radiation used: thus $q = 4\pi/\lambda \sin(\theta/2)$. d spacing values were then calculated using the formula $d = 2\pi/q$.

One-dimensional small-angle X-ray scattering (1D-SAXS) and wide-angle X-ray scattering techniques (WAXS)

To characterise the long-range mesostructure regularity of the film samples, 1D-SAXS measurements were performed in a $\theta/2\theta$ geometry (symmetric reflection) on a PANalytical X´pert Pro. (Cu-Kα radiation, λ = 0.154 nm, 40 kV, 40 mA) equipped with an X Celerator counter. Beam aperture was adjusted using a 1/4° divergence slit for the beam source and scattering slit for the detector to reduce background scattering and limit the beam divergence. The angle of incidence θ was varied from 0.25 to 2.5°. The reflected beam was then passed through another slit to the detector. d spacing values were calculated using the formula $d = \lambda/2 (\sin \theta)$. The WAXS patterns were also collected in the same way, but without the slit.

Fourier transform Infrared spectroscopy (FTIR)

FT-IR spectra were recorded with IFS 25 FT-IR spectrophotometer (Bruker Optics GmbH). The measurements were carried out using the KBr technique in the wavenumber range of 500–4000 cm^{-1}. The spectral resolution was 2 cm^{-1}. The film samples were scratched off from the substrates and mixed with KBr, then pressed into a pellet prior to the measurements.

Elemental analysis (EA)

The measurements were performed on a CHN-Analyzer Carlo Erba 1106 (Thermo Fisher Scientific). In this thesis, the carbon, hydrogen and nitrogen content (wt% C, H, N) was determined for the samples and the oxygen content was derived by subtracting with the wt% of C, H and N content. Oxygen content (wt% O) was determined by subtracting total wt% of C, H and N. Since the measurements were sensitive to amounts of the materials on substrates, corresponding powder samples were also prepared and used for the analysis. The corresponding powder samples were prepared from the same solutions as for the films by evaporating the solvent in Petri dishes at room temperature until dried and then themopolymerised at 100 °C for 24 h, followed by carbonisation at desired temperatures using the same carbonisation protocols for the film samples.

Thermogravimetric analysis (TGA)

TGA analysis was performed under a pure nitrogen atmosphere on a Netzsch STA 409 PC thermobalance (Netzsch) using a heating rate of 1 °C/min, identical to the heating programs for carbonisation of the film samples. The thermogravimetric analyzer was coupled with a Balzers QMG421 quadrupole mass spectrometer (ionization energy 70 eV). A scan from 10 to 100 amu was collected. Due to the limited amounts of the materials on substrates, the corresponding powder samples were also prepared and used for the TGA analysis. The powder composite sample was prepared from the same solution as for the films by evaporating the solvent in Petri dishes at room temperature until dried and then themopolymerised at 100 °C for 24 h.

Physisorption experiments

The area and thickness of a film must be known for physisorption measurements. Therefore, many identical films were prepared via dip-coating on thin Si-wafer substrates that had been polished on both sides, and subjected to the same synthesis procedures for making the film samples, as described above. The film area was measured and the thickness was obtained by cross-section SEM. The films were cut into ~2 mm × ~2 mm pieces. Then, 50 - 100 pieces of the film sample were placed in a physisorption vessel, and degassed at 120 °C for at least 12 h. The measurements were carried out at 77 K with a Quantachrome Autosorb 1 system, using N_2 as the adsorbate. The surface areas were determined by the Brunauer-Emmett–Teller (BET) method.[118] The BET values are reported in m^2/cm^3 by normalizing the absolute values obtained from the measurements with the substrate geometrical dimensions in volume. Barrett-Joyner-Halenda (BJH),[119] non-local density functional theory (NLDFT) as well as quenched-state density functional theory (QSDFT)[120, 121] models were used to obtain pore size distributions (PSDs) using the adsorption branches of the N_2 isotherms. Total pore volumes were estimated from the adsorbed amount at $p/p_0 = 0.95$.

Kr adsorption measurements were carried out at 77 K also with the Quantachrome Autosorb 1 system, using Kr as the adsorbate. The BET values using this gas probe were calculated and reported the same way as for N_2 sorption experiments by using the geometrical dimensions of Kr.

3.5 Catalytic testing in hydrogenation of 1,3-butadiene

The catalytic performance of selected templated porous catalyst coatings was investigated using a model reaction, the gas-phase hydrogenation of 1,3-butadiene. The catalytic performance was studied at temperatures between 35 and 80 °C. Catalyst films containing Pd particles were coated on both sides of grinded and pre-calcined steel plates (plate size 27 mm × 30 mm, and thicknesses of 0.5 and 0.25 mm for 5- and 10-plate reactors, respectively).
For each catalytic run, 5 (or 10) identical steel plates with the same thickness (0.5 mm for 5 plates, and 0.25 mm for 10 plates) were stacked parallel into the reactor housing. Figure 3.3 shows five stainless steel plates coated with Pd-containing mesoporous carbon catalyst films and the reactor with the catalyst plates. The direction of gas flow is indicated with red arrows.

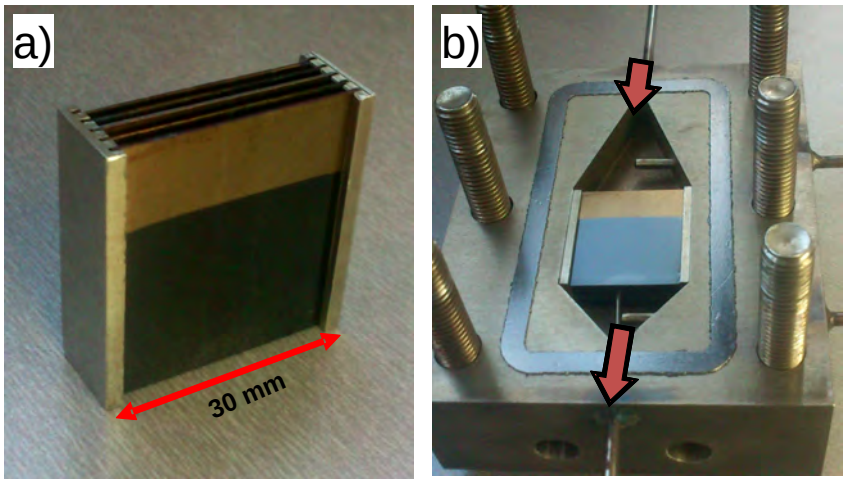

Figure 3.3. a) five stainless steel plates coated with Pd containing mesoporous carbon catalyst films. b) the (open) reactor with the catalyst plates. The direction of gas flow is indicated with red arrows.

A testing setup and procedure similar to the one described by Cukic et al. and Ortel et al. [113, 122] were used. A reaction mixture consisting of 5% butadiene (2.5 purity), 10% hydrogen (5.0 purity), and 85% nitrogen (5.0 purity) was passed through the reactor at a flow rate of 30 mL/min (STP) at 1.05 bar. The catalyst was then heated to 80 °C under reactive gas flow and equilibrated to reaction conditions for several hours. Afterwards, the temperature was gradually decreased stepwise from 80 °C, 72 °C, 64 °C, 56 °C, 48 °C, 40 °C and finally to 35 °C with a dwell time of 60 min for each temperature set point. Analysis of the gas products was continuously performed every 7 min by online gas chromatograph (Agilent GC 7890 equipped with FID, TCD and columns HP Plot Al_2O_3, Molsieve 5A, HP Plot Q and DB FFAP.)

Chapter 4
Micelle-templated mesoporous carbon coatings

4.1 Preparation of the dip-coating solutions based on RF polymer as a precursor and F127 as a template under acidic conditions

Tanaka et al.[49] employed acidic conditions to successfully prepare mesoporous carbon films with contracted *Im3m* structure(or *Fmmm* as they reported) after carbonisation at 800 °C. Nevertheless, the procedure faces some challenges, for example, they found that by using either resorcinol or phlorogucinol alone in an EtOH/H_2O solutions, heterogeneous films without well-ordered pore structure were obtained. This observation was attributed to the fast and strong interactions between F127 template and resorcinol or phlorogucinol precursors, leading to too large phologlucinol- or resorcinol-formaldehyde clusters which deposited on the substrates during the spin-coating. Besides the work by Tanaka, irrespective of the film morphology, Dai et al. synthesize mesoporous carbons using only resorcinol-formaldehyde as a carbon precursor under acidic conditions.[54] More interestingly, their method seems easy to handle and even much faster than the resol precursor approach. The strategy started from simply mixing F127 with resorcinol (1:1 wt ratio) in 3 M HCl and EtOH, followed by addition of formaldehyde. Only about 11 minutes after the addition of formaldehyde, the precipitation occurs due to the strong interactions through $I^+X^-S^+$ mechanism, which is a composite of RF cluster and F127. This precipitated composite was afterwards separated and undergo thermal treatment to obtained mesoporous carbon powders with a hexagonal structures (*p6mm*). More interestingly, if the precipitate is once redissolved in a THF/EtOH mixture, a clear solution is obtained; after the evaporation of the solvent and carbonisation, the better homogeneity of the composite is obtained. This 'precipitation-redispersion' method has been employed by Dai et al. for several publications; however, insights into the mesostructure, especially in the film morphology produced in their work have never been studied.[116, 117, 123, 124]

Inspired by the synthesis approaches by both Tanaka et al. and Dai et al. which also leads to small pore shrinkage compared to the resol precursor route, I have modified the reported synthesis by Dai et al. based on using RF as a carbon precursor and F127 as a template.[54] In the synthesis method developed in this thesis, the weight ratio of F127 to the resorcinol was adjusted to 1:3, instead of 1:1 of Dai's method, while keeping the other conditions the same. This change led to earlier precipitation of the RF/F127 composite (only about 4 min after addition of formaldehyde). The precipitation was continued for a few more minutes (10 min in total after the addition of formaldehyde) in order to further polymerise the RF clusters. Subsequent centrifugation at 3500 rpm for 5 min was carried out to separate the RF/F127 composite from the EtOH/H_2O mixture, followed by redispersion in THF. I found that THF

not only was the best solvent for this purpose but also suitable for the subsequent dip-coating method, which needs a volatile solvent for the EISA process. Unlike Dai's system where a hexagonal mesostructure (*p6mm*) is obtained, the change in the F127 to resorcinol weight ratio to 1:3 leads to the final cubic mesostructure, which is preferable when deposited on 2D-confined substrate surface (See Chapter 3 Experimental). As demonstrated in Chapter 2 and in my published review,[28] several parameters and synthesis conditions could effect the quality of the resulting mesoporous carbons. Longer polymerisation times than 14 min led to a composite which was not dissolvable in the THF or any other solvents, while shorter times of polymerisation before centrifugation results in a film without a well-ordered mesopore structure. The dip-coating solution is stable after keeping for 2 days (shown later in the effect of aging the dip-coating solution). This facile and fast synthesis procedure to obtain the dip-coating solution is named in this thesis 'precipitation-redispersion'. Shown later for the mesoporous carbon films with large pore size, this approach has been extended to other block-copolymers in order to control pore size and morphology.

4.2 Thermal stability of the resorcinol-formaldehyde (RF) matrix and removal of the templates

Since the materials prepared in this thesis are based on the 'precipitation-redispersion' method employing RF as a carbon precursor, unlike those obtained based on the resol precursor,[14, 48] investigation of the thermal stability of the as-made RF/block-copolymer composites has been performed in order to choose suitable temperatures for carbonisation with respect to each polymer template.

Since the small amount of the RF/block-copolymer composites in the form of films results in a large error in TGA analysis, their corresponding powders prepared in the same way as the films were employed instead. The pyrolysis behavior of the as-made composites was monitored by TGA at a heating rate of 1 °C/min under a nitrogen atmosphere, identical to the heat treatment protocol used for carbonisation of the films. For comparison, the decomposition behaviour of the polymer templates was also analysed under identical conditions. The TGA curves of those samples are presented in Figure 4.1.

The TGA curves of F127 and PIB-PEO 3000 show a sharp weight loss in the temperature range of ~300−400 °C, with almost no residue left at 400 °C, indicating that both F127 and PIB-PEO 3000 are nearly completely decomposed before 400 °C. In contrast, 10k-PB has a slightly higher thermal stability and completely decomposes at ~450 °C.

The RF resin polymer shows a gradual weight loss up to 700 °C. Over the whole temperature range, the RF polymer undergoes decomposition and condensation reactions[125] and finally a carbon residue of approximately 15 wt % is left at 900 °C. This indicates that the RF matrix possesses high thermal stability compared to the polymer templates and exists even after carbonisation at 900 °C. For all the composites, a large weight loss appears in the range between 300 and 400 °C, which is attributed to the decomposition of the templates. However,

for the RF/10k-PB composite, a second step decomposition in the range 400 to ~450 °C is observed.

These results clearly indicate that all the polymer templates can be completely removed by simply pyrolysis even under a N_2 atmosphere in the temperature range 300-450 °C. The weight loss of the composites between 400 and ~600 °C for RF/F127 and RF/PIB-PEO 3000 composites and between 450 and ~600 °C for RF/10k-PB composite is attributed to further release of hydrocarbons, oxygen, and other fragments from the RF precursor matrix.[54] According to the information obtained from the TGA analysis, the minimum pyrolysis temperatures to completely remove each template can be selected. Furthermore, pyrolysis can be performed even up to 1000 °C without a complete loss of the RF precursor matrix.

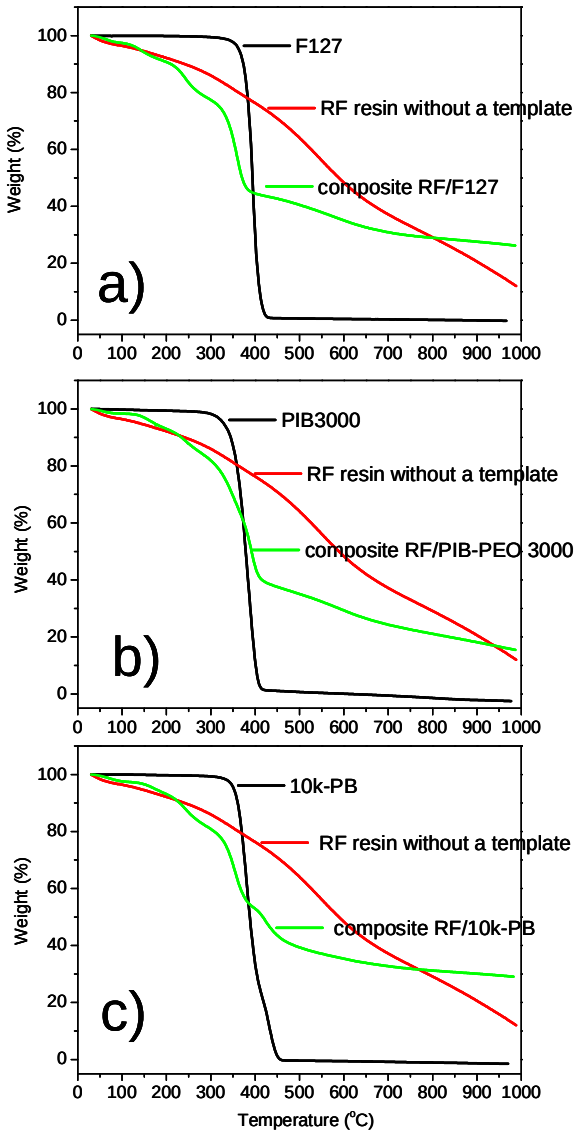

Figure 4.1. TGA curves of the templates polymers used in the thesis: a) F127, b) PIB-PEO 3000 and c) 10k-PB. RF resin made without polymer templates and the as-made composite RF/polymer templates. Heating rate was 1 °C/min under N_2 atmosphere, identical to that used for carbonisation of samples.

4.3 Films templated with F127

4.3.1 General features and morphology of the films

Figure 4.2 shows a photograph of films prepared on silicon wafers thermopolymerised at 100 °C and carbonised at 600 °C (~1.5 cm × ~3 cm) as well as one prepared on a precalcined-steel (~1 cm × ~2 cm). All films are continuous macroscopic crack-free and adhere tightly to the substrates. The films cover all area of dip-coating part of the substrates. The film thermopolymerised at 100 °C shows transparent features but after carbonisation at 600 °C, the film turns black and is no longer transparent.

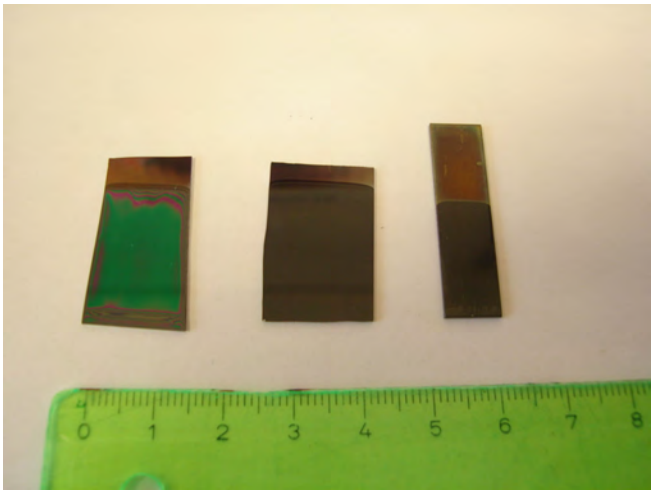

Figure 4.2. Photographs of films prepared on Si-wafers: (left) as prepared and cured at 100 °C, (middle) after carbonisation at 600 °C and (right) film prepared on a precalcined steel plate with a surface roughness (R_a) of ~0.55 µm and carbonised at 600 °C. All films were prepared at the withdrawal speed of 60 mm/min, 30%RH at 25 °C.

SEM

Figure 4.3 presents top-view and cross-section scanning electron microscope (SEM) images obtained from the film coated on a silicon wafer at a withdrawal speed of 60 mm/min and and carbonised at 600 °C. The top-view image at low magnification (Figure 4.3a) confirms the macroscopic crack-free morphology of the film throughout the area observed. Furthermore, the SEM images in Figure 4.3c and e present the well-ordered mesostructure with high quality and regularity in the areas observed.

The pores are arranged in an ordered fashion with a nearly hexagonal packing. The uniform pore size is ~8 nm in diameter, as determined by ImageJ program. More importantly, all pores on the top surface are open in a spherical shape. By careful determination with the FFT image on the corresponding SEM image (Figure 4.3e), it is found that, in fact, the order is not a perfect hexagonal packing, but a centred rectangular shape, i.e. this is only an apparent distorted hexagon. This observation can be explained by the preferred orientation of the body centered cubic (*Im3m*) mesostructure in (110) plane relative to the substrate surface.

The morphology of the cross-section view of the film was further investigated by cross-sectional SEM images (Figure 4.3b,d,f).

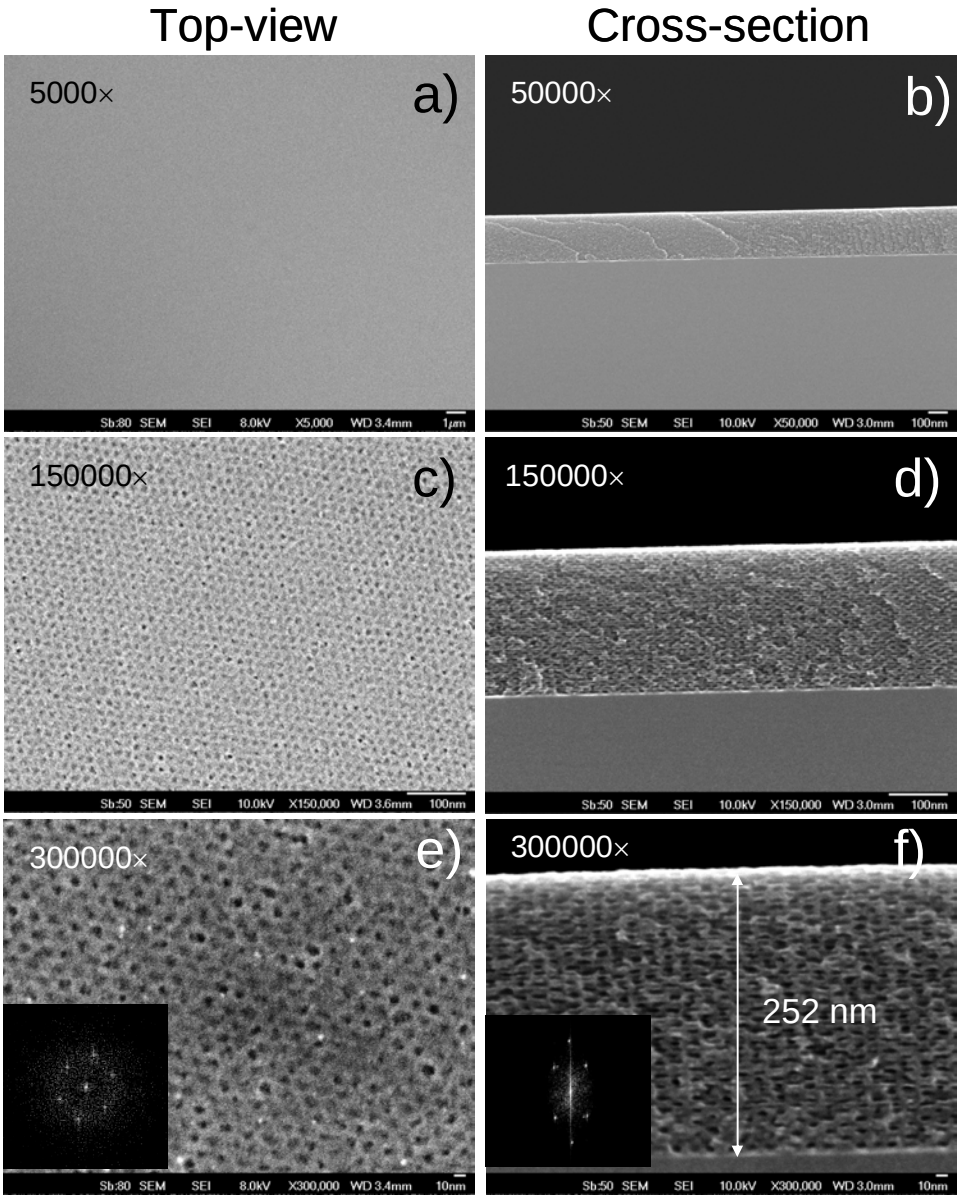

Figure 4.3. Top-view and cross-section SEM images of the mesoporous carbon film prepared on a silicon wafer at a dipping speed of 60 mm/min, carbonised at 600 °C. a) Top-view image at magnifications of 5000×, proving a crack-free film. c) and e) Top-view images at magnifications of 150000× and 300000×, respectively, showing the pore order on the top surface. Inset in e) shows a FFT image, proving the nearly ordered hexagonal closed packing on the top surface. b) Cross-section image at a magnification of 50000×. d) and f) Cross-section images at magnifications of 150000× and 300000×, respectively, showing the elliptical pore shape. Inset in f) shows a FFT image, proving the contraction in Z direction.

Cross-sectional SEM images prove homogeneity of the film with porosity throughout the cross-section area and show a film thickness of 252 nm. A periodic pore structure is observed. However, in contrast to the pores seen from the top view images, the pores seen from the cross-sectional view possess an elliptical shape. This behaviour is not surprising, as it is well known that mesostructured materials confined on substrates normally undergo anisotropic

contraction upon drying and high thermal treatment.[18, 19, 26, 126, 127] A diameter of the pores normal to the substrate (Z direction) is ~3-5 nm, whereas that parallel to the substrate (XY directions) is ~8 nm, which is similar to the pore diameter seen from the top view. This finding confirms again that the contraction indeed happens only in the Z direction, and not in X and Y directions. Moreover, I notice no collapse of the templated mesopores when looking throughout the cross-section areas. By considering the distance between two adjacent layers from the SEM image as well as from the FFT image, we obtain a distance of 4-5 nm. By looking closer at the cross-section images in Figure 4.3d, two different domains are observed. However, there is no evidence of existence of hexagonal elongated pores. Overall, it can be concluded from the SEM results that the film possess a contracted 3D cubic mesostructure without the existence of a cylindrical pore morphology.

TEM

Transmission electron microscopy (TEM) images of the carbon film scratched off the Si-wafer are shown in Figure 4.4. The TEM image viewed along a (110) direction reveals large domains of a cubic arrangement of mesopores with the size of ~8 nm in diameter (Figure 4.4a) even after carbonisation at 600 °C, further confirming the results from SEM. In addition, from this image, mesoporosity is observed throughout the specimen. Figure 4.4b shows the TEM image of the same material, but investigated in a different area. Although, the image can be mistaken for the presence of cylindrical mesopores, closer examination proves the existence of the apparent lines composed of individual pores. The appearance of this hexagonal-like structure originates from the investigation along either [10-1] or [010] zone axis of the contracted cubic *Im3m* structure.[25] Due to the low contrast images, it was difficult to find the domains showing the elliptical pores.

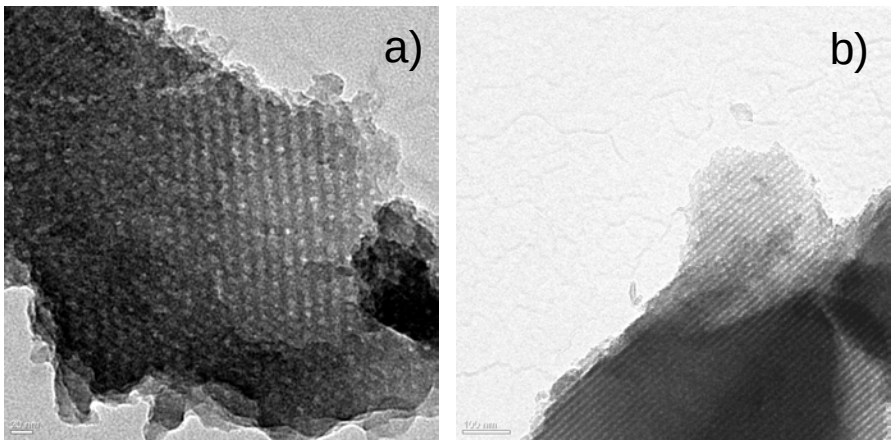

Figure 4.4. TEM images of the carbon film carbonised at 600 °C. The sample specimens were prepared by scracted off the film from the substrate and dropped onto a TEM grid. a) Image viewed along (110) direction, showing a regular pore arrangement. b) Image showing the pore arrangement along [010] zone axis.

However, SEM and TEM are only techniques used to investigate the morphology locally. Therefore, we cannot exclude the possibility of existence of other phase systems. For this

reason, I further conducted two-dimensional small-angle X-ray scattering (2D-SAXS) measurements.

2D-SAXS:β = 90°

The 2D-SAXS pattern measure in transmission mode at the incident angle β = 90° (perpendicular to the substrate surface) features isotropic diffraction rings without an indication of in-plane contraction (Figure 4.5a). The appearance of the circular diffraction rings confirms a random orientation of mesostructured domains within the plane parallel to the substrate surface. The 1D-integral curve from the 2D-SAXS pattern (Figure 4.5b) presents several well-defined reflections, suggesting a highly ordered morphology in plane. The *d*-spacings from those reflections are found to be 13.6, 10.1, 7.9, and 6.8 nm. By comparing the ratio of the *d*-spacings, it is found that the *d*-spacings can be attributed to 1-10, 002, 1-12, and 2-20 reflections, resembling those of the cubic *Im3m* structure.[20, 128]

2D-SAXS:β = 20°

Figure 4.5c shows the 2D-SAXS pattern for the film carbonised at 600 °C for the beam incident angle β = 20°. Distinct reflection spots and a very weak ellipsoidal circle are generated. The very weak ellipsoidal circle corresponds to domains with the same cubic structure, but has a random poly-orientation with respect to the substrate plane. One possible explanation for the existence of these poly-oriented domains is the rapid organization of the system, where THF is used as a solvent. In other words, the fast evaporation of THF leads to a very short time for the organised domains to homogeneously align themselves with the air and substrate surface. This similar behavior has been previously observed for mesoporous TiO_2 films with the cubic *Im3m* structure prepared by dip-coating.[126, 127]

The intensity of the reflection spots on the ellipsoidal ring is more pronounced than that of the weak elliptical circle, indicating that the oriented phase is dominant. Nevertheless, it is difficult to determine a portion of these poly-oriented domains with respect to the oriented one. The distinct reflection spots can be indexed in terms of a body centered cubic (BCC) mesostructure (*Im3m*) with (110) orientation. In fact, to be more certain, the distorted BCC mesostructure cannot be distinguished as a perfect *Im3m* structure because the contraction causes the structure to convert into other morphology, Therefore, for the sake of better understanding and clarity for this mesostructure obtained here, it is more recommendable to classify the material as a 'contracted BCC *Im3m* structure' with (110) orientation. In general, the (110) reflection should clearly be observed (Figure 4.5c). However, in our case, this (110) reflection disappears due to the high incident angle (β = 20°) used.[128] In fact, the disappearance of the (110) reflection for the *Im3m* mesostructure at high incident angles $\beta >$ 6° is normal and was previously observed by our group.[129]

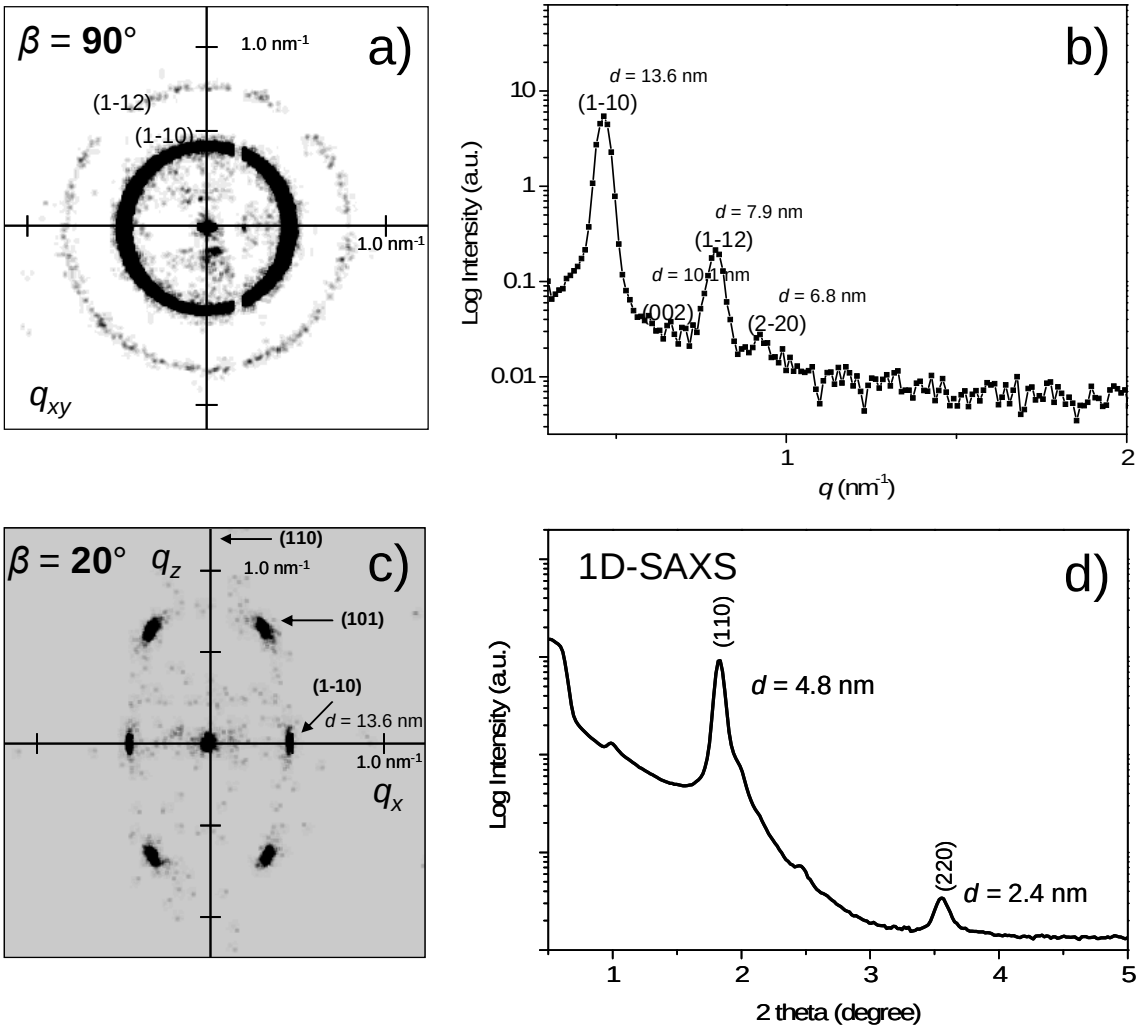

Figure 4.5. SAXS analysis in transmission configuration at two beam incident angles (β = 90° and 20°); (a, b, and c) and 1D-SAXS (d) of the carbon film carbonised at 600 °C. a) 2D-SAXS image at β = 90°, featuring isotropic diffraction rings. b) Corresponding 1D integral curve of the pattern in a). The lattice parameter (*d)* is calculated using the expression $d = 2\pi/q$. c) 2D-SAXS pattern at β = 20°; the reflection spots are indexed according to the *Im3m* structure with (110) orientation. d) 1D-SAXS pattern recorded in θ-2θ geometry (symmetric reflection or Bragg-Bretano geometry); the reflections are indexed according to the *Im3m* structure with (110) orientation.

1D-SAXS

The 2D-SAXS measurements were complemented by 1D-SAXS measurements performed in θ-2θ geometry (symmetric reflection or Bragg-Bretano geometry). The 1D-SAXS results provide the information on the mesostructure only in the Z direction (off-plane structure) for such contracted mesostructures. However, for the well-known mesostructure systems such as *Im3m*, the 1D-SAXS measurements facilitate calculation of the *d*-spacing in the Z direction, and this value can be used to compare shrinkage behaviour of mesostructured films. Furthermore, 1D-SAXS patterns of various thin film samples can easily be obtained with a facile experimental set-up. Figure 4.5d presents 1D-SAXS pattern of the carbon film carbonised at 600 °C. Typical features of the two equidistant reflections at 2θ of 1.8 and 3.6 are noticeable, which can be indexed to (110) and (220) reflections. The appearance of these

reflections complements the 2D-SAXS interpretation, especially regarding the disappearance of the (110) reflection from the 2D-SAXS pattern (Figure 4.5c, $\beta = 20°$). The *d*-spacing value calculated according to the (110) reflection is 4.8 nm, which is consistent with the distance between layers observed by cross-section SEM measurements (Figure 4.3f).

N_2 sorption

To study the mesoporosity and especially the accessibility to the pores, N_2 sorption experiments were employed for the film carbonised at 600 °C and dip coated at a withdrawal speed of 300 mm/min. In essence of this technique, usually to investigate porosity of mesostructured films, a reasonable sufficient amount of materials is desirable to prevent the fluctuation of the measurements, thereby resulting in reasonable data evaluation. Therefore, several identical films were coated on double-side polished Si-wafers at a withdrawal speed of 300 mm/min. In accordance with Landau-Levich's law, thicker films were obtained in order to have sufficient amount of materials for reliable N_2 sorption studies. Note that by increasing the withdrawal speed of the dip-coating up to 300 mm/min, the thickness can be increased, while the mesostructure stays constant, as will be shown later, providing validity to the use of thicker films for the N_2 sorption analysis.

Figure 4.6a shows a nitrogen sorption isotherm for the film carbonised at 600 °C. The isotherm features a well-defined typical type IV curve with a distinct hyteresis loop and condensation step, indicative of uniform cage-like mesopore architecture. However, the desorption branch does not close at low relative pressures. This behaviour, nevertheless, is a common feature observed for porous polymers or carbon materials which are not fully carbonised. Unlike in porous metal oxides, this is because the N_2 molecules can be tightly trapped in the pore walls of the carbon materials and swell the wall matrix during condensation, resulting in a delay in desorption kinetics when the emptying of the pores occurs.[83, 121] The BET surface area is 523 m^2/cm^3, and the pore volume is calculated to be 0.45 cm^3/cm^3 using quenched-state density functional theory (QSDFT)[120] model applied on the adsorption branch of the isotherm. Note that the units per film volume are used in this case since the weight and density of the material were difficult to determine. However, the high surface area and pore volume further confirm that the film is highly porous and the pores are accessible to nitrogen molecules. The fact that the desorption branch does not close at low relative pressure reasonably excludes the use of this branch for the determination of pore size distribution.

The calculation using the adsorption branch and Barrett-Joyner-Halenda (BJH) model indicates the existence of a narrow mesopore size distribution centred at 4.7 nm (Figure 4.6b). This value is slightly higher than that previously reported (4.3 nm) using also the BJH for adsorption branch but from the resol-precursor system and identical treatment procedure and temperature.[20]

I chose to determine the mesopore size using the BJH model applied to the adsorption branch for the sake of comparison; however, this model could lead to wrong interpretation of the pore size distribution because the BJH model is based on the Kelvin's equation and only applies to cylindrical pore morphology.[119, 120]

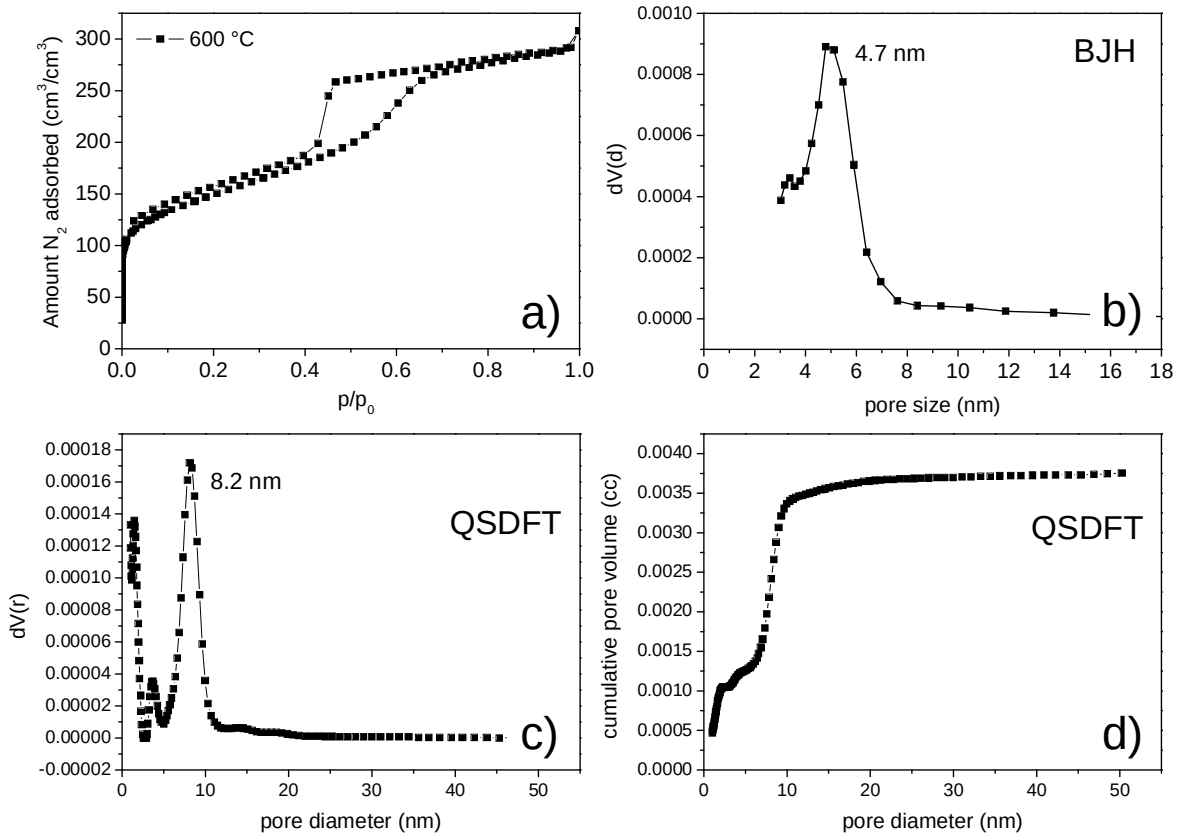

Figure 4.6. Nitrogen sorption analysis of the carbon film, templated using F127, dip-coated at 300 mm/min, carbonised at 600 °C. a) N_2 sorption isotherm. b) BJH pore size distribution calculated from the adsorption branch. c) Pore size distribution calculated from QSDFT model from the adsorption branch based on spherical pore shape. d) Cumulative pore volume distribution, also calculated using QSDFT model.

For the above reason, I also applied the QSDFT model to the adsorption branch to obtain the pore size distribution in both the micropore and mesopore regions. Figure 4.6c,d shows both a cumulative pore size distribution and differentiated pore size distribution for both micro- and mesopore regions. The mesopore volume is about 74% of the total pore volume, which was calculated based on the QSDFT model. The micropore volume determined using the same model is found to be 0.117 cm^3/cm^3, which possesses about 26 % of the total pore volume. The presence of the microporosity partly contributes to the connectivity of and accessibility to the templated ordered mesopores. The microporosity can result either from the intrinsic porosity due to the release of small molecules from the pore walls upon carbonisation or from the direct templating with the PEO moiety of the F127 polymer. The mesoporoe size from the QSDFT model is found to be centred at 8.2 nm, which is about two times larger than that calculated using the BJH model.

Carbon wall composition, as evidenced by elemental analysis, WAXS and, FT-IR

Besides the mesostructure, the microstructure of the film has also been studied to investigate the nature of the pore wall composition of the carbon. Due to the presence of strong reflections of the Si wafers used as substrates in wide-angle X-ray scattering (WAXS) analysis, I instead prepared corresponding carbon materials in the form of powder by using the identical dip-coating solutions for the films. The dip-coating solution was poured into Petri dishes for drying. The dried powder material was then subject to thermal treatment and carbonisation in the same way as for the film materials. It is assumed that there should be no difference in the carbon microstructure in the form of both powder and film based on resin precursors. The WAXS pattern of a powder carbon sample corresponding to the film carbonised at 600 °C is presented in Figure 4.7.

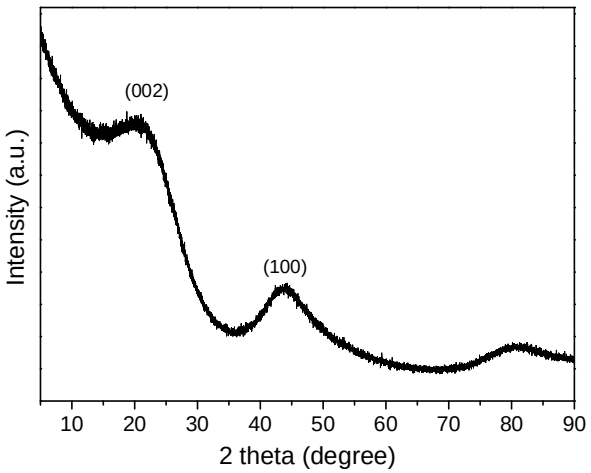

Figure 4.7. WAXS pattern of the carbon film carbonised at 600 °C. The material used for the WAXS measurement was prepared in a powder form using the same coating solution for the film, followed by thermopolymerisation and carbonisation the same way as for the film.

The pattern shows a very weak diffraction shoulder at $2\theta \sim 24°$ and a broad reflection at ~44°, which correspond to (002) and (100) reflections of a non-graphitic type carbon material, respectively.[15, 59] The (002) and (100) reflections are related to interlayer (off-plane) and intralayer (in-plane) scattering of the graphene stacks, respectively. This observation can be interpreted as the aromatization and condensation of the RF precursor upon carbonisation at this temperature (600 °C). The characteristic WAXS pattern proves that the wall matrix is already composed of carbon atoms which arrange in a rather disordered fashion. The WAXS results correspond to those from elemental analysis for which ~ 89 wt% of carbon content is detected (C: H: O = 88.8: 2.4: 8.8 wt%). The rather broad reflections in the WAXS pattern indicate a typical feature of non-graphitic carbon microstructure (a weakly ordered, bended form of graphitic carbon).[59]

Fourier transformed infrared (FT-IR) spectrum of the film carbonised at 600 °C (referred to Figure 4.12, shown later) was measured to track changes of oxygen functionalities. It is clear that characteristic vibration bands for oxygen functionalities almost disappear after

carbonisation at 600 °C, indicating that high carbon content and low oxygen content are detected in this material. This result is in good agreement with the results obtained from WAXS and elemental analysis.

4.3.2 Influence of carbonisation temperature on mesostructure, porosity, and carbon wall composition

To elucidate the change in the mesostructure as a function of carbonisation temperature, different carbonisation temperatures have been applied.

SEM

Figure 4.8 presents top-view and cross-section SEM images of the carbon films carbonised at 800 °C, and at a low magnification (Figure 4.8a, 50000×), there is no evidence of macroscopic cracks. It is evident that, although high temperature treatment is used, the ordered pore structure is preserved and shows similar features to those of the film carbonised at 600 °C (Figure 4.3).

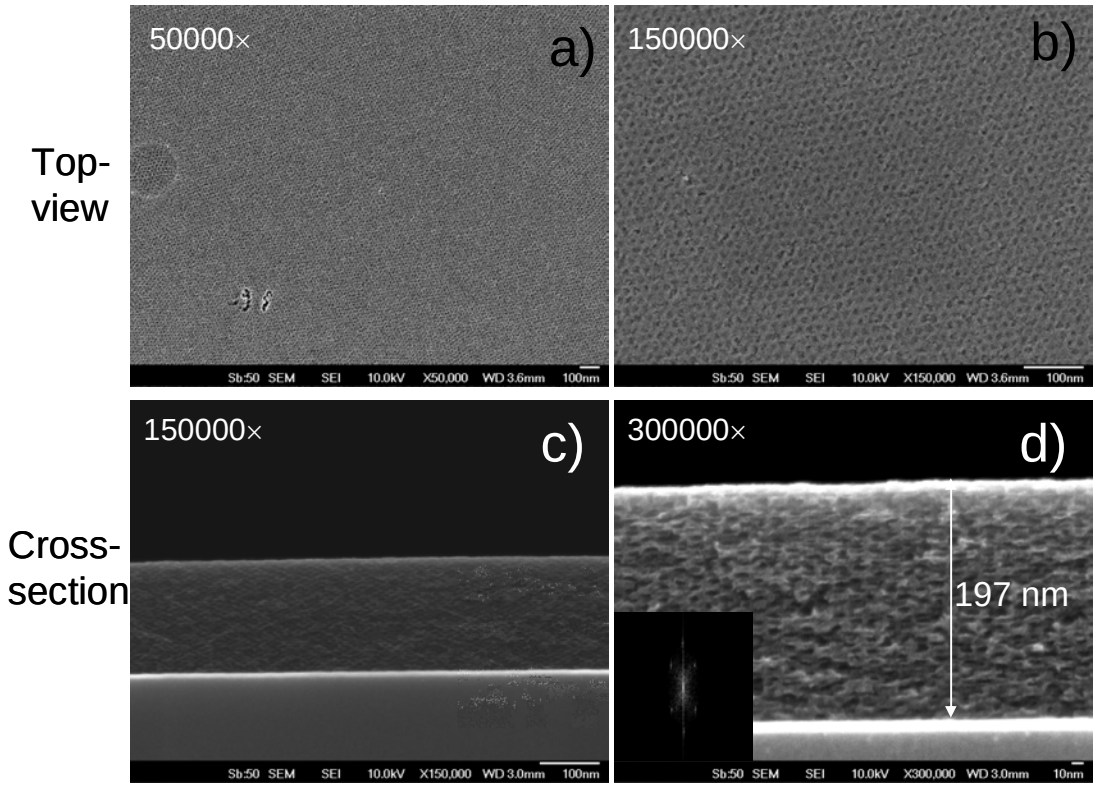

Figure 4.8. SEM images of the mesoporous carbon film prepared on a silicon wafer at a dipping speed of 60 mm/min, carbonised at 800 °C. a) and b) Top-view images at magnifications of 50000× and 150000×, respectively, proving a crack-free film and proving the reservation of the pore order on the top surface. c) and d) Cross-section images at magnifications of 150000× and 300000×, respectively. Inset in d) shows the FFT image of the images d).

From the top-view SEM images (Figure 4.8a,b), the pore arrangement is uniform and the pore size is found to be ~8 nm, similar to that carbonised at 600 °C. However, the walls possess some broken smaller pores. Cross-section SEM images of this sample (Figure 4.8c,d) show a film thickness of 197 nm, a few nm smaller than that carbonised at 600 °C (252 nm). The pores are elliptical in shape, similar to ones carbonised at 600 °C, but with a smaller distance of ~4 nm between two adjacent layers. The decrease in the film thickness confirms that the shrinkage in the Z direction further occurs as the carbonisation temperature is increased from 600 to 800 °C.

The distance between two adjacent layers (~4 nm) corresponds to the *d*-spacing obtained using 2D- and 1D-SAXS, as will be discussed later. It is evident that no collapse of the pores is observed throughout the cross-section area, as can be seen from the Figure 4.8c,d. Overall, from the SEM investigation, the fact that the sample can be carbonised at 800 °C without considerable loss of periodic mesoporosity indicates that the carbons obtained through the synthetic procedure is of high thermal stability.

2D-SAXS:β = 20°

To further investigate the ordered morphology of the pore system as a function of carbonisation temperature, 2D-SAXS experiments were carried out. Figure 4.9a (first column) shows the 2D-SAXS patterns of the films carbonised at three different temperatures (400, 600 and 800 °C) measured with an incident angle β = 20°. By increasing the carbonisation temperature, the shape of the 2D-SAXS patterns becomes more elliptical, indicating shrinkage of the mesotructure in the Z direction. In contrast, the lateral dimension parallel to the substrate remains constant, as evidenced by the unchanged position of the in-plane (1-10) reflection spots (in X direction). Furthermore, the distinct off-specular (101) reflection spots still exist for all different carbonisation temperatures, but shift towards the higher q_z values, when increasing the carbonisation temperature (the dash green lines in Figure 4.9a). The existence of the (101) reflection spots, along with the (1-10) reflections confirms that the contracted BCC *Im3m* mesostructure with the preferred orientation is preserved. The *d*-spacing in the Z direction (110) decreases from 7.0 nm to 5.0 nm and to 4.1 nm, determined from the 2D-SAXS patterns (β = 20°), upon increasing the carbonisation temperature from 400 to 600 and to 800 °C, respectively. The values correspond to the contractions of 48 %, 63 % and 69 %, based on the assumption that the in-plane (1-10) signals correspond to the original perfect BCC structure (without contraction) and the contraction is calculated using

$$\%contraction = \left(\frac{d_{(1-10)} - d_{(110)}}{d_{(1-10)}} \right) \times 100$$

2D-SAXS:β = 90°

To determine the change in in-plane structure, 2D-SAXS patterns and their corresponding integral curves were collected in transmission mode at β = 90° (Figure 4.9b,c ; middle and last columns). All the integral curves (Figure 4.9c) show similar patterns with several well-resolved peaks attributed to 1-10, 002, 1-12, and 2-20 reflections with *d*-spacing values of ~

13.6, 10.1, 7.9, and 6.8 nm, respectively. These results confirm the presence of randomly oriented polycrystalline domains parallel to the substrate for all the materials. These similarities of the patterns prove that there is almost no change in the in-plane mesostructure upon carbonisation. The lattice spacings (*d*-spacings) for the first reflection calculated from the 1D-integral curves of all the samples are found to be 13.6 nm (Figure 4.9c), which are consistent with the values from the (1-10) reflections for the 2D-SAXS patterns of all materials measured at $\beta = 20°$.

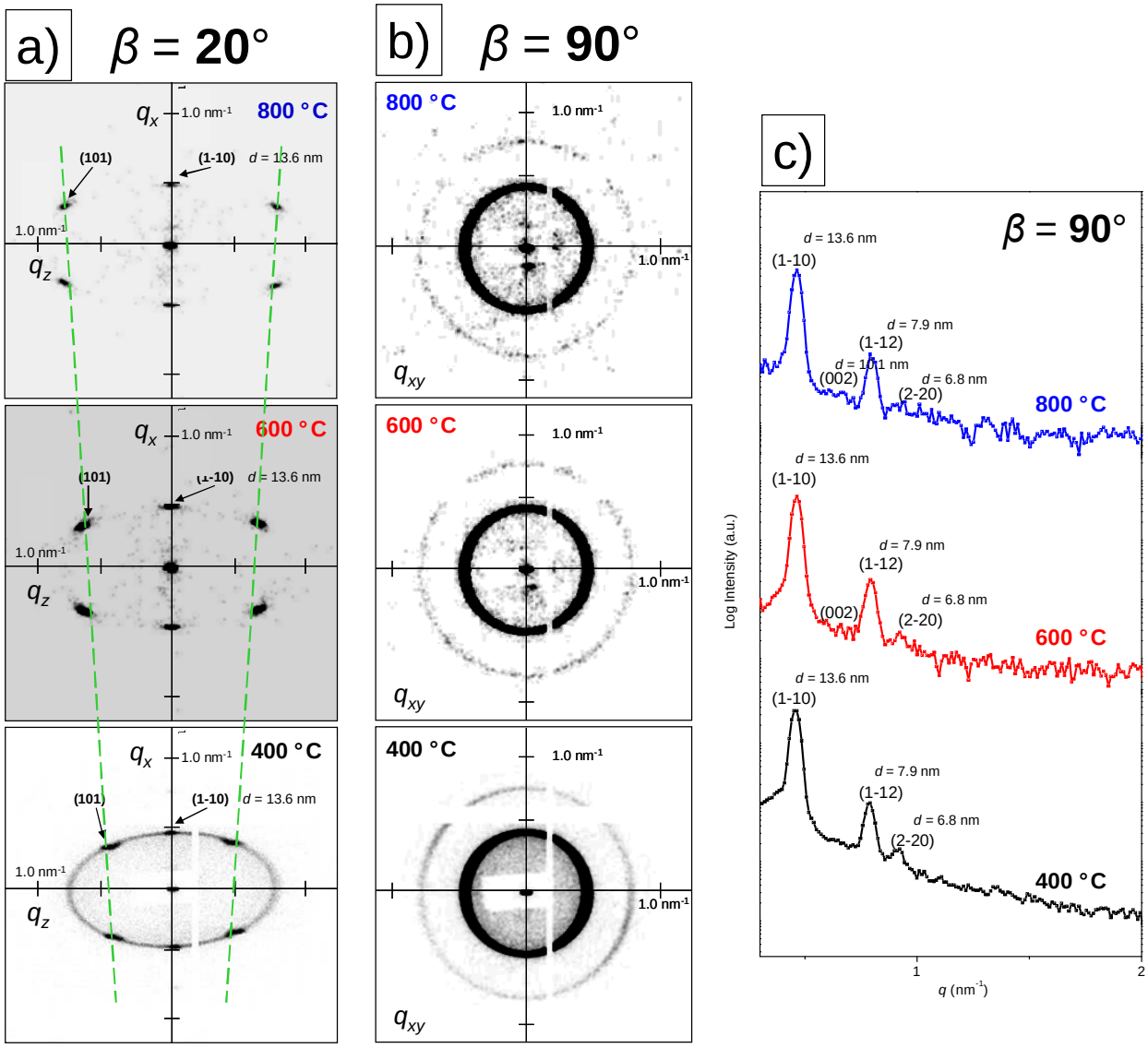

Figure 4.9. 2D-SAXS analysis in transmission configuration at two beam incident angles $\beta = 20°$ (a; first column) and $\beta = 90°$ (b, c; middle and last columns) of the carbon films dip-coated at a speed of 60 mm/min carbonised at 400, 600 and 800 °C. a) 2D-SAXS patterns recorded at an incident angle $\beta = 20°$. The dash green lines in a) indicate the change in position of the (101) reflection spots, when increasing the carbonisation temperature. b) 2D-SAXS images recorded at $\beta = 90°$, featuring isotropic diffraction rings. c) Corresponding 1D-integral curves of the patterns in b). The lattice parameter (*d*) is calculated using the expression $d = 2\pi/q$.

1D-SAXS

The *d*-spacing values calculated from the 2D-SAXS are in agreement with those obtained by 1D-SAXS (Figure 4.10). Figure 4.10 presents the change in the 1D-SAXS profiles as the F127/RF resin composite films are carbonised at different temperatures.

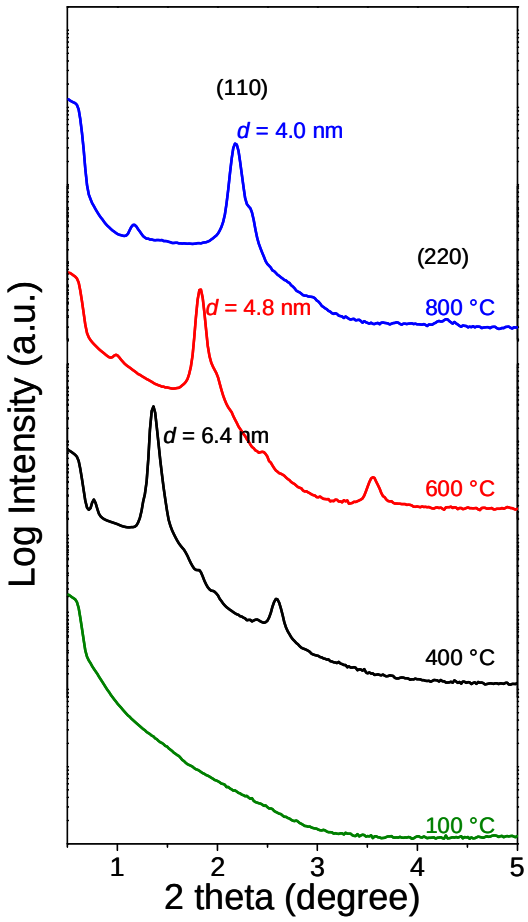

Figure 4.10. 1D-SAXS patterns performed in θ-2θ geometry (symmetric reflection or Bragg-Bretano geometry) of the carbon films dip-coated at a speed of 60 mm/min carbonised at 400, 600 and 800 °C as well as that of the film after thermopolymerisation at 100 °C .

The resin film thermopolymerised at 100 °C exhibit no reflections in the 1D-SAXS pattern. The 1D-SAXS data for this film are consistent with those obtained by 2D-SAXS measurements where no reflection spots and rings can be seen (data not shown). It is interesting to note that this observation is in contrast to that in previous reports based on using the resol as a carbon precursor.[20, 55] This behaviour can result either from absence of an ordered mesostructure of the F127/RF composite or more likely from the lack of electron contrast between PEO chains of the F127 micelles and the RF resin framework. Recently, Schuster et al. reported that heat treatment over 100 °C only results in a mesostructure formation of the resol/F127 composite films, as determined by SAXS analysis.[26] However, in contrast to their observation, Godflab et al. employed electron spin resonance spectroscopy (ESR) to investigate the mesostructure formation of the resol/F127 composite,[55] and found that in fact a cubic structure of the composite already forms during the thermopolymerisation

at 100 °C. Furthermore, in their work, reflections indicating the cubic mesostructure could clearly be observed for the polymerised composite in a 1D-SAXS pattern. Based on the system here employing the RF polymer, it would be worth studying the mesostructure formation mechanism in detail. According to the 1D-SAXS pattern shown here, we can conclude that the RF polymer composite has different crosslinking and templating behaviours compared to the resol precursor.

Upon increasing the carbonisation temperature, two reflections are clearly observed for all the materials carbonised at 400, 600 an 800 °C, which can be indexed to (110) and (220) reflections according to the BCC *Im3m* mesostructure. The fact that F127 template is completely removed before 400 °C in the N_2 atmosphere, as proved by the TGA results in a significant (110) reflection at 2θ of 1.5° and (220) reflection at $2\theta \sim 2.7°$ in the 1D-SAXS pattern. This appearance of the pronounced reflections is due to the high degree of mesostructure order and enhanced electron contrast between the RF resin matrix and the templated pores. Changes in mesostructure upon an increase in carbonisation temperature can be explained by the shift of the primary (110) reflection towards higher 2θ. The shift of this (110) reflection clearly indicates a contraction in the Z direction and a decrease in *d*-spacing during the carbonisation process. The *d*-spacing values determined from the 1D-SAXS patterns are found to be 6.4, 4.8 and 4.0 nm for the films carbonised at 400, 600 and 800 °C, respectively. The *d*-spacing values obtained using 1D-SAXS measurements are in agreement with those from the 2D-SAXS data. Furthermore, the decrease of the *d*-spacing can also be reflected by a decrease in the film thickness. For instance, a decrease in the d-spacing of 16.6% from the films carbonised at 800 °C and 600 °C results from the reduction in the film thickness of 21.8% (252 nm for the film carbonised at 600 °C, and 197 nm for the film carbonised at 800 °C).

N_2 sorption

Figure 4.11a illustrates N_2 sorption isotherms for the films dip-coated at a speed of 300 mm/min. All the isotherms feature well-defined typical type IV curves with a distinct hyteresis loop and condensation step, indicative of a uniform cage-like mesopore architecture. However, the desorption branches for all materials do not close at low relative pressures. This behaviour, nevertheless, is a normal feature observed for some types of porous polymers or carbon materials based on resin-type precursors even after carbonisation at 800 °C, as explained earlier above and in the literature.[121]

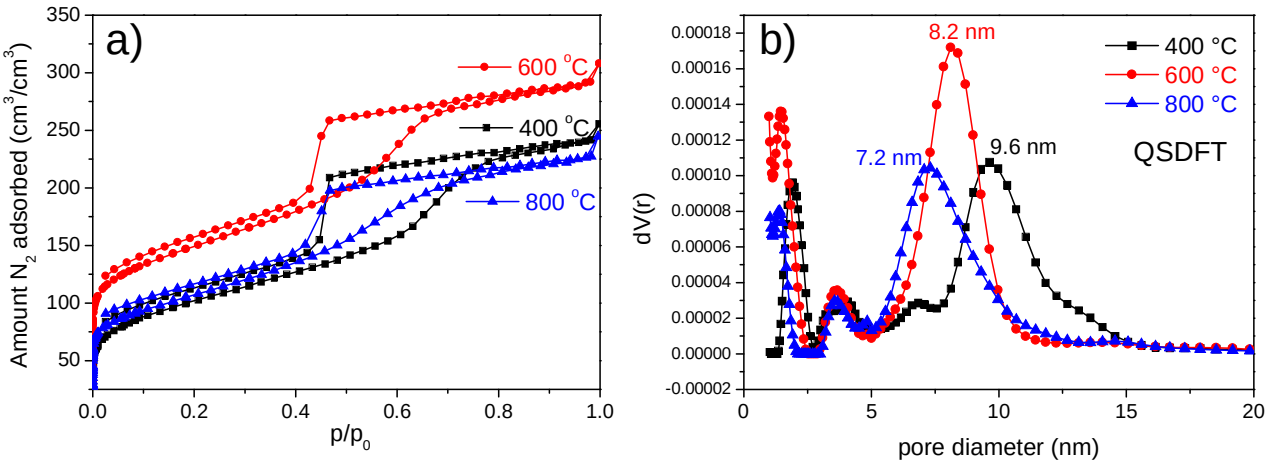

Figure 4.11. N_2 sorption analysis of the carbon films, templated using F127, dip-coated at 300 mm/min, carbonised at 400, 600 and 800 °C. a) N_2 sorption isotherms. b) Pore size distributions (PSDs) calculated using QSDFT model applied on the adsorption branches.

The BET surface areas and pore volumes of the materials are shown in Table 4.1. The high surface areas and pore volumes further confirm that all the films carbonised at different temperatures are highly porous and the pores are accessible to nitrogen molecules. The pronounced mesoporosity of the film carbonised at 400 °C provides evidence that the template completely decomposes even at a temperature as low as 400 °C under an inert atmosphere, resulting in templated mesopores.

Table 4.1. Porous textural properties of mesoporous carbon films templated using F127, dip-coated at 300 mm/min and carbonised at different temperatures

Sample	Carbonisation temperature (°C)	BET surface area (m^2/cm^3)	Total pore volume (cm^3/cm^3)	Microporosity (volume%)[a]	Mesoporosity (volume%)[a]	Mesopore size (nm)[b]	C : H : O[c] (wt%)
C-400	400	353	0.37	14	86	9.6	72.5 : 4.8 : 22.7
C-600	600	523	0.45	26	74	8.2	88.8 : 2.4 : 8.8
C-800	800	369	0.35	20	80	7.2	89.4 : 2.2 : 8.4

[a] the relative volume is determined from cumulative pore size distribution using QSDFT model applied to adsorption branch for spherical pores.
[b] obtained from pore size distribution using QSDFT model applied to adsorption branch for spherical pores.
[c] oxygen content (wt% O) was determined by subtracting total wt% of C, H and N.

By increasing the carbonisation temperature from 400 °C to 600 °C, the BET surface area increases. This can be attributed to the generation of microporosity upon the increase in the temperature to 600 °C, as evidenced by the microposity analysis using QSDFT model applied

to the adsorption branches (see Table 4.1). In contrast, further increasing the temperature to 800 °C causes a decrease in both the surface area and total pore volume. This is because pore dimension in Z direction decreases due to larger contraction of the pores in the Z direction, therefore leading to less porosity. Furthermore, there is also a slight decrease in microporosity. The decrease in the pore dimension reduces both the surface area and total pore volume.

Mesopore sizes were also calculated using QSDFT model on the adsorption branches (model for spherical pores). The results reveal narrow pore size distributions (PSDs) for all the materials (Figure 4.11b). The mesopore sizes are centered at 9.6, 8.2 and 7.2 nm for the films carbonised at 400, 600 and 800 °C, respectively, indicating that the apparent mesopore size decreases with increasing the carbonisation temperature. However, it is important to note that this analysis only provides qualitative information about mesopore size because in fact the mesopores are elliptical in shape as proved by SEM and SAXS discussed earlier, whereas the model kernel provided by QSDFT here represents the pores in the spherical shape. The change in the mesopore size appears to be related to the change in contraction and *d*-spacing, i.e. the increase in mesopore size is consistent with lower contraction and higher *d*-spacing.

Carbon wall composition, as evidenced by elemental analysis, WAXS and, FT-IR

To elucidate also the composition and structure of the carbon frameworks of the films as a function of the heat treatment temperature, Fourier transform infrared (FT-IR) spectroscopy, elemental analysis and WAXS were employed.
Figure 4.12 presents FT-IR spectra of the films carbonised at different temperatures of 400, 600 and 800 °C, respectively as well as from the RF/F127 composite after themopolymerisation at 100 °C.
The FT-IR spectrum of the composite material thermopolymerised at 100 °C shows a strong but broad band at ~3400 cm^{-1} corresponding to −OH stretching, suggesting the existence of a large amount of phenolic −OH group and un-cross-linked resorcinol molecules. The broad characteristic of this absorption band arises from intermolecular H-bonding. The band at about 1475 cm^{-1} is caused by C−H bending of an aliphatic bridge structure. Several bands at 1085 cm^{-1} (intense band) and 2800−3000 cm^{-1} can be assigned to the C−O and C−H stretching of the template F127. After carbonisation at 400 °C under an inert atmosphere, the bands at 1085 and 2800−3000 cm^{-1} completely disappear, further confirming evidence of template decomposition and removal.

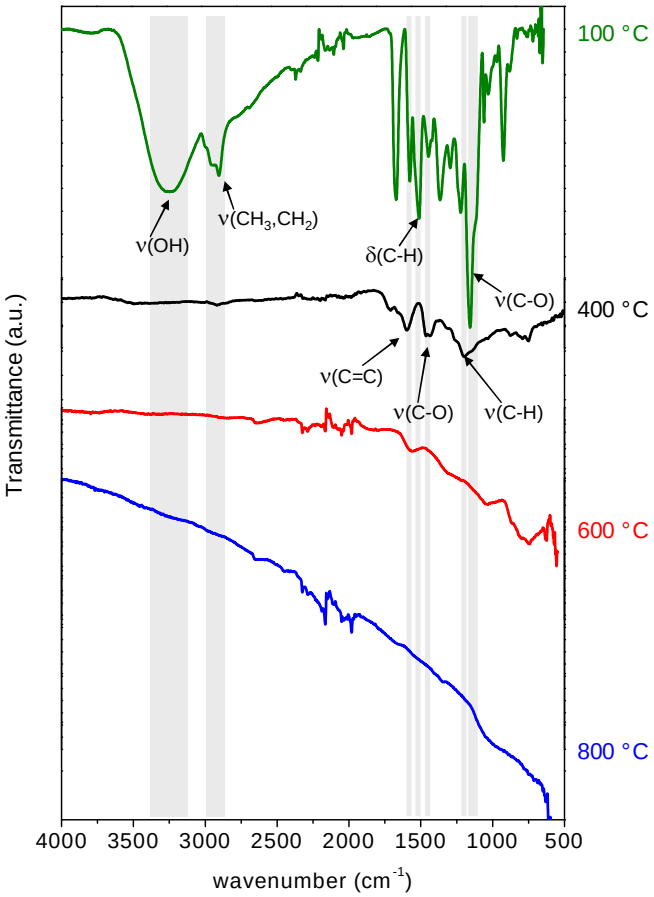

Figure 4.12. FT-IR spectra of the RF/F127 composite thermorpolymerised at 100 °C and corresponding carbon films carbonised at different temperatures.

Moreover, although the FT-IR spectrum of the material carbonised at 400 °C exhibits broad bands, the major bands at 1584, 1444, and 1185 cm^{-1}, corresponding to the stretching skeletal vibration of C=C and the stretching vibrations of C−O and C−H, can be observed. The fact that the stretching vibration of C−O still exists for this sample indicates that the material carbonised at this temperature still possesses a large amount of oxygen.[14, 48] This results is in consistence with those obtained by elemental analysis, which found about 22.7 wt% of oxygen (C: H: O = 72.5: 4.8: 22.7 wt%). It is shown that the relative intensity of all characteristic bands decreases and almost completely disappears above 600 °C (and also for the material carbonised at 800 °C). The spectra of both materials carbonised at 600 and 800 °C are rather featureless because the developed carbon framework results in strong adsorption of the IR radiation, which is related to higher carbon contents and less amount of oxygen functionality. This observation is in agreement with the elemental analysis for both the samples carbonised at 600 °C (C: H: O = 88.8: 2.4: 8.8 wt%) and 800 °C (C: H: O = 89.4: 2.4: 8.4 wt%), respectively.

WAXS measurements were performed to investigate the microstructural order of the obtained carbon films as a function of the carbonisation temperature, as shown in Figure 4.13. The broad peak centered at 2θ of ~ 22° for the material carbonised at 400 °C corresponds to the amorphous structure of the polymer-like carbon materials. However, it contains a number of hetero-atoms, which in this case are oxygen functionalities. These functionalities expand interlayer spacing of the RF polymeric structure, therefore resulting in a lower 2θ value in comparison with the normal value of carbon materials (2θ (002) is 26°). The (100) reflection at 2θ ~ 44° related to in-plane scattering and characteristic of a turbostratic-type carbon becomes shaper for both the carbon materials after carbonization at 600 and 800 °C in comparison with the material carbonised at 400 °C due to an increase in degree of aromatization and further condensation of the materials upon heating to these temperatures. For both the materials carbonised at 600 and 800 °C, the (002) reflection at 2θ ~ 24° corresponding to interlayer of the graphitic units is less-well defined, indicating that the carbon microstructure based on the RF precursor in the present study presents a turbostratic-type carbon order of small and poorly oriented graphitic units. The difficulty in graphitization of the carbon framework at low carbonisation temperature is a normal feature of the carbon precursors based on the phenolic resins.[59, 117, 130]

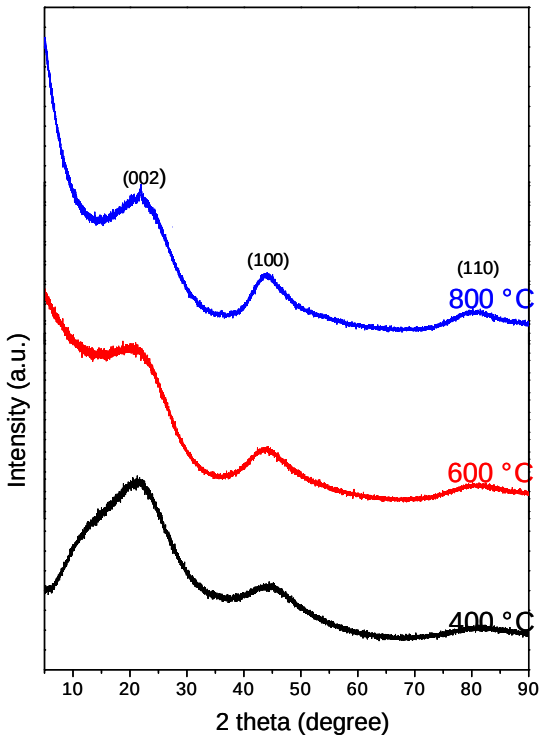

Figure 4.13. WAXS patterns of the carbon films carbonised at different temperatures of 400, 600, and 800 °C. The materials used for the WAXS measurements were prepared in a powder form using the same coating solutions for the films, followed by thermopolymerisation and carbonisation the same way as for the films.

As evidenced from the FT-IR, elemental analysis and WAXS results, a large oxygen content (22.7 wt%), which is only slightly lower than that for pure RF resin (~30 wt),[12] and a typical feature of resin polymer indicate that the film carbonised at 400 °C is not fully carbonised,

and is most likely a polymer film. However, a temperature of at least 600 °C is required to completely carbonise the RF precursor matrix, although the films carbonised at 600 and 800 °C still contain small amount of oxygen.

4.3.3 Effect of aging the dip-coating solution on mesostructure of the films

Keeping the dip-coating solution over time is a critical issue for reproducibility of the materials. The resol route is advantageous concerning this issue since the dip-coating solution is not reactive under ambient conditions. Zhao et al. explained that the resol molecules weakly interact with each other, and therefore macrophase separation is prevented. Consequently, the dip-coating solution stays intact over a long period (over months).[14, 131]
Herein, it is shown that there are no changes in the mesostructure of films prepared from the same solution based on the solution of resorcinol/formaldehyde and F127 in THF after the solution was stored for 2 days under ambient conditions. The solution stored for 2 days showed no changes in colour and fluidity. Figure 4.14 compares SEM images of a film prepared from a fresh solution that prepared from the 2 day-aged solution. Both the films were synthesized by the identical dip-coating and thermal treatment procedures (themopolymerisation at 100 °C and carbonisation at 600 °C). Both the films possess almost identical film thicknesses (252 and 249 nm). Furthermore, the high magnification SEM images (Figure 4.14c,d) confirm that the cubic mesostructure and porosity are well retained for the film dip-coated from the aged solution.

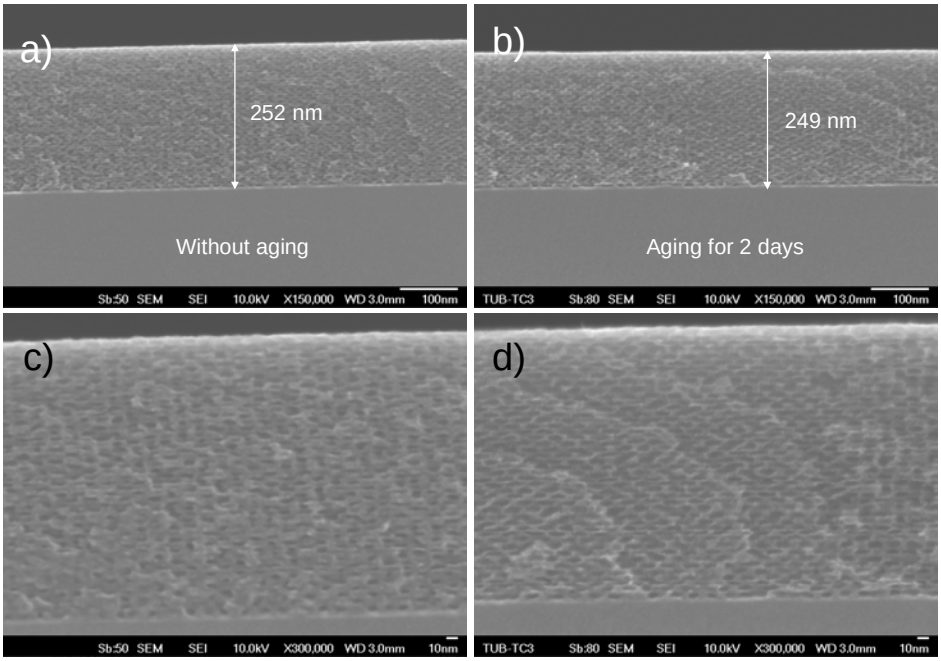

Figure 4.14. Cross-section SEM images of the materials dip-coated from the same dip-coating solution. a) and c) immediately after dip-coating solution was prepared; b) and d) after keeping the dip-coating solution for 2 days. Both the film were prepared at the same speed of dip-coating at 60 mm/min and under the same conditions, followed by carbonisation at 600 °C.

1D-SAXS analysis of both the films (Figure 4.15) further reveals no changes in mesostructure order and contraction behaviour The *d*-spacings for the first reflection (110) of both films are found to be almost identical (*d*-spacings = 4.8 and 4.7 nm).

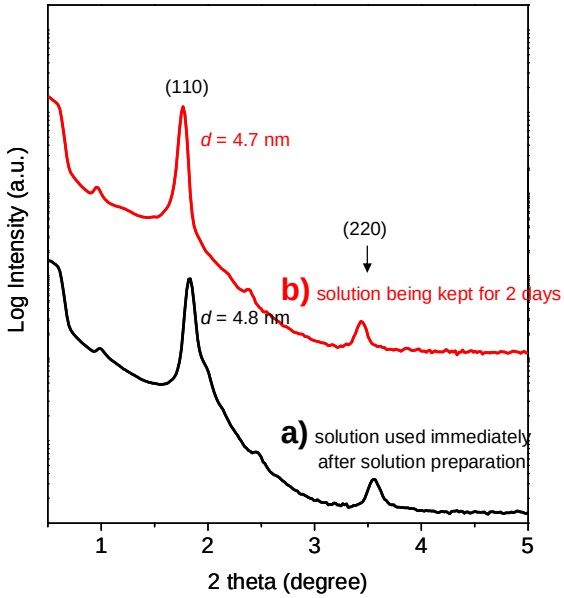

Figure 4.15. 1D-SAXS patterns of the carbon films prepared from a) the solution used immediately after the solution preparation and b) the same solution after being stored for 2 days. Both the films were dip-coated at a speed of 60 mm/min under the same conditions, followed by carbonisation at 600 °C.

Although the starting synthesis conditions for the dip-coating solution are extremely acidic (3M HCl is used in a mixture of EtOH/water), an exchange of the solvent with THF, the system becomes less reactive, therefore preventing the RF clusters from further polymerising. One possible explanation is related to the ability of THF to stabilise the RF clusters in comparison with the EtOH/H_2O mixture.[5, 50] It can be concluded that the RF clusters in the presence of F127 in THF are stable and not reactive under ambient conditions over a certain time. This stability of the RF clusters in the THF solution in the presence of F127 over a certain period of time is considered important to the reproducibility of the resulting mesostructure carbon films.

4.3.4 Effect of dip-coating speed on thickness and mesostructure

An increase in the film thickness in general is expected to lead to higher surface area and pore volume of films. Moreover, repeated coating/calcination cycles can be carried out, which however often lead to degradation of the porous system and loss of porosity.[127, 132-136] Increasing the withdrawal speed during the dip-coating is one way of increasing the film thicknes. However, for metal oxides, this procedure often results in macroscopic cracks when the thickness is beyond 500 nm.[136, 137] I show that by employing the dip-coating solution developed in this thesis, the thickness of carbon films can easily be tuned by only adjusting the withdrawal dip-coating speed, while retaining an ordered mesostructure. Figure 4.16

presents cross-section SEM images of the carbon films carbonised at 600 °C, but dip-coated at different withdrawal speeds of dip-coating. It is evident that by adjusting the withdrawal speed, films with different thicknesses ranging from ~250 to 820 nm were obtained. As can clearly be seen from the SEM images, increasing the withdrawal velocity produces thicker films, whereas the cubic mesopore structure appears to be preserved (Figure 4.16c, inset). All films prepared at higher speeds are macroscopically crack-free.

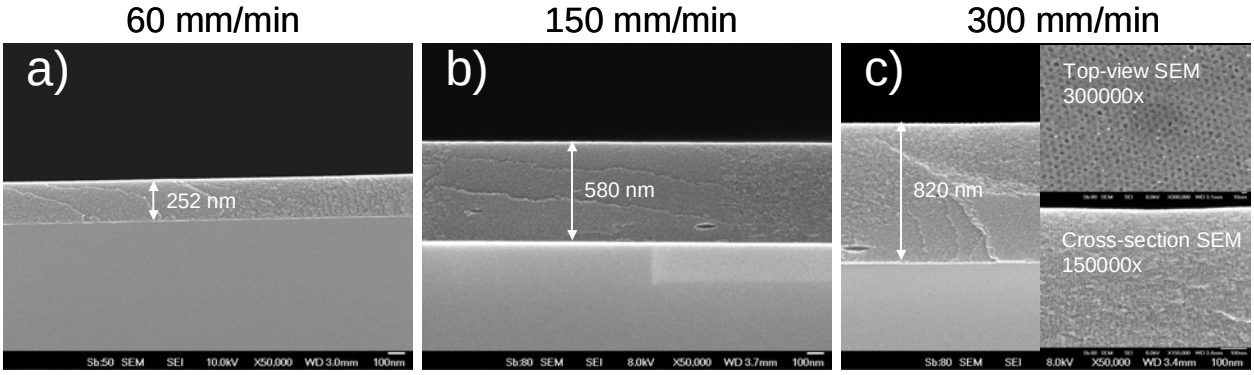

Figure 4.16. Cross-section SEM images of mesoporous carbon films prepared at different withdrawal speeds of dip-coating a) at 60 mm/min, b) 150 mm/min and c) 300 mm/min. Insets in c) represents top-view and cross-section SEM images at higher magnification for the same material. All the films were carbonised at 600 °C.

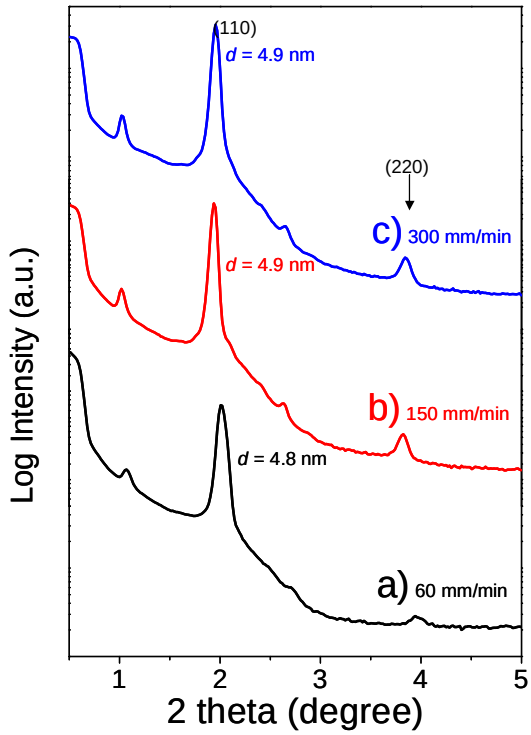

Figure 4.17. 1D-SAXS patterns of mesoporous carbon films on carbonised at 600 °C prepared at different withdrawal speeds of dip-coating, a) at 60 mm/min, b) 150 mm/min and c) 300 mm/min.

To further prove that the mesostructure order of the films is preserved, 1D-SAXS measurements were performed. The 1D-SAXS patterns of the corresponding materials are shown in Figure 4.17.
All the 1D-SAXS patterns feature distinct (110) and (220) reflections. No noticeable changes in the SAXS patterns and *d*-spacing of the (110) reflection are observed, except that the intensity of the (110) and (220) reflections slightly increases with an increase in the film thickness up to 820 nm.
A comparison of the 1D-SAXS patterns leads to the conclusion that the contraction behaviour in the Z direction for the films carbonised at 600 °C is identical for all the films with different thicknesses obtained in the present work, leading to the preservation of the mesopore order and lattice spacing. I also found that by using different carbonisation temperatures (400 and 800 °C), the films with different thicknesses still possess the same mesostructure and lattice spacing (data not shown).
The successful synthesis of the thicker films with the same mesostructure is beneficial to sorption analysis with N_2 as a gas probe because use of thicker films with an identical mesotructure can be representatives for the thinner ones.

4.4 Mesoporous carbon films templated with PIB-PEO 3000

As shown in the previous section, mesoporous carbon films with a 3D cubic pore structure can be obtained using the commercially available Pluronic F127 polymer as a template. Nevertheless, for many applications of mesoporous carbons, especially for catalysis, membranes and sensing, pore sizes obtained using the Pluronic polymers (~2-8 nm) are not effective to the underlying applications in which larger molecules are involved. In fact, the first report of mesoporous carbon films utilised a block copolymer (PS-*b*-P4VP) to obtain large vertically aligned cylindrical mesopores of ~33 nm in diameter. However, this procedure includes a time consuming multi-step approach.[38] Besides the facile synthetic approach using F127 (precipitation-redispersion) shown in the previous section, I have employed two characteristic different polymers, namely poly(isobutylene)-*b*-poly(ethylene oxide) (PIB-PEO 3000)[114, 138] and PEO-*b*-PBO-*b*-PEO (referred to as 10k-PB)[37] as templates in an attempt to generate uniform pores with diameters larger than 10 nm. In previous work,[37, 114, 138] it was demonstrated that these copolymers usually exhibit good templating properties due to the large hydrophobic-hydrophilic contrast between the hydrophobic blocks (PIB or PB) and hydrophilic blocks (PEO). Furthermore, they were successfully employed as the templates for preparation of various mesoporous metal oxide films.[37, 114, 138, 139]

4.4.1 General synthesis procedure of the dip-coating solution based on PIB-PEO 3000

Synthesis procedure for the synthesis of a dip-coating solution with a diblock polymer, PIB-PEO 3000 is similar to that with F127. Due to the shorter PEO block of the PIB-PEO 3000

(PEO_{45}) than that of F127 (PEO_{106}), interactions of this polymer with the RF precursor under identical acidic conditions could have been weaker than those of F127, and should have resulted in the later time of the phase separation. However, it was observed that the RF/PIB-PEO 3000 system took the similar time (~4 min) to that of RF/F127 system for the phase separation to occur in an EtOH/H_2O mixed solvent at identical HCl concentration (3M HCl) (see Chapter 3 Experimental for the details). It has previously been reported that, under acidic conditions, interactions between the block-copolymer template and the resin precursor clusters can be enhanced either by employing the phenol derivatives with a larger amount of -OH groups due to enhanced H-bonding[44] or by increasing the concentration of the acid.[54, 83]
In the present study, since the lower amount of PIB-PEO 3000 (165 mg) was used, I observed the early precipitation of the PIB-PEO 3000/RF composite in an EtOH/H_2O solvent. One possible explanation for this observation is that the RF precursor can crosslink faster since dilution effect by the polymer becomes smaller. From this finding, the synthesis procedure for carbon films based on PIB-PEO 3000 has to be adjusted accordingly to achieve a homogeneous dispersion containing both RF clusters and PIB-PEO polymer without macroscopic phase separation. THF was also used to redissolve the PIB-PEO 3000/RF composite, which had been precipitated out off the EtOH/H_2O mixture.
The resulting dip-coating solution was employed for the dip-coating process. In this case, 20% relative humidity (RH) was used instead of 30%RH (for the F127/RF) at 25 °C because over 20% RH, dip-coated films became turbid and were not homogeneous during the dip-coating process. According to the previous reports on synthesis of mesoporous metal oxide films, the rather low RH results in very fast evaporation of the solvent, leading to rather poor organisation of the precursor clusters and polymer template;[88, 89, 140] therefore, RH lower than 20% was not selected.

4.4.2 General features and morphology of the films

SEM

Carbon films were prepared via dip-coating from the dip-coating solution based on the THF solvent, the dip-coated films were themopolymerised at 100 °C, follow by carbonisation under an inert atmosphere. According to the TGA results, the minimum temperature of 400 °C is needed to completely remove the PIB-PEO 3000 template (see Section 4.2 and Figure 4.1). Figure 4.18 shows the top view SEM images of a carbon film templated with this polymer, dip-coated at the withdrawal speed of 600 mm/min and carbonised at 600 °. The SEM image at low magnification (Figure 4.18a) indicates that the surface is flat a homogeneous and macroscopic crack-free morphology throughout the area is observed. Furthermore, the higher magnification SEM images in Figure 4.18b, c present the opening uniform pores with a size of ~ 12 nm in diameter. The pores seen from the top-view images appear spherical in shape. The FFT image in Figure 4.18b reveals an isotropic ring, indicative of locally ordered mesopore arrangement of different oriented domains on the top surface.

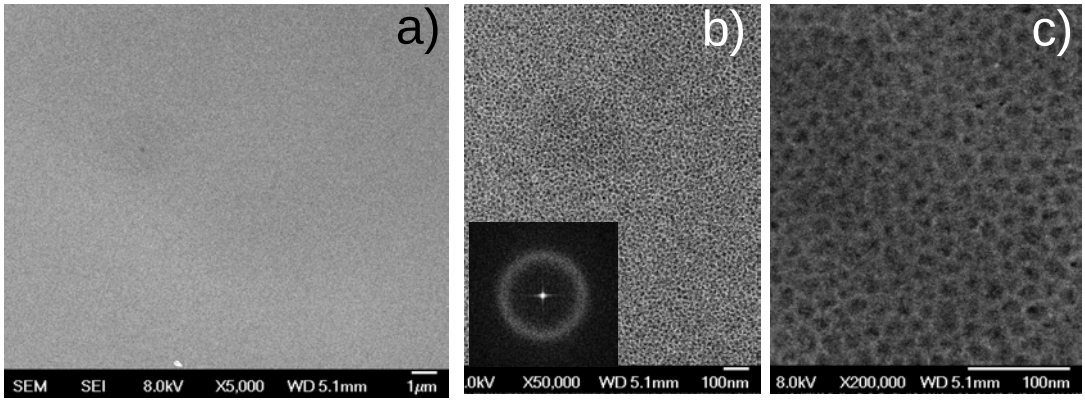

Figure 4.18. Top-view SEM images of the mesoporous carbon film templated with PIB-PEO 3000 at a dipping speed of 600 mm/min, carbonised at 600 °C, a) at magnifications of 5000×, proving a crack-free film; b) and c) at magnifications of 50000× and 200000×, respectively, showing the uniform pores on the top surface. Inset in b) shows a FFT image of the corresponding image.

Cross-section SEM images were also recorded to observe the pore morphology across the film thickness, and shown in Figure 4.19. The thickness of the film dip-coated at 600 mm/min and carbonised at 600 °C is ~ 640 nm.

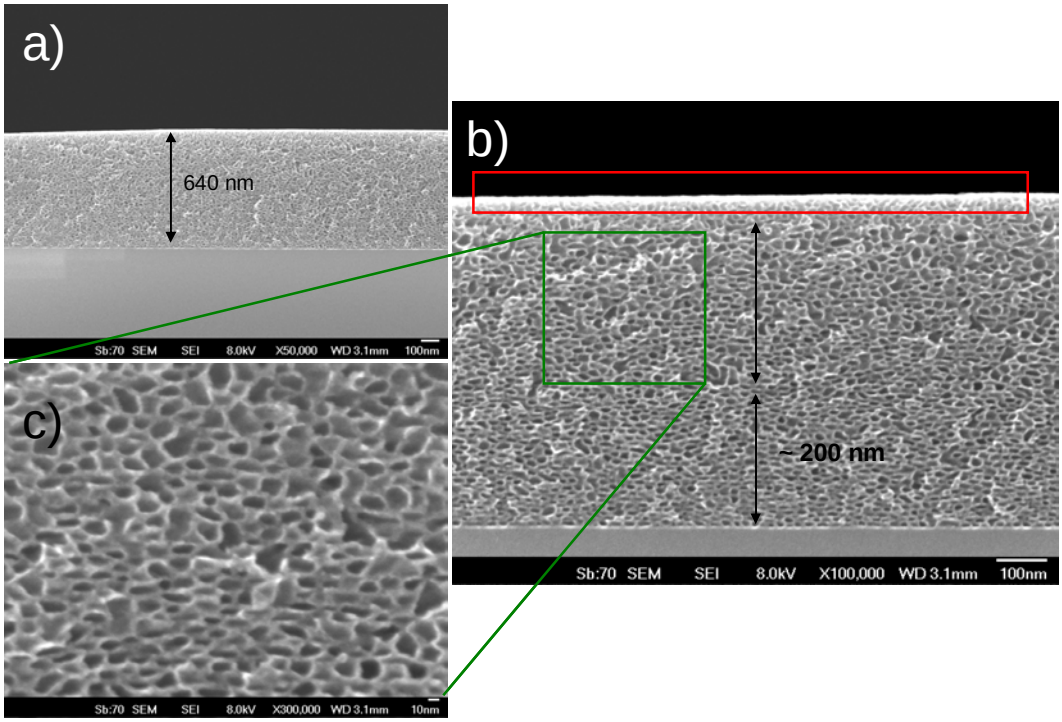

Figure 4.19. Cross-section SEM images of the mesoporous carbon film prepared with PIB-PEO 3000 on a silicon wafer at a dipping speed of 600 mm/min, carbonised at 600 °C, a) at magnifications of 50000×; b) and c) at magnifications of 100000× and 300000× (which is also a zoom-in image from b), respectively. The pores in c) are neither spherical nor elliptical in shape.

Although the film is highly porous, the film lacks a long-range order. Furthermore, the pores are not uniform throughout the film thickness. In the top layer of ~30 nm, pores seem to be smaller than those observed in the middle of the film with the pore size of ~12 nm in diameter in the direction parallel to the substrate surface (XY direction). Pores in the bottom layers of about 200 nm from the substrate surface appear to be rather elliptical in shape, which is induced by contraction and show a uniform morphology (Figure 4.19b). The pore diameter in the direction parallel to the substrate is found to be ~12 nm. However, the pores in the middle of the film (indicated in the Figure 4.19b,c) are differently shaped and have no preferred orientation. Additionally, the pore sizes are in a wide range of ~10-35 nm, most of them being larger than 20 nm. These large pore sizes are larger than the expected size of the micelle core of the PIB-PEO 3000 (12-15 nm).[114, 138] In any case, the pore wall thickness of ~6 nm appears to be the similar for all the pores throughout the film thickness.

TEM

Figure 4.20 presents TEM images of the corresponding film. The images further confirm that the material is highly porous. The TEM images in Figure 4.20a prove the existence of different pore sizes and the pores seem spherical in shape, which is likely to be recorded in a direction perpendicular to the top surface of the film. The contraction of the mesopore structure is confirmed by TEM image in figure 4.20b. More importantly, when assuming the long axes of the pores, the pores in two different regions indicated by the arrows are different in size (12 nm vs. 35 nm), which is in agreement with the SEM observation.

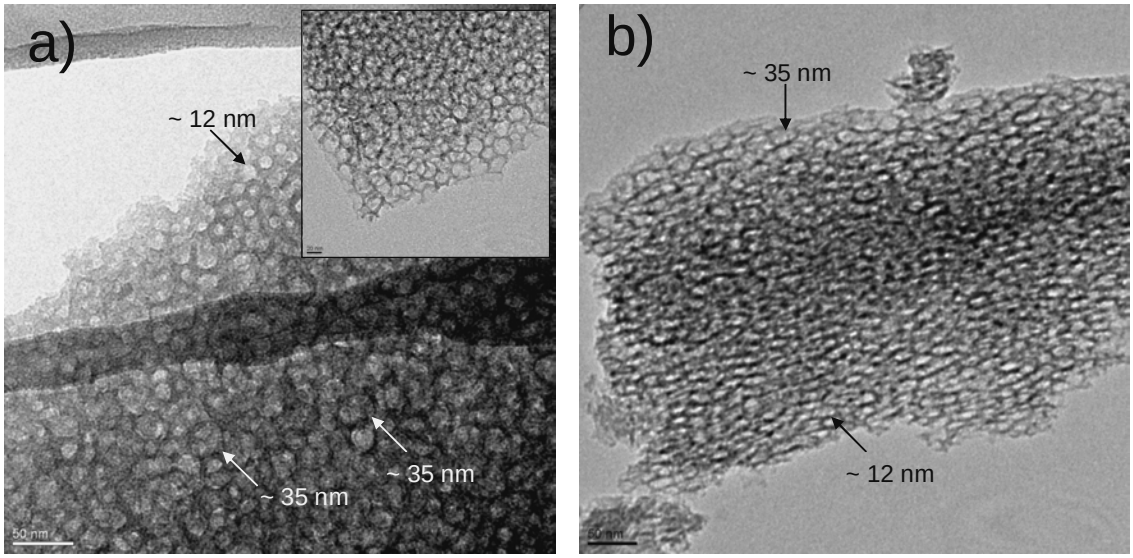

Figure 4.20. TEM images of the carbon film templated by PIB-PEO 3000 at a dipping speed of 600 mm/min, and carbonised at 600 °C; a) showing almost spherical pore shape (viewed perpendicular to the substrate surface) and the arrows indicate different pore sizes, b) showing a deformed feature of the templated pores induced by contraction of the film and the arrows indicate different pore sizes. The inset in a) show a higher magnification image. The TEM specimen was prepared by scratching off some parts of the film with a razor blade, dispersed in ethanol and dropped on a TEM grid.

4.4.3 Influence of carbonisation temperature on mesostructure and porosity

SEM

Similar to the films templated by F127, the change in thickness due to carbonisation temperature was also investigated for films templated with PIB-PEO 3000. After carbonisation at 800 °C, film thickness decreases to ~550 nm, as shown in Figure 4.21, in comparison with that at 600 °C (640 nm). This decrease in film thickness confirms the further contraction in the Z direction. Nevertheless, the mesopores are well preserved, and no collapse of the mesopores is observed even after carbonisation at 800 °C.

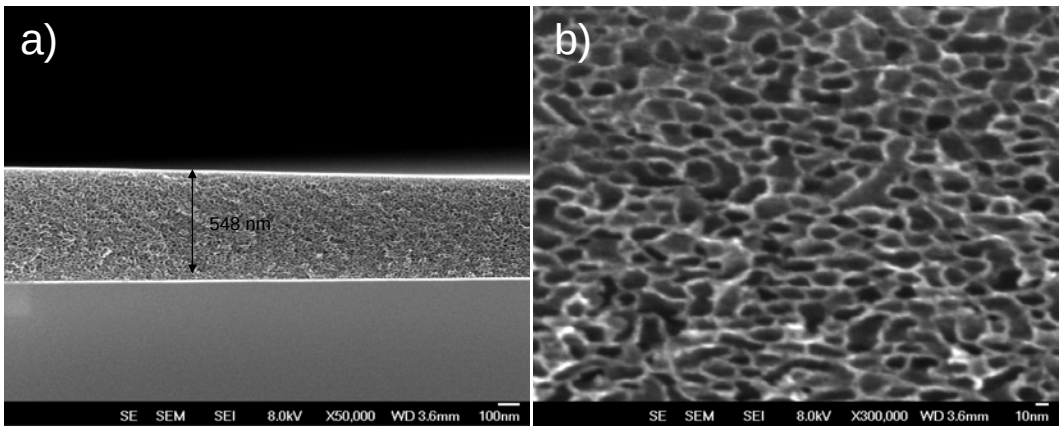

Figure 4.21. Cross-section SEM images of a mesoporous carbon film prepared with PIB-PEO 3000 at a dipping speed of 600 mm/min, carbonised at 800 °C, a) at a magnification of 50000× and b) at a magnification of 300000× imaged from the middle area of the film, still showing a pore disorder.

1D-SAXS

Figure 4.22 presents 1D-SAXS patterns of the films templated with PIB-PEO 3000 and carbonised at three different temperatures. The rather broad reflections of the 1D-SAXS patterns agree well with the somehow disordered nature of the mesopore arrangement of the films. The local maximum of each pattern can be attributed to a broad second-order Bragg maximum of disturbed mesostructure. Because the setup used for the measurements cannot resolve such large mesostructures, the corresponding first-order Bragg maximum could not be observed. A shift of the second maximum to larger scattering vector (*s*) when increasing the carbonisation temperature further proves the contraction of the films in the Z direction. However, the change in *d*-spacing is difficult to determine due to the rather disorder of the mesostructure prepared using this large PIB-PEO 3000 template.

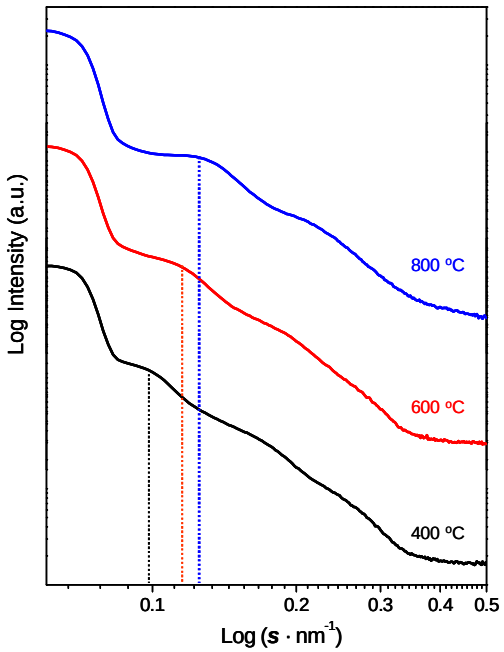

Figure 4.22. 1D-SAXS patterns recorded in θ-2θ geometry (symmetric reflection or Bragg-Bretano geometry) of the carbon films templated using PIB-PEO 3000, dip-coated at the same speed of 600 mm/min and carbonised at 400, 600 and 800 °C. s is the scattering vector, given by $s = 2\sin(\theta)/\lambda$..

N_2 sorption

N_2 physisorption was used to characterise the porosity of the films carbonised at different temperatures. Figure 4.23a shows nitrogen sorption isotherms for the films dip-coated at a speed of 600 mm/min and carbonised at different temperatures of 400, 600, and 800 °C. All the isotherms feature a well-defined typical type IV curve with a distinct large hysteresis loop and condensation step, indicating the presence of mesopore architecture. The fact that all the isotherms possess rather large hysteresis loops and that the condensation step ranges from ~0.4 - ~0.8 p/p_0 implies that mesopore sizes should be bigger than 10 nm.[120] However, the desorption branches for all samples do not close at low relative pressures. This behaviour is a normal feature observed for some types of porous polymers or carbon materials based on resin-type precursors even after carbonisation at 800 °C, as discussed previously (see Section 4.3.2).

The BET surface areas and pore volumes of the films are shown in Table 4.2. The high surface areas and pore volumes indicate that all the films carbonised at different temperatures are highly porous and the pores are accessible to nitrogen molecules. The pronounced mesoporosity of the film carbonised at 400 °C provides evidence that the template completely decomposes even at a temperature as low as 400 °C under an inert atmosphere, which is in agreement with the TGA results (see Figure 4.1).

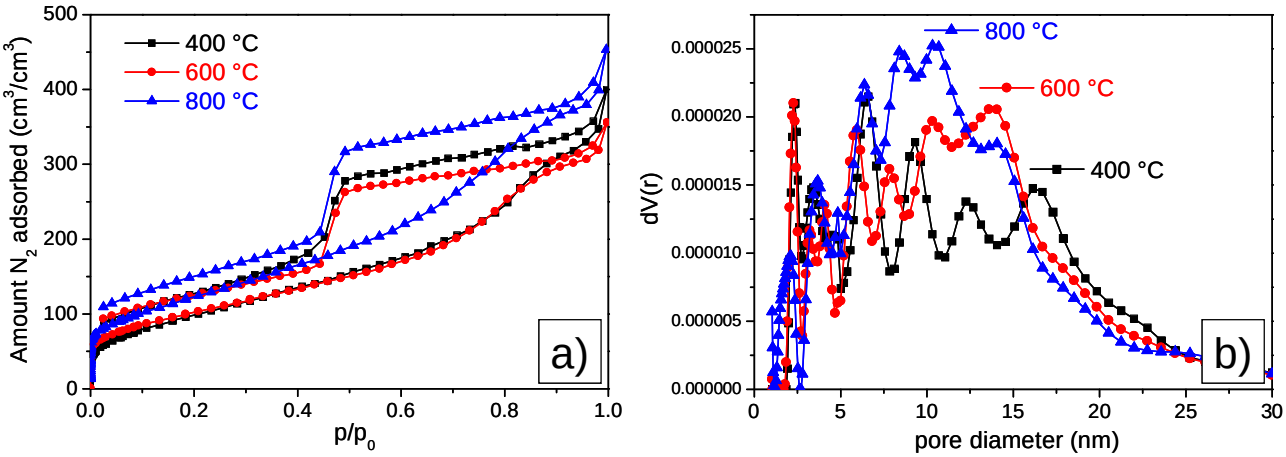

Figure 4.23. N_2 sorption analysis of the carbon films, templated using PIB-PEO 3000, dip-coated at 600 mm/min, carbonised at 400, 600, and 800 °C. a) N_2 sorption isotherms. b) Pore size distributions (PSDs) calculated using QSDFT model applied on the adsorption branches.

It is obvious that increasing carbonisation temperature had no significant influence on the BET surface area of the films, in contrast to the case where F127 was employed (see section 4.3.2). More interestingly, the relative amounts of microporosity (volume%) in all materials are found to be lower than 7%, in comparison with their total pore volumes. Pore size distributions (PSDs) calculated using QSDFT applied to the adsorption branches are presented in Figure 4.23b. All the distributions are broad and pore sizes range from ~5 nm – 20 nm. The rather broad feature of the pore size distributions is consistent with the SEM results, which prove that the pores are not uniform in size. However, it is noticeable that the maxima for all the pore size distributions are located at about 10 – 15 nm. From the sorption and SEM analysis, it is indicated that the pore sizes of the carbon films templated with PIB-PEO 3000 are bigger than those obtained for the films templated using F127 for all studied carbonisation temperatures.

Table 4.2. Porous textural properties of mesoporous carbon films templated using PIB-PEO 3000, dip-coated at 600 mm/min and carbonised at different temperatures

Sample	Carbonisation temperature (°C)	BET surface area (m^2/cm^3)	Total pore volume (cm^3/cm^3)	Microporosity (volume%)[a]
C-400	400	373	0.54	0.1
C-600	600	367	0.49	6.8
C-800	800	451	0.62	5.8

[a] the relative volume is determined from cumulative pore size distribution using QSDFT model applied to adsorption branch for spherical pores

4.4.4 Effect of withdrawal speed on thickness and mesostructure of the films templated using PIB-PEO 3000

Similar to the systems employing F127 as a template, to obtain films with different thicknesses, the withdrawal velocity during the dip-coating was adjusted.
Increasing the velocity produced thicker films, while the mesoporosity in all the films remains intact, as observed by comparing the cross-section SEM images in Figures 4.24.

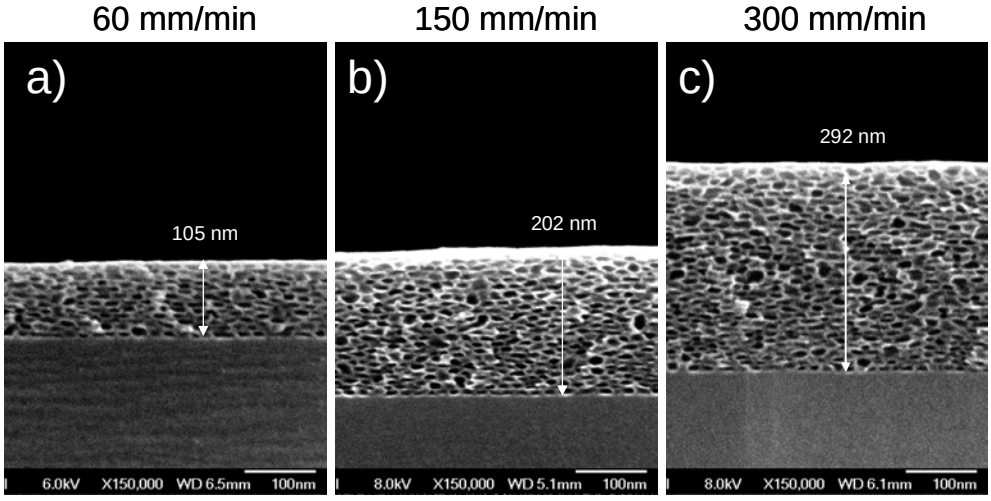

Figure 4.24. Cross-sectional SEM images of mesoporous carbon films on Si-wafers prepared using PIB-PEO 3000 as a template, at different withdrawal speeds of dip-coating; a) at 60 mm/min, b) 150 mm/min and c) 300 mm/min. All the films were carbonised at 600 °C.

By applying the same dip-coating solution developed in this thesis, the film thickness is lowered to 292, 202 and 105 nm when the withdrawal speeds are 300, 150, and 60 mm/min, respectively. It is interesting to note that the presence of the un-uniform pores larger than 20 nm, which are typical observed for the film dip-coated at the speed of 600 mm/min, becomes less noticeable with a decrease in the withdrawal speed. The uniform templated mesopores in the films with thicknesses lower than 200 nm, especially those dip-coated at 60, 150 mm/min, are almost elliptical in shape. A diameter of the pores normal to the substrate (Z direction) is ~7 nm, whereas that parallel to the substrate (XY directions, in-plane) is ~12 nm. For these films, the pore sizes larger than 20 nm are diminished throughout the area observed. From the SEM results, we can conclude that for the carbon films templated by PIB-PEO 3000 prepared using the dip-coating solution developed in this thesis, a degree of mesoscopic order and uniformity of mesopore size can be improved by lowering the film thickness (down to ~200 nm) under identical dip-coating conditions.

4.5 Mesoporous carbon films templated with PEO_{213}-*b*-PB_{184}-*b*-PEO_{213} (10k-PB)

To further increase the pore size of mesoporous carbon films, a polymer with higher molecular weight and especially the hydrophobic block (PEO-*b*-PBO-*b*-PEO, M_w of PB block is 10000 g/mol; here referred to as 10k-PB) has been employed in this thesis. This polymer has previously been employed for the synthesis of large-pore mesoporous coatings with various metal oxides.[37, 139, 141] In addition, the polymer has proved to be a successful template to obtain a 3D pore structure and large mesopore size (pore sizes ranging between 16-23 nm, depending on metal oxide materials).
The synthesis procedure for the synthesis of a dip-coating solution with 10k-PB is similar to those with F127 and PIB-PEO 3000. However, the synthesis procedure was slightly adjusted by changing the ratio of the precursor to the template, as well as the amounts of HCl solution and solvents in order to obtain a homogeneous dispersion containing the RF clusters and the 10k-PB polymer in THF as a solvent, which was found to be the best solvent (see Chapter 3 Experimental).
The resulting dip-coating solution was subsequently employed for the dip-coating process, which was carried out under suitable conditions (30%RH and 25 °C), where the good quality of the dip-coated films based on this polymer was observed.
After the dip-coating process, the dip-coated films were thermopolymerised at 100 °C, followed by carbonisation under an inert atmosphere where temperatures as high as 600 °C were employed since according to the TGA results on this polymer, at 400 °C, the polymer is not completely removed under an inert atmosphere (see Figure 4.1 for the TGA results).

Figure 4.25a,b shows top-view SEM images obtained from a mesoporous carbon film templated using 10k-PB as a structural directing agent, dip-coated at a withdrawal speed of 600 mm/min and after complete removal of the polymer at 600 °C. The images show rather disordered, but macroscopically homogeneous features with ~17-23 nm diameter pores. The film is crack free, and the pores in spherical shape are open at the surface. Recorded in the cross-section SEM images, the film possesses a thickness of ~190 nm and is porous across the whole cross-section area without any indication of pore collapse (Figure 4.25c,d). However, the porous system observed for this film appears to lack the long-range order.
Elliptical deformation of the pore shape upon carbonisation due to uniaxial contraction is also clearly observed for this film. The high magnification SEM image (Figure 4.25d) demonstrates the pore dimension to be about 18-23 nm in width (XY direction) and ~6 nm in height (Z direction). By assuming that the initially spherical shape of the pores should be about 18-23 nm in diameter (according to the diameter in the Z direction), the deformation of the pores is about 70%. This high contraction behaviour corresponds well to shrinkage and pore deformation reported for TiO_2 mesoporous systems using the same polymer.[37]
The dip-coating at higher withdrawal speeds in order to obtained films with larger thicknesses could not be performed due to the limited maximum speed of the dip-coating machine (600 mm/min) and the low viscosity of the dip-coating solution.

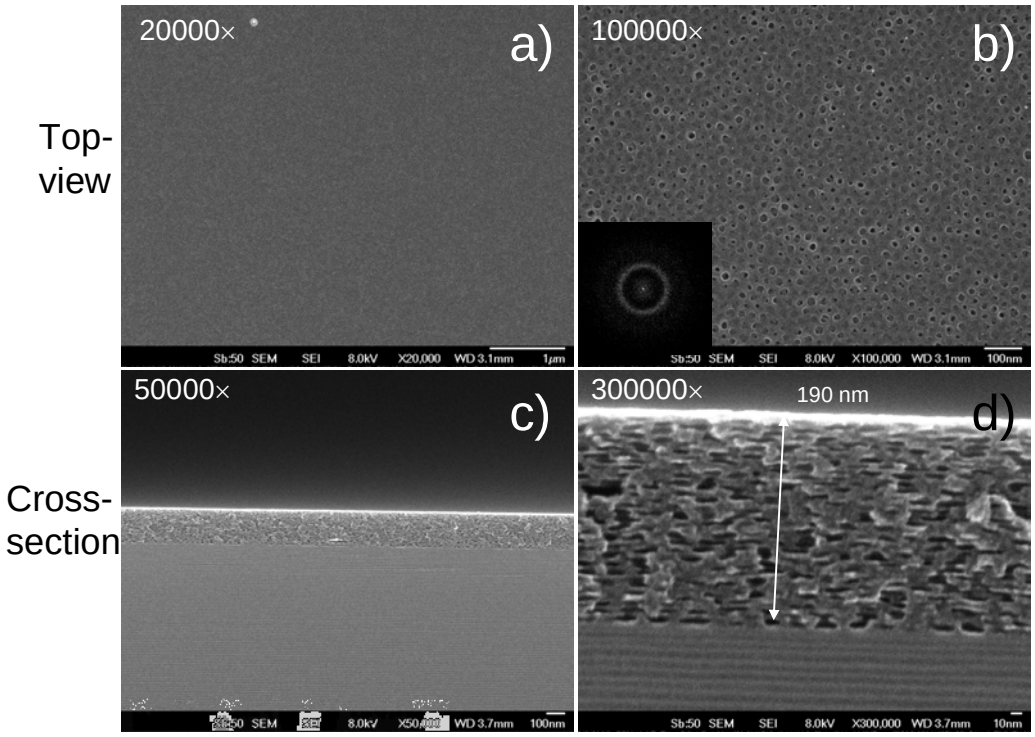

Figure 4.25. SEM images of a mesoporous carbon film prepared using 10k-PB polymer at a dipping speed of 600 mm/min, carbonised at 600 °C. a) and b) Top-view images at magnifications of 20000× and 100000×, respectively, proving a crack-free film and proving the reservation of the open mesopores on the top surface. c) and d) Cross-section images at magnifications of 50000× and 300000×, respectively. Inset in b) shows the FFT image of the corresponding image.

4.6 Coating on stainless steel substrates

As shown in the previous section and in the literature, most synthesis reported for mesoporous metal oxide and carbon coatings up to date employed silicon wafer, or other flat substrates, whereas commercially important materials such as stainless steel have been reported in a few studies. Furthermore, to the best of our knowledge, mesoporous carbon coatings with well-defined mesostructure prepared through the micelle-templated strategy have not been reported so far using steel substrates. Yet, stainless steel remains one of the most practical substrates because of its wide industrial use, and many applications, including heterogeneous catalysis where the mesoporous carbon coatings would be attractive catalyst-support materials employable in chemical reactors.[115, 142]

In this section, we here report the successful synthesis of mesoporous carbon coatings on such stainless steel surface while retaining well-defined mesostructure.

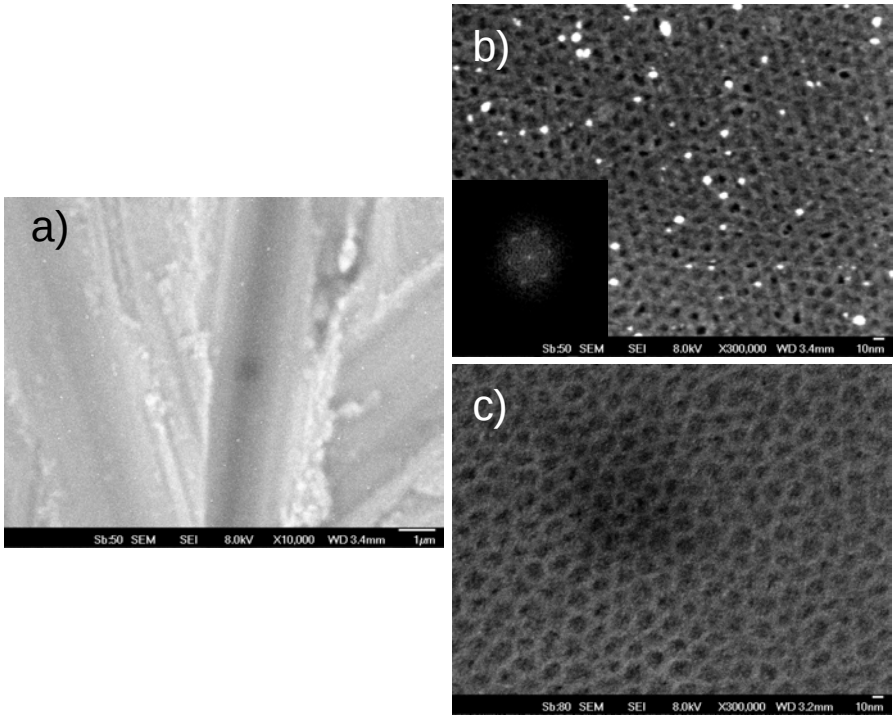

Figure 4.26. Top-view SEM images of the mesoporous carbon films coated on 1.4301 grinded and passivated steel plates with R_a ~ 0.55 µm; a) film templated with F127 at a dipping speed of 60 mm/min, carbonised at 600 °, at magnification of 10000×, proving a crack-free film; and b) at magnification of 300000×, showing the uniform pores on the top surface, similar to those observed on Si-wafers. Inset in a) shows a FFT image of the corresponding image. c) SEM image of the carbon film templated with PIB-PEO 3000 at a dipping speed of 60 mm/min, carbonised at 600 °, at a magnification of 300000×.

The surface of steel plates (grade 1.4301) was passivated prior to coating as described in the experimental section. The polishing/grinding, followed by passivation of the steel substrates yields a surface roughness (R_a) of ~0.55 µm. Dip-coating on these polished, grinded and passivated steel substrates with the dip-coating solutions based on F127 and PIB-PEO 3000 was performed under identical conditions to those for Si-wafer substrates. The dip-coating on the steel substrates produces good quality coatings of the films, which cover the coated area of the substrates throughout the coating process, thermal polymerisation as well as carbonisation of the films. Figure 4.26 presents SEM images of films templated with F127 and PIB-PEO 3000 dip-coated at a withdrawal speed of 60 mm/min, and carbonised at 600 °C. The low magnification SEM images confirm complete substrate coverage and good film integrity, as well as a few isolated fractures generally found in the scratches generated by grinding. Furthermore, no macroscopic cracks are present throughout the coated area observed. By examining at higher magnification of 300000×, both the films templated with F127 and PIB-PEO 3000 appear extensively porous. Moreover, they show narrow pore size distributions of ~8 nm and ~12 nm in diameter for the films templated by F127 and PIB-PEO 3000, respectively. These pore sizes observed by top-view SEM are similar to those prepared on Si-wafers, indicating that the dip-coating process is not affected by the texture produced on the steel substrates by grinding used in this study.

4.7 Discussion

Influence of templates on the film properties

The previous section presents the successful synthesis of carbon films templated with three types of block-copolymers. The synthesis is based on redissolving-casting by means of the dip-coating process. The evaporation-induced self-assembly (EISA) during the dip-coating is responsible for the formation of RF/the block-copolymer composites For each polymer system, some optimisation of the dip-coating conditions (temperature and %RH) was required in order to obtain the best quality of coatings without phase separation or de-wetting.
The dip-coated composite films are subsequently subject to the themopolymerisation at 100 °C, followed by carbonisation at higher temperatures to remove the templates and increase the carbon content. Characterisation by SEM as well as SAXS analysis proves that all the materials prepared with all the three templates possess 3D-mesostructure, e.g. the templated mesopores are open in all directions (XYZ).

Table 4.3 summarises the pore sizes observed on the top surface of the films templated with all the polymers as a function of molar mass of the hydrophobic block of the respective polymer templates. The pore sizes (in-plane, XY) were determined using top-view SEM from the films with the film thicknesses of ~200 nm and carbonised at the same temperature of 600 °C. I have chosen only the films with the thickness of about 200 nm since the pore sizes from the films based on different polymers show monomodal pore size distributions, which should only result from the templating effect replicating individual micelles sizes.

Table 4.3. Molecular weight (M_w) of the template molecules, and corresponding pore size (in diameter) observed in the carbon films coatings with the thickness of about 200 nm. All the coatings were carbonised at 600 °C

Polymer Template	Pore size in diameter ± S.D.[a] (nm)	Template M_w (g/mol)	Hydrohobic part M_w (g/mol)	Thickness of the films used for the determination (nm)
F127	8.0 ± 1.0	12600	4060	252
PIB-PEO 3000	12.2 ± 1.6	7050	2980	202
10k-PB	20.3 ± 3.1	28740	10000	190

[a] obtained from measurements using imageJ program on 100 pores from top-view SEM images

From Table 4.3, it can be seen that the size of the templated mesopores (in-plane) can be tuned using the different polymers. However, the pore size does not scale directly with the molecular weight of the hydrophobic block, for example, when comparing the pore sizes obtained by F127 (8 nm) and from PIB-PEO 3000 (12 nm). The reason could be that even though PIB-PEO has a shorter hydrophobic length, it forms a bigger micelle size due to the

larger hydrophobic volume in comparison with F127.[143] Another reason is related to H-bonding interactions between the PEO block of both the polymers and the H atoms of the RF precursor. Due to the longer PEO block, the RF clusters can more efficiently penetrate the micelle corona of the F127 micelles, resulting in the close contact between RF clusters and the F127 micelle core at the interface, in comparison with a shorter PEO block of PIB-PEO 3000. By using PIB-PEO 3000, pore sizes over 10 nm have been achieved previously for templated mesoporous metal oxide films.[114, 138] By employing a larger polymer, 10k-PB, possessing both high MW and large hydrophobic block, as a template, the pore size can reach ~20 nm in diameter. All the materials prepared using these different polymers (with the thickness of about 200 nm for each sample) show a degree of order to some extent and a uniform pore size, according to the SEM analysis. Moreover, all the materials posses a 3D mesostructure. The film templated by F127 shows a very large long-range degree of order for a contracted 3D cubic mesostructure (contracted *Im3m*), as confirmed by SEM and SAXS analysis. For the films prepared using PIB-PEO 3000, the degree of order is lower. One explanation for this lower degree of order for this PIB-PEO 3000-based film is probably related to the different synthesis condition (30%RH for F127-based films, and 20%RH for PIB-PEO 3000-based films at 25 °C). This effect resulting in poor order for the films based on PIB-PEO 3000 can be more clearly observed when increasing the film thickness, as shown below.

Increasing the film thickness

As shown earlier, by adjusting the withdrawal speed, the thickness of the films based on both F127 and PIB-PEO 3000 were easily adjusted. In general, the film thickness could be increased by increasing the withdrawal speed of the dip-coating.

The thickness of the films templated using F127 can reach ~820 nm when dip-coated at a speed of 300 mm/min, followed by carbonisation at 600 °C, while the contracted cubic mesostructure is perfectly maintained (with an in-plane uniform pore size of ~8 nm). In contrast, an increase in the film thickness beyond 200 nm, the films templated using PIB-PEO 3000 begin to show disordered regularity of the pores, especially on the area close to the top of the film/air interface. Besides the disordered arrangements of the pores, the pore sizes in this region of interest are in a wide range of ~10- 35 nm. Most of them are larger than 20 nm, as confirmed by SEM, TEM and pore size distribution (QSDFT) by sorption analysis. Interestingly, however, the appearance of the disordered large pores becomes diminished by lowering the film thickness (about ≤ 200 nm). At these thicknesses, the uniform PIB-PEO 3000-templated pores (~ 12 nm, in-plane pore size) are more effectively arranged into a closely packed mesostructure. It is obvious that in case of PIB-PEO 3000 templated films, the mesopore arrangements are strongly influenced by the withdrawal speed. Such a big difference between F127 and PIB-PEO 3000 in inducing the degree of mesostructure order for thick films (> 200 nm) is probably related to the interactions between the polymer templates, the RF clusters and solvent (THF).

In fact, Dai et al. previously demonstrated that the periodicity and pore size distribution of resulting carbons can depend largely on the processing conditions of the phase-segregate polymer phase,[44] for example, the evaporation of the solvent. In other words, they found that

when the polymeric precursor (the RF in our case) undergoes fast cross-linking step, while the microphase separation has not reach an equilibrium, a wormy structure is likely to be obtained.[12, 44] Therefore, microphase separation can be facilitated, and a highly ordered structure is obtained by well-controlled solvent evaporation. This similar observation is well-known for the microphase separation of polymer blends.[144, 145]

According to the EISA process, during evaporation of THF from the deposited film, the concentration of the template polymer is enriched, driving the organisation of the RF clusters/polymer composite into a periodic liquid crystalline mesophase.[14, 88] However, the gradient of solvent concentration can be varied as a function of the thickness of the film.

The use of THF as a solvent to re-dissolve the RF clusters/polymer composites is probably the reason for the formation of the pore disorder in PIB-PEO 3000 templated films. One possible explanation could be that the RF clusters are cross-linked concomitantly with the fast evaporation of THF, therefore resulting in the loss of the precursor mobility. As a result, a kinetically trapped mesostructure might be formed.[144, 145] In the case of PIB-PEO 3000-templated films, the fast withdrawal speed (also resulting in a thick film) provides different concentration gradients of the solvent across the thickness. THF molecules can partly interfere with the self-assembly of the PIB-PEO 3000 micelles by swelling the micelles, then resulting in an irregular order of the large pores (10-35 nm). The irregularity of the peculiar large pores can be reduced by lowering the withdrawal speed, which also results in thinner films (down to 200 nm in thickness). In contrast, the withdrawal speed has no influence on the mesostructure order and packing degree of the mesopores in the films templated using F127, even though the thickness is increased to ~820 nm.

Effect of carbonisation temperature

Templating with all the polymers used in this thesis leads to the formation of porous films contracted in the Z direction (perpendicular to the substrate surface) as a result of high temperature carbonisation. Films templated using F127 and dip-coated at 60 mm/min show contractions of 48%, 63% and 69% after carbonisation at 400, 600, and 800 °C, respectively, as determined by 2D-SAXS analysis (see Section 4.3.3)

Films templated with PIB-PEO 3000 and 10k-BP also show the contraction behaviour. Nevertheless, due to lower uniformity of the templated mesopores of these films, a direct comparison of the contraction behaviour among the films templated using all the different polymers is difficult.

For the F127-templated films, it is obvious that the decrease in pore size in the Z direction is closely related to the increase in carbonisation temperature, while the pore size in the XY dimension (~8 nm, in-plane pores) stays constant. The change in the pore size in the Z direction is also reflected by QSDFT pore size distributions. The pore size distributions (PSDs) are, however, narrow, confirming the preservation of the uniformed templated pores even after the large contraction. All the films possess large surface areas and pore volumes (Table 4.1).

It is interesting to note that the materials templated with F127 possess a degree of microporosity to some extent. Even after the temperature as low as 400 °C is employed, the

film possesses 14% micropore volume. Furthermore, a large increase in micropore volume is observed when increasing the carbonisation temperature to 600 °C (26% micropore volume). This large increase is related to the formation of gases from the decomposition of the RF matrix, which is in accordance with the TGA and elemental analysis. The release of the decomposed species from 400-600 °C also results in a huge relative contraction of the films (15%). Increasing carbonisation temperature to 800 °C has no further influence on the microporosity probably because the rigid carbon framework already formed at 600 °C. In contrast to F127-templated films, the PIB-PEO 3000-templated films show very low microporosity (up to ~7%) for all carbonisation temperatures, especially the film carbonised at 400 °C (Table 4.2).

Considering the fact that both F127 and PIB-PEO 3000 completely decompose at 400 °C, the PEO block of both polymers should be responsible for this difference in microporosity. The large contribution to the microporosity for the materials carbonised at 400 °C is generated from the strong interactions between the PEO chains and the RF clusters in the micelle corona. Therefore, the trapping of the PEO chains, followed by their removal via carbonisation at 400 °C produced PEO-templated micropores. Since F127 possesses longer PEO blocks than PIB-PEO 3000, this phenomena is more pronounced for the materials templated with F127. This similar behaviour was previously observed by Ikkala et al. for templated phenolic resin,[57] and Smarsly et al. for templated SiO_2 materials.[146]

4.8 Conclusions

A facile synthesis strategy has been developed for the preparation of crack- free mesoporous carbon coatings. The strategy is based on the preparation of dip-coating solutions through simple 'precipitation-redispersion' method, followed by the evaporation-induced self-assembly process (EISA) via dip-coating technique. The successful synthesis relies on the organic-organic self-assembly of resorcinol-formaldehyde and the block copolymers used as structure directing agents. The composite films are directly converted into mesoporous carbon films by carbonisation. The pore size of such coatings can be tuned by choice of the polymer templates. By using F127 as a template and appropriate ratio of the carbon precursor to the template, the resulting films possess a highly ordered cubic *Im3m* contracted mesostructure, high surface area and pore volume. The thickness of the F127-templated films can be easily tuned (the thickness up to 820 nm) by adjusting the withdrawal speed of dip-coating, while the mesostructure is maintained. In contrast, the speed of dip-coating largely influences the mesostructure order of films templated by PIB-PEO 3000.

The developed method not only offers coating on Si-wafer substrates, but also on steel substrates, which could be beneficial to industrial applications. Furthermore, the preparation of carbon coatings on steel substrates has no influence on the mesostructure of the films. It is believed that the facile method can be applied to the synthesis of a variety of mesostructured carbon films, including the coatings containing other active species, as well as coating on different kinds of substrates, e.g. glassy carbon, which can be applicable for the applications in catalysis and energy storage.

Chapter 5
Mesoporous carbon coatings containing Pd and Pt and application in hydrogenation of 1,3-butadiene

When used as catalyst supports, mesoporous carbons can offer advantages in mass transfer and better accessibility to reactant molecules over their microporous counterparts Therefore, it is interesting to incorporate catalytically active metal species into mesoporous carbons for the preparation of the catalysts, while the ordered mesostructure is retained.
In comparison with conventional postsynthesis of catalyts loaded on carbon supports, through various methods such as impregnation,[147, 148] adsorption,[149] or ion exchange,[150] the direct incorporation of metal precursors during the synthesis of the mesoporous carbons is a very attractive procedure in terms of cost effectiveness. Furthermore, according to the previous reports,[5, 90, 101] introducing the metal precursors in situ into the carbon precursor matrix enables a homogeneous dispersion of active species throughout the carbon precursor matrix. These active species are probably stable against serious sintering at high temperature treatment.

Although much success has been achieved in the incorporation of metal component into the carbon matrix by such one-pot synthesis, the resulting carbon gels often possess no well-defined pore structure.[5] In the past few years, there have been many reports on direct incorporation of metal species into the ordered mesoporous carbons through the organic–organic self-assembly induced by triblock copolymers.[90, 91, 93, 151] Nevertheless, most of the materials are in the powder form.

On the basis of the developed synthesis method to prepare mesostructure carbon films, described in the Chapter 4, I have extended the method in order to incorporate metal active species into mesoporous carbon films through a one-pot procedure. Such catalytic films based have never been reported before.
This chapter focuses on the preparation method and catalytic testing of the coatings. The active phase (Pd and Pt particles in this case) is homogeneously dispersed in the mesoporous carbon films. The resulting catalyst coatings are tested in the gas-phase hydrogenation of 1,3-butadiene. In addition, the characterisation of the catalytic carbon coatings is also provided in this chapter.

5.1 Pd-containing mesoporous carbon coatings templated with F127

5.1.1 Preparation of precursor solution containing Pd precursor

To synthesize Pd/C films in a one-pot procedure, a stable solution containing both the RF carbon precursor, F127 as a pore template and Pd source must be employed. The preparation of this solution is similar to that of the solution for carbon films without metal, except a certain amount of the Pd source ($Pd(acac)_2$) is first dissolved in THF, and then the Pd solution is further mixed at room temperature with the RF/F127 composite gel obtained by centrifugation until an orange solution is obtained. I observed no precipitation, which indicates compatibility of all the precursor components (see Chapter 3 Experimental section for the details). The resulting solution was used for dip-coating. Catalyst films employed for testing in 1,3-butadiene hydrogenation were coated on grinded and pre-calcined steel plates using the same coating solution. All coatings on both Si-wafers and steel substrates are of high quality without any de-wetting observed. After dip-coating, the coated films were thermally treated with the same manner as described in the previous chapters (see Chapters 3 and 4). All the synthesis procedure until achieving the dip-coating solution took only about 30 min, so that this developed method seems to be practical even in large-scale application.

5.1.2 Characteristics of the films containing Pd nanoparticles (1%Pd 1/C-600)

The Pd content of the prepared films is related to the carbon fraction of the employed amounts of resorcinol and formaldehyde. Two films were prepared with Pd loadings of 0.5 and 1 wt% with respect to content of carbon in the RF precursor. The films are designated as '0.5%Pd/C-X' and '1%Pd/C-X', where 0.5%Pd and 1%Pd represent the Pd content with respect to carbon in the RF, and X represents the carbonisation temperature. In case of Pt-containing carbon films, the materials are denoted using '1%Pt/C-X'.

SEM

Figure 5.1 shows top-view and cross-section SEM images of 1%Pd/C-600, the material containing about 1%wt Pd, dip-coated at 60 mm/min and carbonised at 600°C. The top-view image recorded at a low magnification (Figure 5.1 first row) indicates high coating quality of the film. The film exhibits crack-free morphology on a large scale.

Examination of the pores from the top-view SEM images is rather difficult due to an unclear pore order of the open pores, even at a higher magnification (300000×). The FFT image shows no clear spots or rings from the SEM images (Figure 5.1 first row). However, instead of the evident presence of the pores, a few large particles with sizes in the range of 20-50 nm are observed. These large particles were investigated to be Pd.

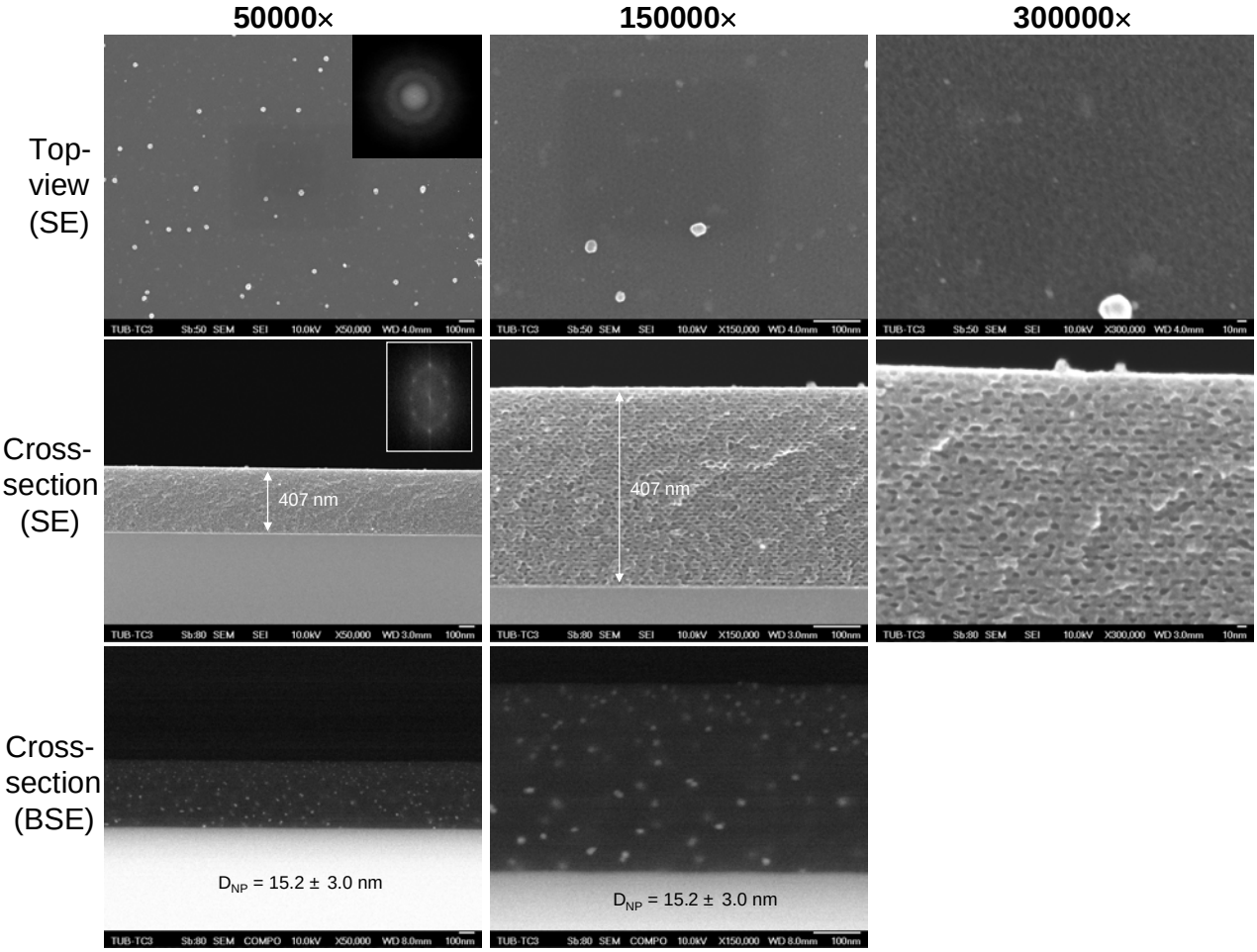

Figure 5.1. SEM images recorded at different magnifications of 50000×, 150000 × and 300000× of a Pd-containing mesoporous carbon film (1% Pd/C) prepared using F127 at a dipping speed of 60 mm/min, carbonised at 600 °C. First row: top-view secondary electron (SE) images, proving a crack-free morphology and the inset in first picture shows the corresponding FFT image. Middle row: cross-section secondary electron (SE) images, confirming the long-range periodicity and templated mesoporoes, as well as the elliptical pore shape and the inset in first picture shows the corresponding FFT image. Bottom row: cross-section back-scattered electron (BSE) SEM images corresponding to the images in the middle row, indicating highly distributed Pd particles and their uniform size of ~ 15 nm.

Cross-section SEM images in a secondary electron mode were recorded and are presented in Figure 5.1 (middle row). From the cross-section images, the thickness of the 1%Pd/C-600 film is found to be 407 nm, which is more than twice as large as the thickness of the Pd-free carbon film prepared at the same speed of 60 mm/min and carbonised at the same temperature (600 °C)(252 nm) (also see Figure 5.4). In contrast to the top-view images, a periodic pore structure is clearly observed throughout the cross-section area. A perfect pore order is further corroborated by the presence of clear spots in the FFT image (middle row, inset in the first image). The pores seen from the cross-sectional images reveal an elliptical shape, confirming the contraction in the Z direction. The diameter of the templated pores parallel to the substrate surface (XY directions or in-plane pores) is ~8 nm, similar to that of the carbon film without the particles. The average diameter of the pores in the Z direction is ~6 nm. This 6-nm pore diameter is slightly higher than that of the film without the particles (3-5 nm). From this

result, it appears that the incorporation of the Pd particles slightly increases the pore dimension in the direction perpendicular to the substrate surface. Besides the pore size, the wall thickness of 1%Pd/C-600 film (7 nm) is slightly larger than that of the film without the particles (6 nm). Furthermore, we notice the absence of a hexagonal pore geometry.

In addition to the pore morphology and size, the Pd particles have also been examined using back-scattered electron (BSE) SEM microscopy. The Pd particles with nearly uniform size are nicely dispersed throughout the matrix, as evidenced by the backscattered electron SEM images (Figure 5.1, bottom row). The averaged particle size amounted to 15.2 ± 3.0 nm. Even though these rather large particles were obtained, there is no evidence of particle agglomeration. Unlike the top-view SEM images where some Pd particles over 20 nm in diameter are found, the cross-section SEM images indicate that smaller Pd particles are formed inside the film. This observation implies the effect of confinement. This behaviour can be explained by the fact that during the pyrolysis, Pd on the external surface (the top surface of the film) sinter into larger clusters since no obstacle hinders the movement of the Pd species. This behaviour has previously been investigated for Pd containing ordered mesoporous carbons prepared through the impregnation method, where large Pd particles over 20 nm in size had been found on the external surface of the carbon support.[92]

TEM

To examine the pore structure and Pd particles of the 1%Pd/C-600 film in more detail, TEM observations were performed. Figure 5.2 illustrates TEM images of the corresponding film.

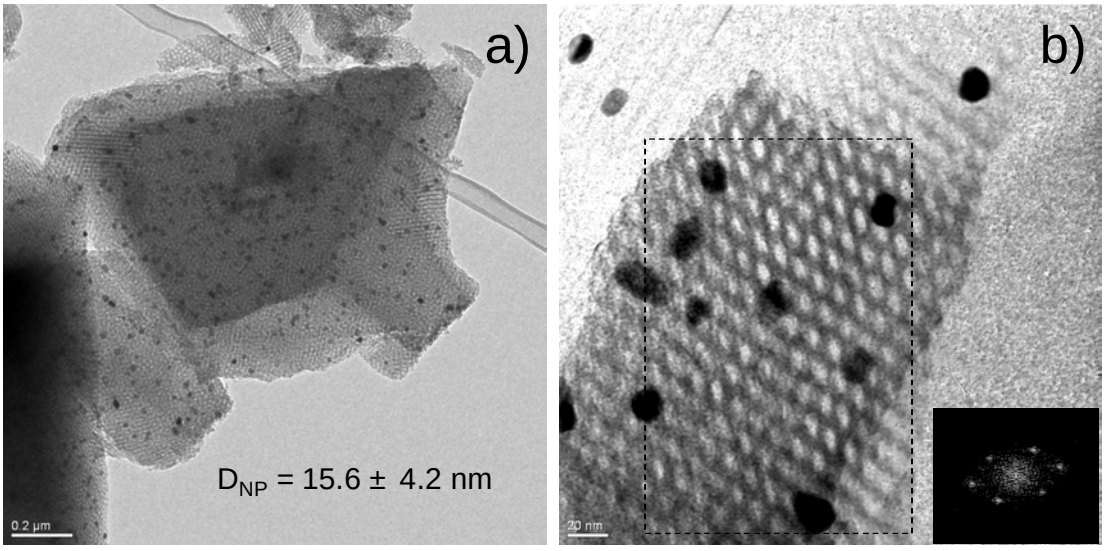

Figure 5.2. TEM images of 1%Pd/C-600 film; a) at a low magnification showing a homogeneous Pd particle distribution with an average size of ~15 nm; and b) at a higher magnification, confirming the elliptical pore shape induced by the contraction of the film: the pore size in XY direction (in-plane pore size) is about 8 nm, while that in Z direction (perpendicular to the substrate surface) is about 6 nm. The inset in b) is a FFT image of the area indicated by the dash frame, further confirming a high degree of pore order and anisotropic pores. The TEM specimen was prepared by scratching off some parts of the film with a razor blade, dispersed in ethanol and dropped on a TEM grid.

The image of Figure 5.2a proves a high degree of porosity of the film over large domains. Furthermore, a distortion of the pores is confirmed by an elliptical shape of the pores, with the pore size in long axis of ~8 nm (in-plane, XY direction parallel to the substrate surface), and that in the short axis of ~6 nm (Z direction perpendicular to the substrate surface). The FFT image made from the selected area in this image further corroborates the uni-axial contraction of the pores. These pore dimensions are in good agreement with those investigated by SEM. By investigating various domains, there is no evidence of the presence of a 2D hexagonal morphology. Therefore, according to the SEM and TEM investigation, the film possesses 3D pore morphology.

Besides the ordered pore structure and uniform pore size, Pd particles with a uniform size of ~15 nm are located inside the material wall matrix, and well dispersed throughout the material without any other larger or smaller particles. The average particle size of ~15 nm determined by TEM (Figure 5.2a,b and Figure 5.3a) is consistent with the particle diameter observed by SEM analysis.

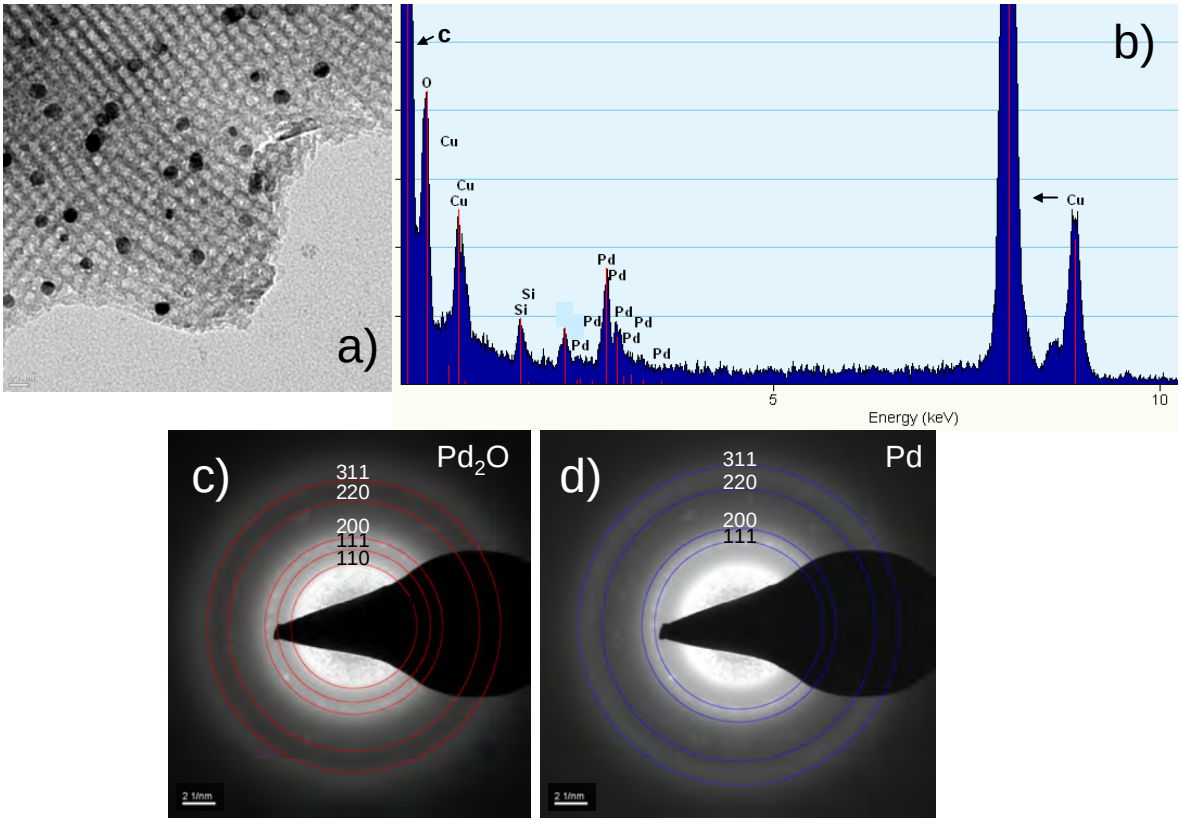

Figure 5.3. a) TEM image of 1%Pd/C-600 film, showing a homogeneous Pd particle distribution, and an ordered pore morphology. b) EDX pattern of the same sample and from a), proving the presence of Pd. The Cu signal is from the TEM grid. c) and d) SAED patterns recorded according to a). Notice that both c) and d) pictures are from the same SAED pattern, but are plotted separately to show the different diffraction rings assigned to Pd_2O (c) and Pd(0) (d), respectively.

The energy dispersive X-ray spectroscopy (EDX) analysis was carried out on the same area of Figure 5.3a, and its spectrum is shown in Figure 5.3b. The EDX pattern reveals the presence of Pd element, along with high content of carbon element, which can be attributed to the carbon matrix of the material.
TEM analysis shows that particle sizes are larger than the pore wall thickness (as determined by the SEM and TEM images to be ~7 nm both in Z and XY directions). It can be concluded that the particles are partly embedded in the carbon pore walls and the rest of them are exposed inside the mesopores. This suggests that a significant portion of the provided Pd nanoparticles is not completely embedded in the carbon pore walls, and is therefore beneficial for surface-catalytic reactions. One possible advantage of this partly embedded particle feature is that the particles are prevented from aggregation under conditions used for catalysis.
The nature and crystallinity of the Pd particles were further studied by selected area electron diffraction (SAED), and the SAED pattern is shown in Figure 5.3c,d. The SAED pattern of the material shows isotropic diffraction rings, along with a few diffraction spots on the rings. The rings positions correspond to reflections associated to both Pd(0) and Pd_2O phases (Figure 5.3d and c). According to the diffraction rings, no other possible PdO_x phases were observed. The presence of the isotropic rings indicates that the particles are composed of randomly oriented Pd(0) or Pd_2O crystallites. On the basis of TEM and SAED analysis, it can be concluded that the synthesis procedure, followed by carbonisation at 600 °C in the absence of air (under an inert atmosphere) results in the formation of both metallic Pd and Pd_2O. Due to limited number of the particles investigated by TEM, the statistic analysis on the Pd phase is difficult. High-resolution TEM (HRTEM) measurements on individual particles were carried out to investigate the nature of the particles in detail. However, the rather unclear images of the particles at high resolutions and the fact that the particles were too thick made the observation of the lattice fringes of selected particles difficult.
Due to a small content of Pd in the material, the reflections associated with Pd phases of the particles could not satisfactorily be observed using WAXS analysis.

5.1.3 Comparison between the films with and without Pd particles

To further investigate changes in the mesostructure upon adding Pd particles, a direct comparison of the SEM and SAXS analysis is performed.

SEM

Figure 5.4 compares cross-section SEM images of the material without Pd (pure carbon film) carbonised at 600 °C and 1%Pd/C-600 film. Besides a higher thickness (from 252 to 406 nm), the pore walls seem to be thicker for 1%Pd/C-600. Reasons for this increase in the film thickness can be attributed to an increase in viscosity of the dip-coating solution upon the addition of Pd precursor, and the Pd precursor could act as a catalyst itself to further polymerise the RF clusters into a bigger size.
The latter also contributes to the slight increase in the pore wall thickness. A similar behaviour has been previously observed for the synthesis of carbon aerogels catalysed by

$PdCl_2$,[125] which resulted in further polymerisation and therefore bigger domain size of the carbon aerogels.

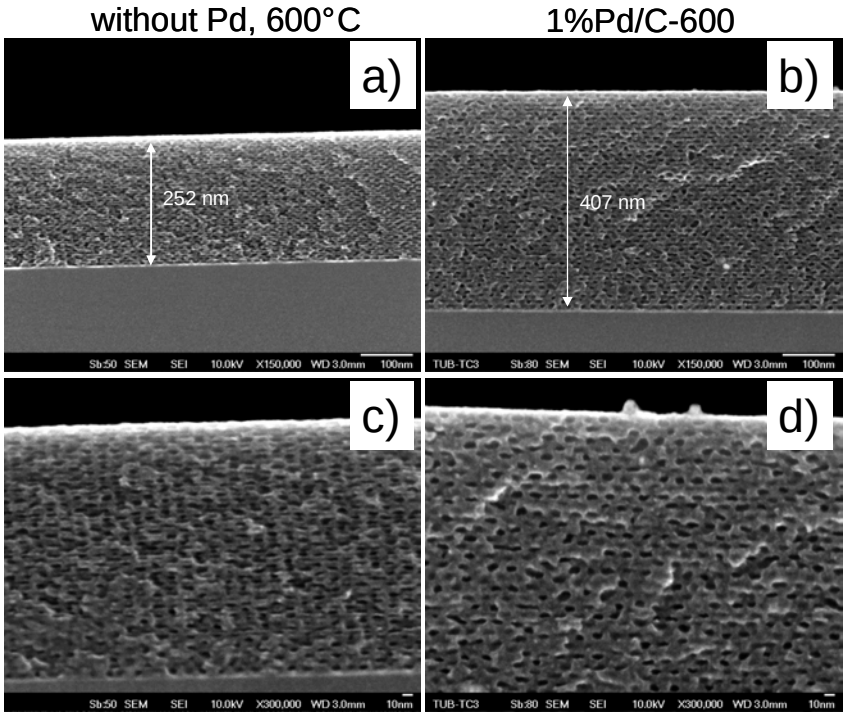

Figure 5.4. Direct comparison of cross-section SEM images. a) and c) Images of the carbon film without Pd particles recorded at magnifications of 150000× and 300000×, respectively. b) and d) Images of 1%Pd/C-600 recorded at magnifications of 150000× and 300000×, respectively. Both the samples prepared using F127 at a dipping speed of 60 mm/min, carbonised at 600 °C.

2D-SAXS: β = 20° and 90°.

To corroborate the presence of ordered mesostructure of 1%Pd/C-600 film, SAXS measurements were carried out. Figure 5.5 presents 2D-SAXS patterns of the film without the Pd particles and 1%Pd/C-600 film, both of them being prepared under the same conditions, measured at incident angles β = 20° and 90°.

The distinct in-plane scattering maxima, as well as the strong off-specular (101) reflection can be indexed in terms of a contracted BCC (*Im3m*) pore structure with (110) orientation for both the material. Nevertheless, it obvious that the 2D-SAXS pattern of 1%Pd/C-600 possesses less anisotropic feature, indicating therefore less shrinkage of the mesostructure in the Z direction. Moreover, *d*-spacings in the Z direction determined using the 2D-SAXS patterns (β = 20°) are 5.0 and 8.5 nm for the film without the Pd particles and 1%Pd/C-600 film, respectively. The values correspond to the contractions of 63% and 41%, based on the assumption that the in-plane (1-10) signals correspond to the original perfect BCC structure (without contraction) and the contraction is calculated using the equation:

$$\%contraction = \left(\frac{d_{(1-10)} - d_{(110)}}{d_{(1-10)}} \right) \times 100$$

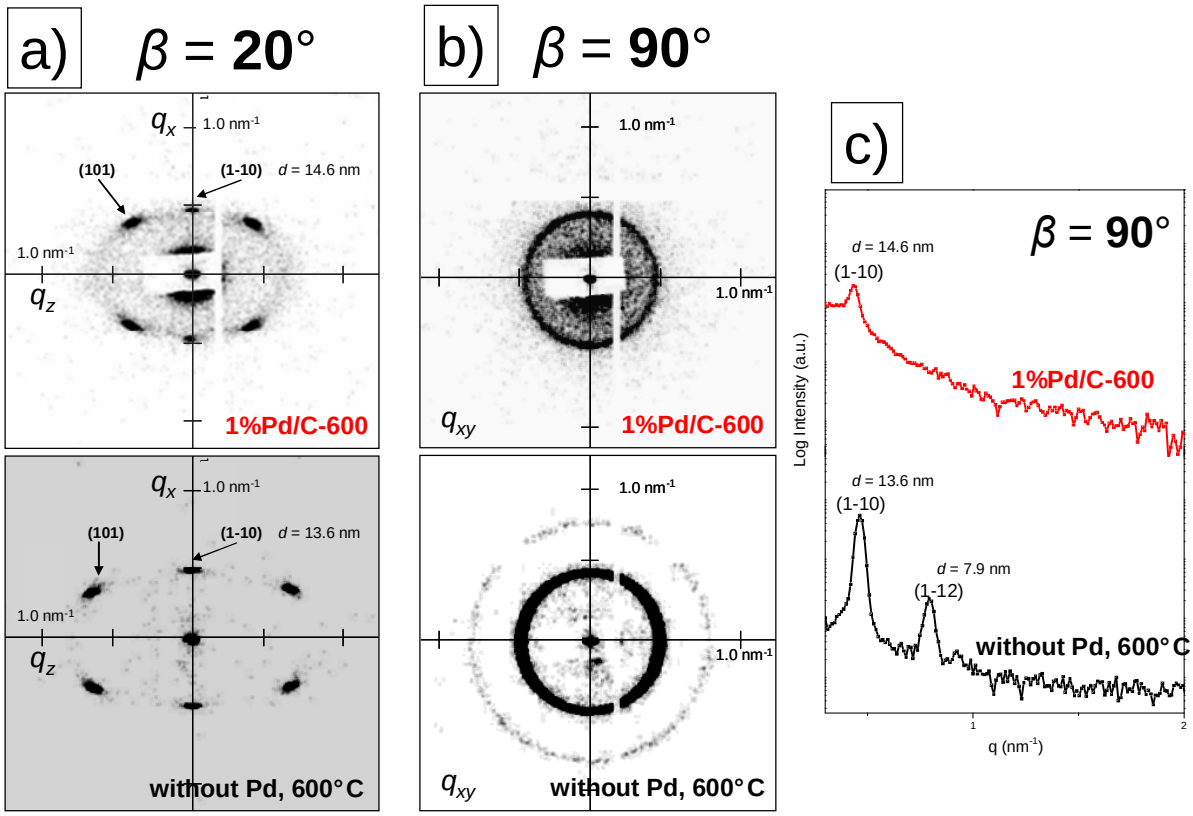

Figure 5.5. 2D-SAXS analysis in transmission configuration at two beam incident angles β = 20° (a; first column) and β = 90° (b, c; middle and last columns) of the film without Pd particles and 1%Pd/C-600 film. a) 2D-SAXS patterns recorded at an incident angle β = 20°: the reflection spots in both patterns are indexed according to the cubic BCC (*Im3m* structure) with (110) orientation. b) 2D-SAXS images recorded at β = 90°, featuring isotropic diffraction rings. c) Corresponding 1D integral curves of the patterns in b). The lattice parameter (*d*) is calculated using the expression $d = 2\pi/q$. Both the samples prepared using F127 at a dipping speed of 60 mm/min, carbonised at 600 °C.

The 2D-SAXS patterns taken at β = 90° for both the materials and their corresponding integral curves (Figure 5.5b,c; middle and last columns) show isotropic diffraction rings, which suggests the presence of polycrystalline domains parallel to the substrate surface, and high degree of in-plane ordering.

Interestingly, even though the integral curve of 1%Pd/C-600 is less resolved in comparison to that of the film without Pd counterpart, its *d*-spacing of the first reflection is slightly higher (14.6 nm vs. 13.6 nm).

Considering the fact that the pore sizes in XY direction (in-plane pore size, ~8 nm) and *d*-spacings of (1-10) reflection are almost the same in both materials), as proved by SEM and 2D-SAXS analysis, the pore wall thicknesses do not significantly differ . This observation is in good agreement with the results from SEM and TEM analysis.

The *d*-spacing values calculated from the 2D-SAXS are in agreement with those obtained by 1D-SAXS (Figure 5.6).

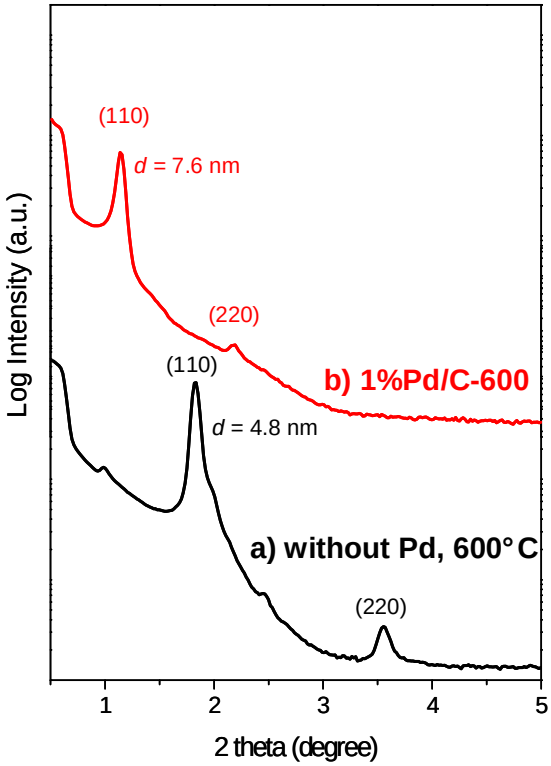

Figure 5.6. 1D-SAXS patterns of the carbon films performed in θ-2θ geometry (symmetric reflection or Bragg-Bretano geometry). a) for the film without Pd particles and b) for 1%Pd/C-600. Both the films were dip-coated at a speed of 60 mm/min under the same conditions, followed by carbonisation at 600 °C.

1D-SAXS

For both materials, two reflections are clearly observed, which can be indexed to (110) and (220) reflections according to the BCC *Im3m* mesostructure (Figure 5.6). The shift of this (110) reflection towards lower 2θ in the 1D-SAXS patterns indicates an increase in *d*-spacing with the increase in Pd content. By adding higher Pd content, the *d*-spacing is increased. This probably implies that Pd precursor can act as a catalyst for the cross-linking of the RF cluster, leading to a larger RF cluster size, and finally resulting in thicker walls. In other words, the higher content of Pd is incorporated, the thicker the pore walls could be achieved.

A film containing half of the Pd content compared to 1%Pd/C-600 (0.5%Pd/C-600) was also prepared by adding half amount of the Pd precursor compared to that for 1%Pd/C-600 film into the dip-coating solution. The Pd particle size of the 0.5%Pd/C-600 film is ~15 nm, similar to that in 1%Pd/C-600 and the particles are well distributed in the material (data not shown). The values for Pd contents measured by wavelength dispersive X-ray spectroscopy (WDX) analysis are found to be 3.1 wt% and 1.5 wt% for 1%Pd/C-600 and 0.5%Pd/C-600, respectively. Note that the Pd content for 0.5%Pd/C-600 is nearly half of that in 1%Pd/C-600, indicating that the Pd content in the carbon films can be adjusted up to 3wt%.

Since electron microscopy and SAXS do not provide insight into the accessibility of pores, Krypton adsorption was performed on 1%Pd/C-600, and its Kr-BET surface area is calculated

to be 587 m^2/cm^3, which is similar to that of carbon film without Pd particles (523 m^2/cm^3, determined by N_2 sorption shown in Chapter 4, Table 4.1). This proves that the presence of Pd particles as high as ~3 wt% does not block the accessibility to the pores.

5.1.4 Effect of carbonisation temperature on Pd particle size and mesostructure

Figure 5.7 shows SEM images of materials prepared by adding the same amount of Pd precursor (1 wt%) and at the same dip-coating speed (60 mm/min), but carbonised at different temperatures. The thickness decreases from 540 to 407 and to 320 nm as the carbonisation temperature increases from 400 to 600 and to 800 °C, respectively, while the mesopore structure is preserved in all materials, as evidenced by cross-section SEM images. The decrease in the film thickness is a typical feature of mesostructure films confined on the substrate surface upon increasing treatment temperature.
It is clear that the mesopore architecture can be retained up to the temperature treatment of 800 °C. However, the pore size in the Z direction slightly decreases to ~5 nm, compared to that of 1%Pd/C-600 (6 nm).

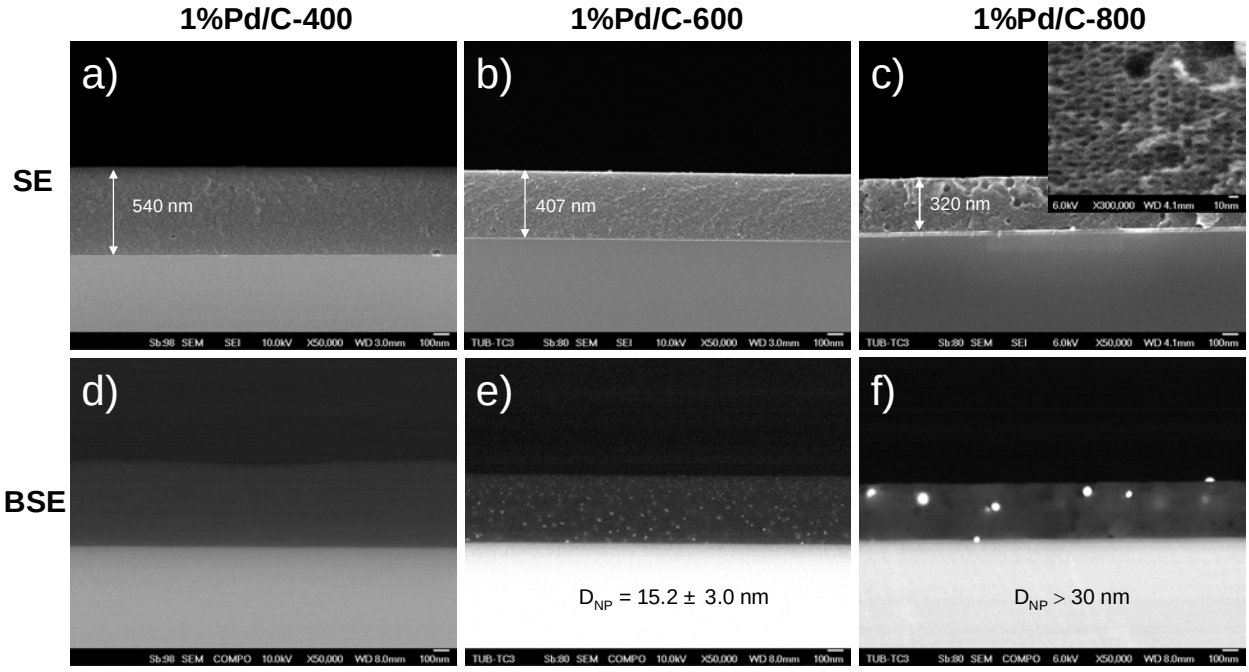

Figure 5.7. Cross-section SEM images of Pd-containing mesoporous carbon films (1%Pd/C) templated using F127 at a dipping speed of 60 mm/min, carbonised at different temperatures recorded at a magnification of 50000× in both secondary electron (SE) (a, b and c) and back-scattered electron (BSE) modes of the corresponding images (d, e and f). a) and d) Images of the film carbonised at 400 °C (1%Pd/C-400); b) and e) of the film carbonised at 600 °C (1%Pd/C-600); and c) and f) of the film carbonised at 800 °C (1%Pd/C-800). The inset in c) is a higher magnification image of 1%Pd/C-800 (300000×). The back scattered SEM images reveal the Pd particles.

Besides the retention of the mesopore structure, changes in Pd particle size were observed. By examining the back scattered cross-section SEM images, it is hard to observe Pd particles, and

then to determine the size of the particles in 1%Pd/C-400, implying that the particles must be too small to be visible with the SEM microscopy. By further increasing the carbonisation temperature, the Pd particle size increases. The average particle size of 1%Pd/C-600 is ~15 nm, while the particles of 1%Pd/C-800 are rather broad in size and possess sizes in the range 30-90 nm. The results indicate that smaller Pd particles tend to sinter into larger ones at elevated temperatures (Figure 5.7d,e,f). It is well known that at higher temperatures metallic species can migrate across a surface and aggregate to form larger particles.[100, 152] The influence of the carbonisation temperature on metal (or metal oxide) nanoparticle size incorporated in situ into soft-templated carbon supports has been previously observed by other researchers.[100, 151, 152]
Based on the findings of the influence of carbonisation temperature on the Pd particle size, we have chosen 1%Pd/C-600 as a model system for catalytic tests for 1,3-butadiene hydrogenation due to its uniform Pd particle size as well as the accessible 3D cubic mesopore structure. (preparation of the catalysts on steel substrates and their catalytic testing results will be shown in section 5.3 and 5.4).

5.1.5 Influence of subsequent temperature treatment of Pd-containing carbon films in air

Pd particles are known as one of the oxidation catalysts.[112] In the presence of oxygen, Pd particles can oxidise organic species at high temperatures. As the amorphous carbon matrix is composed of carbon, oxygen and hydrogen atoms, the stability of the carbon matrix could be affected by the Pd particles in the presence of oxygen at high temperatures.
For this reason, the influence of thermal treatment in air with a catalyst material containing Pd particles on the stability of the mesopore structure was studied.

Experiments were performed on the 1%Pd/C-600 film, which had been carbonised under an inert N_2 atmosphere, and shows a well-ordered mesopore structure and monodispersed particle distribution. The film was divided into several pieces. The pieces of the sample were subjected to heat treatment at different temperatures (400, 450 and 500 °C) for 5 min in a pre-heated muffle filled with stagnant air. The treated film materials were subsequently removed from the oven and cooled down at room temperature. Changes in the quality of the film, mesopore structure, and particle size were monitored by SEM microscopy, as shown in Figure 5.8.
By treating the material at 400 °C for 5 min, the top view SEM image of this material (Figure 5.8a) proves the formation of a few large pores with an irregular shape, which is in contrast to the top surface of the material without the treatment (1%Pd/C-600) (see Figure 5.1 for comparison). This formation of the open, large wormhole-like pores on the top surface is probably attributed to the oxidation of the top layer by oxygen, which has been similarly observed previously by Dai et al.[153] They opened the closed top surface of soft-templated mesoporous carbon membranes using an oxygen plasma exposure. Another reason could be

that the Pd particles themselves catalyse the conversion of the carbon matrix, resulting in the movement of the particles around the surrounding matrix.

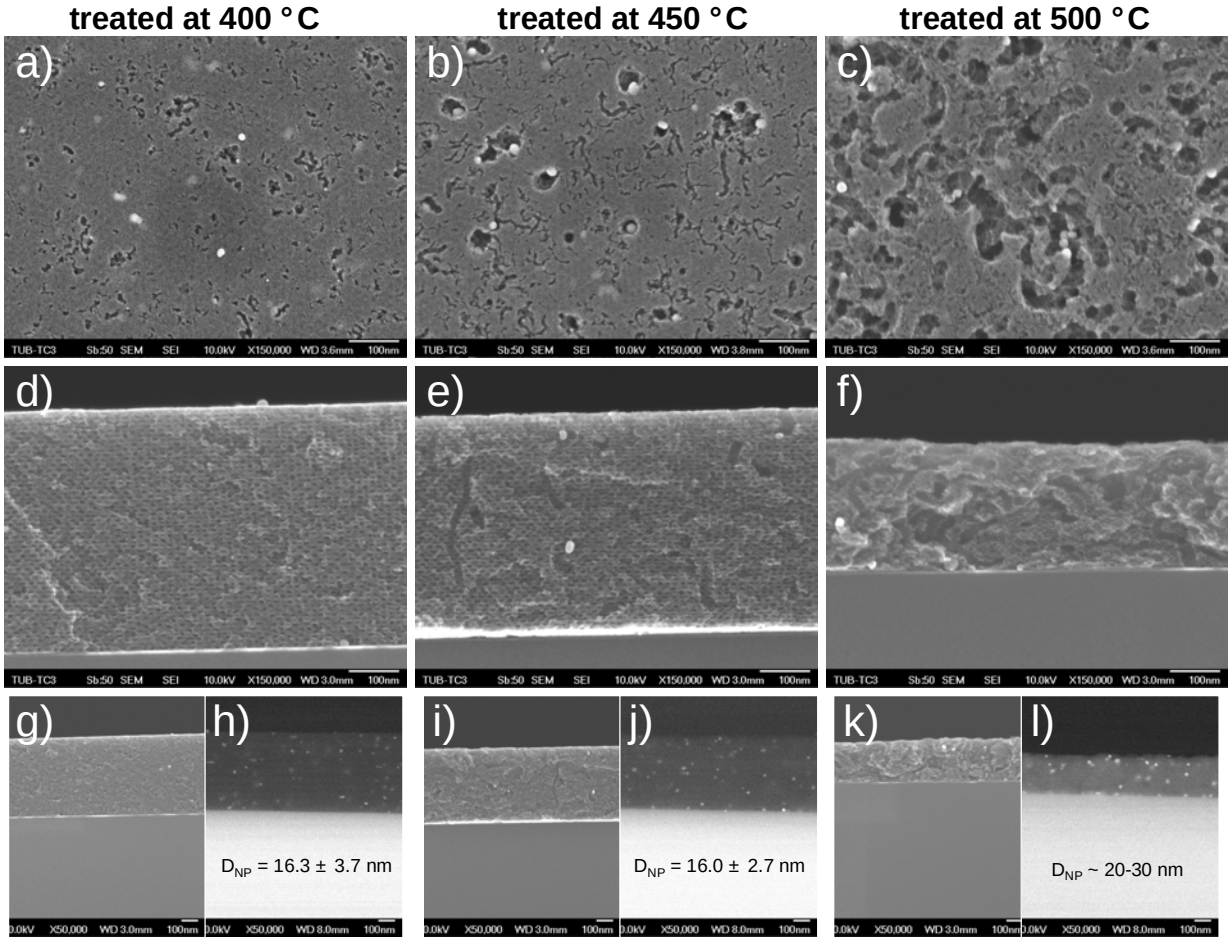

Figure 5.8. Top view (a-c) and cross-section (d-l) SEM images of Pd-containing mesoporous carbon films prepared in the identical manner as 1%Pd/C-600, followed by treatment in air at different temperatures for 5 min. a), d), g) and h) Images for the material after being treated at 400°C. b), e), i) and j) images for the material after being treated at 450°C. c), f), k) and l) Images for the material after being treated at 500°C. h), j) and l) are cross-section back-scattered electron SEM images (at a magnification of 50000×) of the corresponding images g), i) and k), respectively, showing Pd particle size and distribution.

However, the film thickness and the mesopore structure remain unchanged with the same templated pore size (8 and 6-nm pore sizes in XY and Z directions, respectively), as evidenced by the cross-section SEM image in Figure 5.8d, similar to those of 1%Pd/C-600. Moreover, the averaged particle size (~16 nm) remains similar to that of the untreated sample, and the particles are still well distributed (Figure 5.8h). Increasing the temperature to 450 °C caused further formation of the large wormhole-like pores on the top surface (Figure 5.8b). Besides that, these large wormhole-like pores are clearly seen across the film thickness (Figure 5.8e). The formation of these pores is likely to result from the movement of the Pd particles. Nevertheless, the pore structure and particle size stay unchanged (Figure 5.8e,j). Further increasing treatment temperature to 500 °C not only resulted in the formation of even larger wormhole-like pores both on top surface and across the film thickness, but also

decreased the film thickness to ~250 nm (Figure 5.8c,f). The mesopore structure seems to largely degrade. Furthermore, the Pd particles become larger with sizes of 20-30 nm (Figure 5.8i).

5.2 Pt-containing mesoporous carbon coatings templated with F127

Nanostructured Pt-containing porous carbon materials are known to be attractive candidates for electrocatalysis and various other heterogeneous reactions.[97, 149, 154, 155] In this respect, mesoporous carbons can be employed as catalyst supports for Pt particles. Therefore, facile synthesis strategies for preparation of mesoporous carbons containing Pt, especially in the form of materials coatings are desirable.

In the previous section (5.1), I have shown the facile synthesis of Pd-containing mesoporous carbon films with a 3D mesopore structure. To investigate the applicability of the facile synthesis strategy via the organic-organic self-assembly, similar materials were prepared by employing $Pt(NO_3)_2$ instead of $Pd(acac)_2$ as a metal precursor. The materials were prepared in the same way as for Pd-containing carbon films, except that $Pt(NO_3)_2$ was used as Pt source. To investigate the pore morphology and Pt particle size of the films, SEM microscopy was utilised.

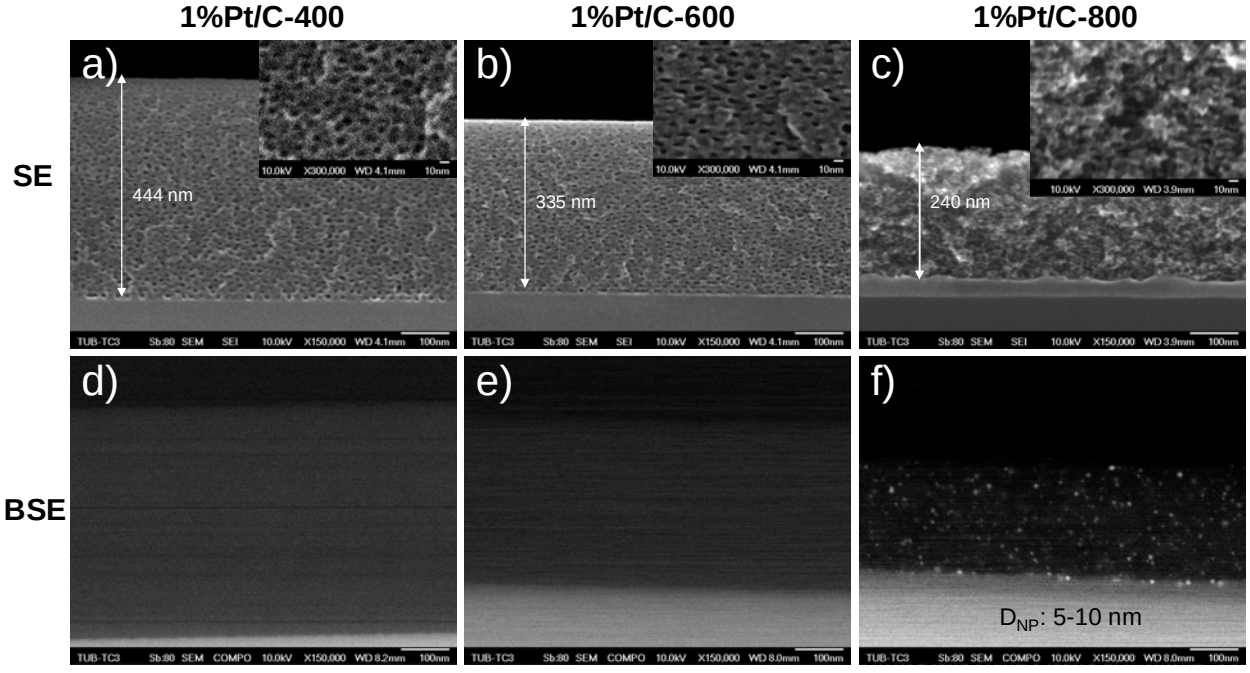

Figure 5.9. Cross-section SEM images of Pt-containing mesoporous carbon films (1%Pt/C) prepared using F127 at a dipping speed of 60 mm/min, carbonised at different temperatures recorded at a magnification of 150000× in both secondary electron (SE) (a, b and c) and back-scattered electron (BSE) modes of the corresponding images (d, e and f). a) and d) Images of the film carbonised at 400 °C (1%Pt/C-400); b) and e) of the film carbonised at 600 °C (1%Pt/C-600); and c) and f) of the film carbonised at 800 °C (1%Pt/C-800). The insets in a), b) and c) are higher magnification images of their corresponding images (300000×). f) Back-scattered SEM image of 1%Pt/C-800 reveals Pt particles sizes in the range 5-10 nm.

Figure 5.9 displays cross-section SEM images of materials prepared by adding the same amount of Pt precursor (1 wt%) and at the same dip-coating speed (60 mm/min), but carbonised at different temperatures. The film thickness decreased from 444 to 335, and to 240 nm as the carbonisation temperature increased from 400 to 600, and to 800 °C, respectively. The mesopore structure was preserved in 1%Pt/C-400 and 1%Pt/C-600, as evidenced by cross-section SEM images (Figure 5.9a,b), which is similar to that of the films containing Pd carbonised at the same temperatures. The pores in both materials posses an elliptical shape, as shown in the insets in Figure 5.9a,b. The pore sizes in long axis are ~8 nm (in-plane, XY direction parallel to the substrate surface), and those in the short axis are ~6 nm (Z direction perpendicular to the substrate surface) for both materials. In contrast, for the film carbonised at 800 °C (1%Pt/C-800), the long-range order of the templated pores seem to be lost (Figure 5.9c); yet, the templated pores can still be seen (inset in Figure 5.9c).
To investigate the Pt particle size and particle distribution, back-scattered electron SEM images were recorded for all materials, and are shown in Figure 5.9d,e,f. 1%Pt/C-800 has Pt particles with sizes of 5-10 nm are uniformly dispersed throughout the area observed without particle agglomeration, as shown in Figure 5.9f. Unfortunately, the particle size in 1%Pt/C-400 and 1%Pt/C-600 is difficult to determine probably due to the very small Pt particles, making visibility using SEM microscopy difficult.

Unlike the films containing Pd particles, the Pt-based films possess no large Pt particles formed by aggregation, even after carbonisation at 800 °C. The difference in particle size between Pt- and Pd-containing carbon films can be explained by the nature of the metals themselves. It is well-know that different surface energies of metals leads to different behaviours for the particle growth, leading to various sizes and shapes. The Pt particles smaller than 10 nm obtained in our case is consistent with the work published earlier.[97] Zhao et al. incorporated Pt particles by wet impregnation into the SBA-15 channels followed by deposition of a carbon precursor at 900 °C to encapsulate the Pt particles. They found that the embedded Pt nanoparticles were 4.0-7.5 nm in diameter, even up to loading of 20 wt %. In addition, the Pt particles were well distributed in the carbon matrix.[97] The metal growth behaviours for the Pd and Pt particles could possibly provide an explanation of the difference in the apparent mesopore structure in both 1%Pt/C-800 and 1%Pd/C-800 films.

5.3 Up scaling of Pd-containing mesoporous carbon films for preparation of catalysts on steel substrates and reproducibility

As shown in Chapter 4 (section 4.6), we successfully applied the carbon coatings onto passivated stainless steels used as substrates. In this section, this facile carbon coating procedure was extended to coatings of Pd-containing mesoporous carbon films on such stainless steel surface while retaining well-defined mesostructure. Furthermore, by applying this approach, we are able to upscale to make coatings on several steel plates. Therefore, the steel plates coated with the catalyst films could subsequently be employed as catalyst in a

chemical reactor for testing of 1,3-butadiene hydrogenation (shown later in the catalytic results, section 5.4).

Coupons of stainless steel with three different thicknesses (0.5, 0.25 and 0.1 mm) (material number 1.4301, AISI 304, X5CrNi18-10) cut to 30 x 27 mm dimensions in width were used as substrates. The procedure to treat and passivate the steel surface is shown in Chapter 3. After being polished/grinded and passivated, the steel plates have a surface roughness (R_a) of ~0.55 µm.

The preparation of the dip-coating solution and the film synthesis of the coatings on the steel plates are the same as those for 1%Pd/C-600. Once the fresh dip-coating solution was prepared, the dip-coating was performed on Si-wafer and several steel plates. The same solution was used throughout the dip-coating procedure. Figure 5.10 schematically presents the dipping sequence of all substrates. After dip-coating all substrates, no change in colour and viscosity of the solution was observed. Homogeneous films were observed for all the substrates. The films covered the coated area of the substrates throughout the coating process, thermal polymerisation as well as carbonisation of the films.

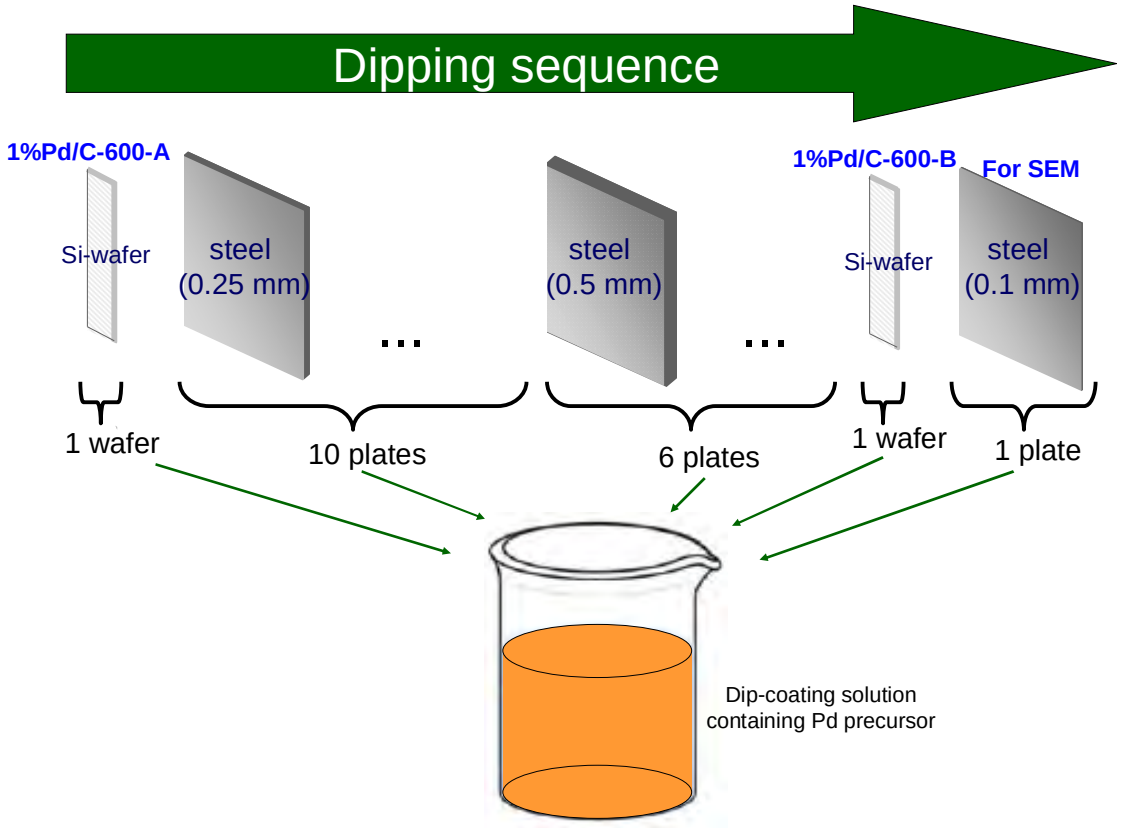

Figure 5.10. Scheme showing the sequence of the dipping procedure. Corresponding samples prepared on Si-wafers are denoted as 1%Pd/C-600-A (the first dipping in the sequence) and 1%Pd/C-600-B (the sample prepared after dipping of several steel plates). The dipping of a steel plate of 0.1 mm-thickness was used for SEM analysis.

To ensure the retention of the mesostructure integrity and particle distribution of the coated, SEM microscopy and 1D-SAXS analysis were carried out. The samples prepared on Si-wafers are denoted as 1%Pd/C-600-A and 1%Pd/C-600-B (see Figure 5.10 for the dipping sequence).Both the 1%Pd/C-600-A and 1%Pd/C-600-B as well as one prepared on a 0.1 mm steel plate possess no macroscopic cracked in a micrometer area, as observed by top-view SEM (data not shown).

Figure 5.11 shows top-view and cross-section SEM images of the 1%Pd/C-600-A and 1%Pd/C-600-B films prepared using the same solution. Note that it took about 1 h before the solution was used to dip-coat 1%Pd/C-600-B.

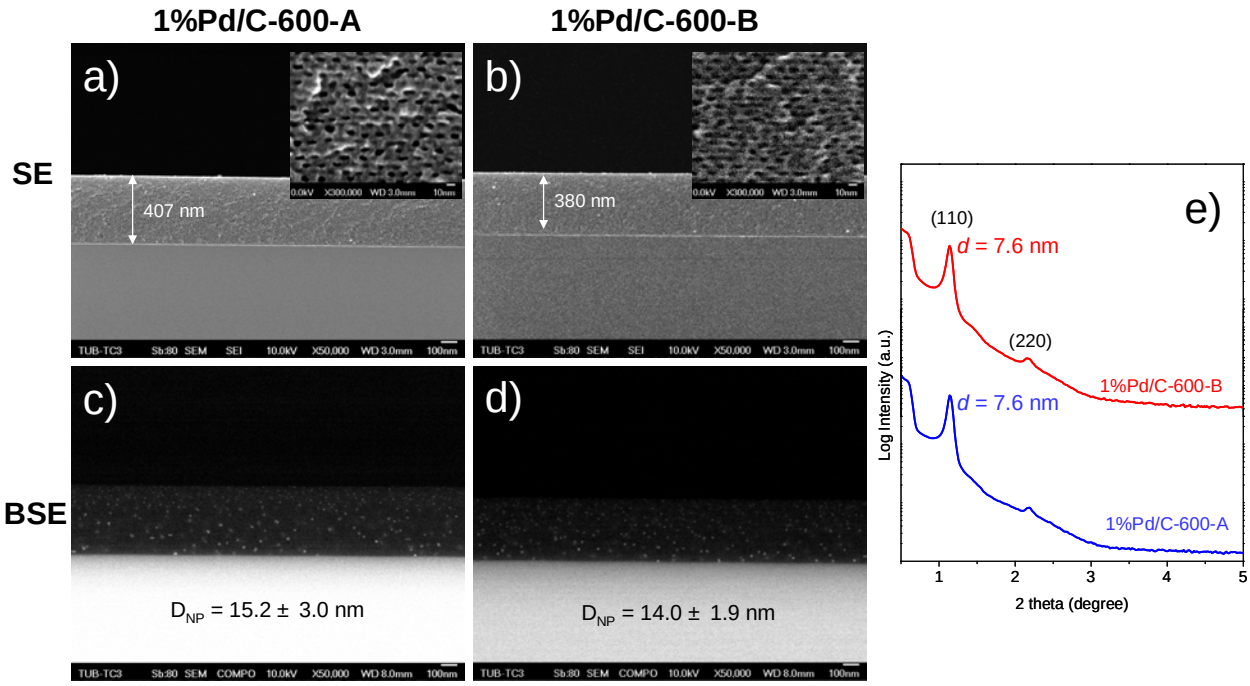

Figure 5.11. Cross-section SEM images (recorded at a magnification of 150000×) and 1D-SAXS patterns of Pd-containing mesoporous carbon catalyst films, 1%Pd/C-600-A and 1%Pd-C-600-B (see Figure 5.10 for the dipping sequence). The films were prepared on Si-wafers using F127 at a dipping speed of 60 mm/min, carbonised at 600°. The images were recorded in both secondary electron (SE) (a, b) and back-scattered electron (BSE) modes of the corresponding images (c, d). a) and c) Images of 1%Pd/C-600-A; b) and d) 1%Pd/C-600-B. The insets in a) and b) are higher magnification images of their corresponding images (300000×). e) 1D-SAXS patterns of 1%Pd/C-600-A (blue curve) and 1%Pd/C-600-B (red curve).

Both 1%Pd/C-600-A and 1%Pd/C-600-B films possess similar film thicknesses of 407 and 380 nm, respectively. (Figure 5.11a,b). Furthermore, the high magnification SEM images (insets in Figure 5.11a, b) confirm that the cubic mesostructure and porosity, pore size (~6 nm for off-plane pores (Z), and ~8 nm for in-plane pores (XY)), are well retained for the 1%Pd/C-600-B film, even after dip-coating 16 steel plates. Back-scattered SEM images (Figure 5.11c,d) reveal the similarities in Pd particle size distribution and size (~14-15 nm) for both the materials.

In addition, 1D-SAXS analysis on both films (Figure 5.11e) further reveals no change in mesostructure ordering and contraction behaviour, as evidenced by the fact that the *d*-spacings for the first reflection (110) of both films are found to be identical (*d*-spacings = 7.6 nm), proving the retention of a cubic *Im3m* mesostructure.

Dip-coating of a steel plate with a thickness of 0.1 mm was done with the identical solution in order to cut the film and investigate influence of steel surface on pore structure and particles. To record cross-section SEM images of the film coated on this steel plate, the substrate was cut by scissors. This led to breaking of the film; yet, the film did not seriously delaminate from the substrate. The SEM image at a low magnification (Figure 5.12a) shows the cracked, but deposited film on the steel substrate. While the substrate surface is rough to some extent, the carbon film has a constant thickness (~400 nm) throughout the area observed, the thickness being similar to that of the film coated on Si-wafer. High magnification SEM images, as well as the FFT image in the inset prove the retention of the pore order of the film, as shown in Figure 5.12c.

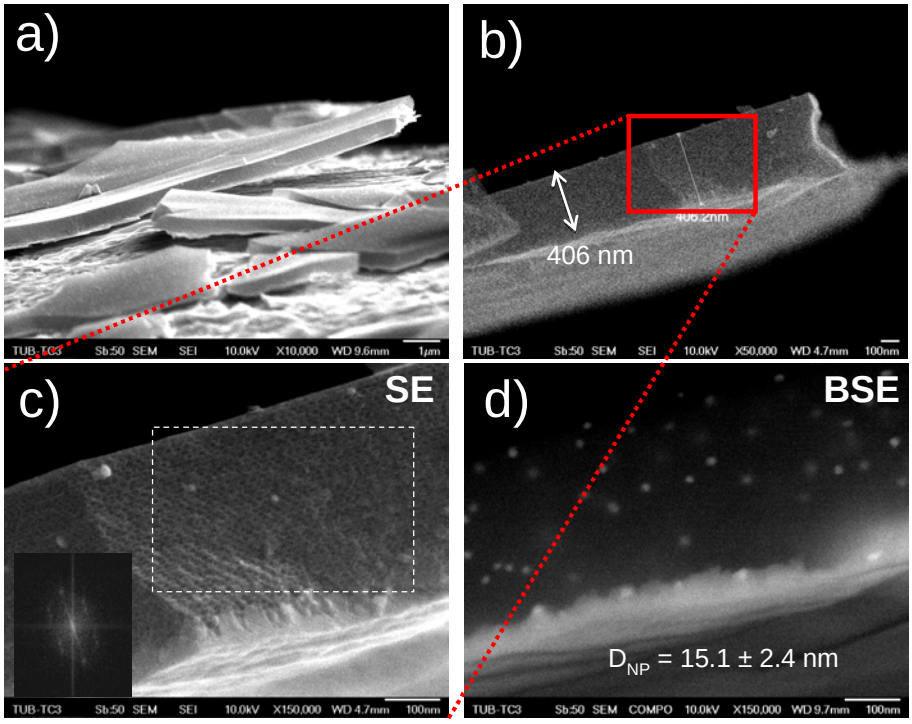

Figure 5.12. SEM images of the Pd-containing carbon film prepared on a 0.1 mm-thick steel plate with the same solution as for the films on Si-wafers, recorded at different magnifications of a) 10000×, b) 50000×, c) and d) 150000×. The film was prepared using F127 at a dipping speed of 60 mm/min, carbonised at 600 °C. a) SEM image, showing both the cracked film caused by cutting and bending of the substrate, and the substrate roughness. b) SEM image (50000×) recorded to see the film cross-section area. c) SEM image at a higher magnification, corresponding to the area highlighted in b), proving the pore ordering throughout the cross-section area. The inset in c) is a FFT image of the area indicated by the dash frame, further confirming a high degree of ordering and anisotropic pores. d) Back-scattered (BSE) SEM image of the corresponding image c), revealing well-distributed Pd particles and an averaged particle size of ~15 nm.

Beside the observed pore order throughout the cross-section area, the pore sizes in both the short and long axes (Z and XY) are observed to be ~6 and ~8 nm, similar to those of the film on Si-wafers. The back-scattered cross-section SEM image (Figure 5.12d) confirms the well-distributed Pd particles with an averaged size of ~15 nm.
The retention of mesopore structure, Pd particle size and distribution on the steel substrates, compared to Si-wafer counterparts, indicates that the dip-coating process is not affected by the scratch texture produced on the steel substrates by grinding used in this study.

In summary, the synthesis method developed in this thesis for Pd-containing mesoporous carbon catalyst films can be extended to coatings on practical steel substrates to be used in a chemical reactor. By using the identical dip-coating solution, several pre-treated steel substrates can be coated, while the mesopore structure and uniform Pd particle size (~15 nm) and good particle distribution can be retained, proving reproducibility of the synthesis procedure. Furthermore, the dip-coating solution is not degraded during the dip-coating of several steel plates, and is stable over a certain period of time (~1 h). The period of dip-coating all the materials presented here is comparatively short, providing advantages to the practical applications in the large scale synthesis.

5.4 Hydrogenation of 1,3-butadiene catalysed using Pd-containing mesoporous carbon catalyst coatings

The catalytic activity and selectivity of the Pd-containing mesoporous carbon catalyst coatings on steel plates were tested in gas-phase hydrogenation of 1,3-butadiene, a reaction relevant to industrial applications.[106, 107]

The first set of experiments was carried out using 5 steel plates (thickness of the substrates is 0.5 mm) coated with Pd-containing mesoporous carbon coatings (prepared in an identical manner to 1%Pd/C-600). The catalyst coatings after carbonisation at 600 °C under N_2 atmosphere with the film thickness of 406 nm and the total catalyst volume of 3.24 mm^3 were first used without further modification and denoted as '*as-made*' materials.
Figure 5.13a depicts 1,3-butadiene conversion as a function of reaction temperature, and Figure 5.13b shows product selectivity plotted versus the conversion. The 1,3-butadiene conversion increased with the reaction temperature and reached about 9% at 80 °C (Figure 5.13a,■). In contrast to such rather low conversion of the as-made catalysts, the selectivity towards all butene products (1-butene, *trans*-2-butene and *cis*-2-butene) is more than 90% over the range of conversions studied, although ~5% of *n*-butane is still observed, as shown in Figure 5.13b.
The conversion of ~9% at 80 °C for the catalyst set studied here is similar to that (~10%) performed using Pd-containing porous TiO_2 coatings reported in the literature.[122] Moreover, the selectivity towards 1-butene for the catalyst set here is about 52-55%, which is in accordance with values reported in for the Pd-containing TiO_2 catalysts in a conversion range

between 0-60% (Figure 5.13,green dash frame).[113, 122] The Arrhenius plot made for this set of the catalysts in the 40-80 °C interval were fitted by a straight line and yields the activation energy (E_a) of 48 kJ/mol from the slope. Values reported in literature range from 62 kJ/mol for Pd/TiO_2[122] to 48-66 kJ/mol[156] and 75 kJ/mol[111] for Pd/Al_2O_3.

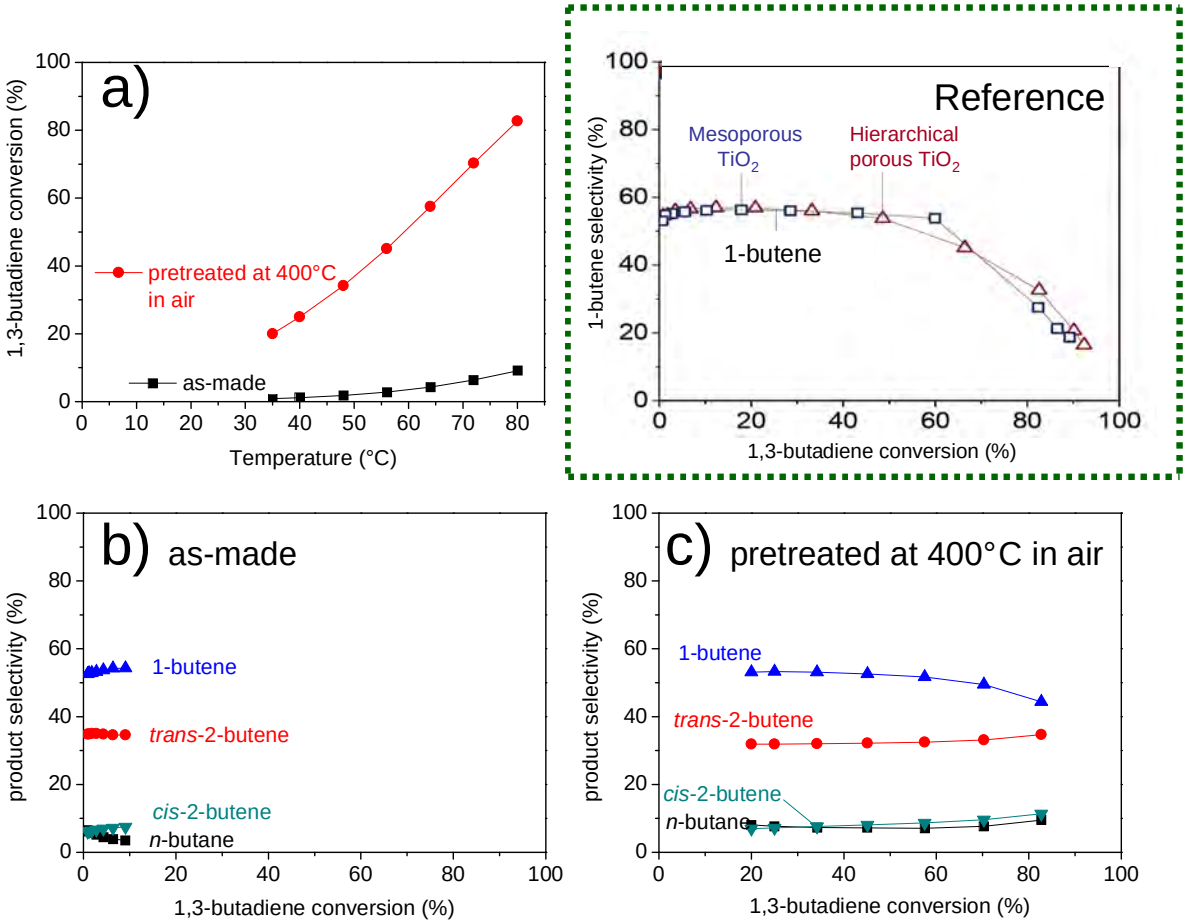

Figure 5.13. Catalytic performance of Pd-containing mesoporous carbon catalyst coatings assembled with 5 steel plates (0.5 mm-thick). The materials were prepared according to the identical procedure for 1%Pd/C-600; those used without further modification denoted as '*as-made*' and those followed by treatment in air at 400 °C for 5 min denoted as '*pretreated at 400 °C in air*'. a) 1,3-butadiene conversion as a function of the reaction temperature: (■) conversion using the as-made coatings, (●) conversion using the same coatings after heat-treatment in air at 400°C for 5 min. b) Selectivity to reaction products using the '*as-made*' materials as a function of conversion. c) Selectivity to reaction products using the materials treated at 400°C in air for 5 min as a function of conversion. The green dash frame depicts selectivity to 1-butene of mesoporous TiO_2 and hiierarchical porous TiO_2 from literature: for comparison.[122]

Nevertheless, the conversion at the maximum temperature tested (80 °C) is still rather low. One possible reason for this could be related to accessibility of the active Pd particles. Based on the SEM and TEM analysis previously shown, the Pd particles could be partly trapped in the pore walls of the carbon matrix or be covered by a thin carbon layer.

For this reason, the catalysts were treated in air in an attempt to remove carbon layers possibly covering the Pd particles. The treatment was performed at 400 °C for 5 min. This temperature was chosen on the basis of observations presented in the pervious section (section 5.1.5). Treating the catalysts at over 450 °C in air destroyed the mesopore structure and led to

larger particles (see Figure 5.8). The treatment of the as-made catalysts at 400 °C for 5 min led to no change in mesopore structure, particle size and distribution, but to active particles. The as-made catalysts followed by this heat-treatment are then denoted as '*pretreated at 400 °C in air*'.

The treated materials were subsequently tested again for hydrogenation of 1,3-butadiene. The treated catalyst set shows higher conversion (more active) for all reaction temperatures, and the highest conversion can even 82% at 80 °C (Figure 5.13a,●). After the air-treatment, the conversion increased from 1% to 20%, 2% to 45%, and 9% to 82%, for the reaction temperatures of 35, 56, and 80 °C, respectively. The Arrhenius plot made for this set of catalysts yields a lower activation energy (E_a) of 31.5 kJ/mol. Moreover, the treated catalysts are still selective towards butene products with small *n*-butane amounts of ~5%, similar to the as-made catalysts without treatment (Figure 5.13c).

For the as-made catalyst set, the trapped particles might have no accessibility to the reactant molecules, leading to low activity of the catalyst. This similar low activity for metal-containing mesoporous carbons prepared by in situ incorporation via soft-templating has been previously observed.[104, 157] For example, Ji et al. synthesized Ru-containing soft-templated ordered mesoporous carbons prepared through the EISA method. The Ru particles were wrapped with carbon, which made them not contact with the reactant molecules during benzene hydrogenation.[104]

As shown in the previous section, the coating of many steel plates is possible using the identical dip-coating solution without changes in mesopore structure, particle size and particle distribution (see section 5.3). To increase 1,3-butadiene conversion in the catalytic reactor, a larger number of the catalyst plates (10 plates) was then introduced in the same reactor. The experiments were performed using 10 steel plates (thickness of the substrates is 0.25 mm) coated with Pd-containing mesoporous carbon coatings (prepared in an identical manner to 1%Pd/C-600, and the catalyst set assembled with 5 steel plates).

The catalytic performance of the set of Pd-containing mesoporous carbon catalyst coatings assembled with 10 steel plates (0.25 mm-thick) in the reactor for gas-phase hydrogenation of 1,3-butadiene is illustrated in Figure 5.14.
As expected, this set of the as-made catalysts (10 plates) prior to the heat treatment in air show more than 2 times higher 1,3-butadiene conversion than the as-made catalyst set assembled with 5 plates for all reaction temperatures (Figures 5.14a,■). By substituting 5 plate-catalyst set with 10 plate-counter part, the conversion increased from 1% to 4%, 2% to 8%, and 3% to 12%, for the reaction temperatures as low as 35, 48, and 56 °C, respectively. The activation energy from the Arrhenius plot for this catalyst set is calculated to be 40.4 kJ/mol. The selectivity towards butene products is similar to that obtained using the 5-plate catalyst counterpart (compare Figures 5.13b and 5.14b) for the range of 1,3-butadiene conversion.

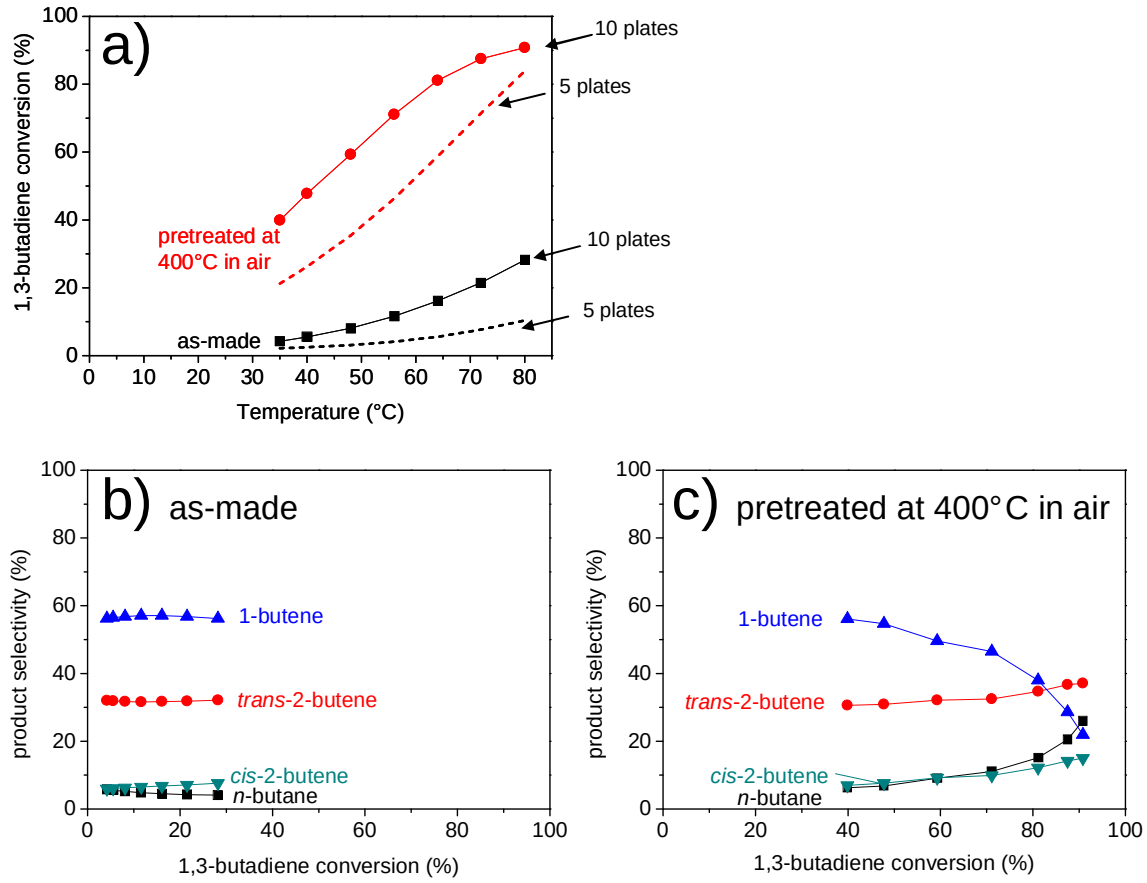

Figure 5.14. Catalytic performance of Pd-containing mesoporous carbon catalyst coatings assembled with 10 steel plates (0.25 mm-thick). The materials were prepared according to the identical procedure for 1%Pd/C-600; those used without further modification denoted as '*as-made*' and those followed by treatment in air at 400 °C for 5 min denoted as '*pretreated at 400 °C in air*'. a) 1,3-butadiene conversion as a function of the reaction temperature: (■) conversion using the as-made coatings, (●) conversion using the same coatings after heat-treatment in air at 400°C for 5 min. The dash lines in a) show direct comparison with the results from the 5-steel plate set. b) Selectivity to reaction products using the '*as-made*' materials as a function of conversion. c) Selectivity to reaction products using the materials treated at 400°C in air for 5 min as a function of conversion.

Similar to the 5-plate catalyst series, after the treatment in air at 400 °C for 5 min, the 'treated' catalyst set assembled with 10 plates gave much higher conversion that the as-made counterpart and the maximum conversion of ~90% can be obtained at 80 °C. The conversion increased from 4% to 40%, 12% to 71%, and 28% to 90%, for the reaction temperatures of 35, 56, and 80 °C, respectively (Figure 5.14a,■ and ●). The selectivity towards all butene products of the treated catalyst set in the range of 1,3-butadiene conversion of 40-50% (Figure 5.14c) still resemble that of the as-made catalyst set for the range of conversion of 4-30% (Figure 5.14b). Furthermore, the selectivity towards 1-butene of ~55% in those conversion regions of both catalyst sets is in line with values reported by previous work on other Pd-containing catalysts.[113, 122] Nevertheless, when high 1,3-butadiene conversion (> ~50%) was achieved, a gradual decrease in the selectivity towards 1-butene was observed in favour of *n*-butane production (Figure 5.14c,▲ and ■). These observations are consistent with the typical behaviour of Pd-based catalysts reported in literature,[158] and can be explained by secondary reactions that further hydrogenate 1-butene or isomerisation of 1-butene.

All the catalysts reported here are stable under reaction conditions, and feature identical activity and selectivity even after several hours, after repeated cycle runs under identical reaction conditions.

In summary, the developed Pd-containing mesoporous carbon catalysts coated on steel substrates approach prove to be highly active and selective in gas-phase hydrogenation of 1,3-butadiene. Their obtained activity and selectivity are comparable to those of catalysts previously reported in literature. Modification by heat-treatment in air at 400 °C results in catalysts with higher conversion as a result of their accessible Pd active particles, while still showing high selectivity. Using more steel plates coated by the Pd-containing mesoporous carbon catalysts in a reactor results in higher conversion, whereas the high selectivity towards butene products can be retained.

5.5 Conclusions

On the basis of facile synthesis approach to ordered mesoporous carbon films with a cubic mesopore architecture (*Im3m*) shown in Chapter 4, the synthesis to ordered mesoporous carbon films containing Pd or Pt particles was successfully extended. The one-pot synthesis employs RF as a carbon precursor, F127 polymer as a structural directing template and $Pd(acac)_2$ or $Pt(NO_3)_2$ as Pd and Pt sources, respectively. Carbonisation temperature was found to have an effect on the particle size for both Pd- and Pt-containing materials. For the Pd-containing carbon film after carbonisation at 600 °C, a Pd loading as high as 3 wt% can be achieved while the *Im3m* mesopore structure, a desirable structure for 2D-confined materials, a high Kr-BET surface area, as well as an uniform Pd particle size (~15 nm), and good particle distribution are obtained. Such synthesis procedure for this material also enables coating of stainless steel substrates, which is the most common reactor material for applications in catalysis. The Pd-containing mesoporous carbon coatings on the steel substrates possess identical features to those on Si-wafer counterparts, and have subsequently been applied to catalytic tests for gas-phase hydrogenation of 1,3-butadiene. The catalytic coatings prove to be active and selective to butenes.
The approach to the synthesis of catalytic coatings based on ordered mesoporous carbons reported in this thesis represents a modular concept for catalytic coatings based on soft-templated mesoporous carbon supports. These experiments have primarily been conducted as proof-of-principle experiments to demonstrate possibility of employing these coating materials as catalyst supports. Further improvements can be performed to obtain high conversion. Moreover, the flexibility of this synthesis approach can readily be extended to incorporate other metal species to suit different applications.

Chapter 6
Conclusion and outlooks

In this thesis, a facile synthesis method for the preparation of mesoporous carbons in film morphology has been developed. The synthesis strategy is based on soft-templating principles using resorcinol-formaldehyde (RF) as a carbon precursor and amphilphilic block-copolymers (F127, PIB-PEO 3000, and 10k-PB) as structural directing soft-templates.
Aiming at a desirable morphology (3 dimensional mesostructure) confined on 2D substrates, the synthesis procedure for the bulk mesoporous carbon powders prepared under acidic conditions was refined and adapted to control the desired morphology.

The film morphology of the resulting mesoporous carbons is achieved by the dip-coating technique through the evaporation-induced self-assembly (EISA) process, followed by thermopolymerisation, and carbonisation at higher temperatures to remove the templates and convert the cross-linked RF into the carbon matrix.

The resulting crack-free films synthesised using F127 as a template possess a contracted 3D cubic mesostructure (*Im3m*). The materials reveal a uniform pore size, and an elliptical mesopore shape due to the contraction in the direction perpendicular to the substrate surface (Z direction). By increasing carbonisation temperature from 400 to 600, and to 800 °C, the pore size in the direction perpendicular to the substrate (off-plane pores, Z direction) decreases from ~6 nm, to ~5 nm, and ~4 nm, respectively, while the pore size in the direction parallel to the substrate surface (in-plane pores, XY direction) is retained as ~8 nm in diameter. By increasing the withdrawal speed of dip-coating, the film thickness of the film carbonised at 600°C also increases, and can be tuned in the range ~250-820 nm. Moreover, the increase in the withdrawal speed of dip-coating has no influence on the mesostructure of the thicker films. The films templated with F127 possess accessible porosity (up to 520 m^2/cm^3 and 0.45 cm^3/cm^3 for N_2 BET surface area, and pore volume, respectively).

The templated pore size can be tuned up to ~20 nm (in-plane pores) by choice of the polymer templates using PIB-PEO 3000 and 10k-PB polymers, and 3D mesopores are still obtained.
For the films templated with PIB-PEO 3000, an increase in withdrawal speed of dip-coating increases the film thickness up to 640 nm, but however influences the mesostructure order.

In Chapter 5, the synthesis procedure has been extended to the synthesis of mesoporous carbon films containing Pd or Pt particles through one pot in situ incorporation of Pd or Pt precursors. The synthesis employs F127 as a template and yields high quality, uniform mesoporous carbon coatings containing either Pd or Pt particles. For the Pd-containing carbon films, a Pd loading as high as 3 wt% is successfully incorporated after carbonisation at 600

°C, while the contracted *Im3m* mesopore structure with the uniform pore sizes of ~8 nm in the XY direction and ~6 nm in the Z direction, can be kept intact. In addition, a thickness of ~400 nm, high Kr-BET surface area of 587 m^2/cm^3, and well-distributed Pd particles with a uniform size of ~15 nm can be obtained. The synthesis procedure for this Pd-containing mesoporous carbon film has been adopted to prepare coatings on polished and precalcined steel plates, which are used as substrates in a catalytic reactor. The synthesis of the catalyst coatings containing Pd particles is comparably simple and short. Therefore, this allows for up scaling for several steel plates, while the catalyst coatings on the steel plates still possess identical features (both mesopore structure, and Pd particles) to those on Si-wafer counterparts. The Pd-containing mesoporous carbon coatings on the steel plates have been tested for gas-phase hydrogenation of 1,3-butadiene. In order to achieve a high activity additional activation in air at 400 °C is required. The catalyst coatings prove to be highly active with the conversion of ~80% at a reaction temperature of 80°C, and high selectivity to butenes of up to ~95%.
The performance of the catalytic reactor can even be improved by applying a higher number of the catalyst plates into the reactor, while the high selectivity remains almost unchanged.

This synthesis approach to catalytic coatings based on ordered mesoporous carbons and the 1,3-butadiene hydrogenation testing reported in this thesis represent a modular concept for catalytic coatings based on the soft-templating principles for carbon materials. Therefore, other gas-phase hydrogenation reactions can be tested by employing catalyst coatings developed here in order to gain insight into the feasibility of applying the coatings for other catalytic reactions. An increase in the film thickness for the mesoporous catalyst coatings, while keeping the mesostructure could also be achieved, so that further studies on the influence of film thickness on the performance of gas-phase reactions can be investigated.

According to the synthesis presented in this thesis, possible further developments can be carried out. For example, preformed colloidal Pd or Pt particles with controlled particle size can be prepared, followed by the incorporation into dip-coating solutions.[122] This could lead to a better control of particle size of nanoparticles. Incorporation of other metal species in situ can be an option to modify mesoporous carbon coatings for various types of catalytic applications.

Alternative carbon precursor and polymerization catalysts containing nitrogen provide the option to also generate nitrogen-doped carbons, materials applicable to electrocatalysis,[155, 159, 160] in a simple one-pot synthesis.[161, 162] Furthermore, the N-doped mesoporous carbons can lead to a very stable and uniform dispersion of Pd nanoparticles, as demonstrated for powder materials.[163] This concept can be directly applied to the system reported in the thesis with an aim to better control Pd or Pt dispersion in the film matrix.

Moreover, the concept of micelle-templated mesopores can be combined with strategies of macro-pore formation, resulting in hierarchical meso-macroporous carbon materials.[164]

This strategy can be employed to prepare hierarchical meso-macroporus carbons in the form of films, which could be beneficial to the diffusion control.

Finally, the mechanisms of self-assembly and the chemical interactions between precursors and templates as well as the influence of the preparation conditions deserve further investigation, since the mechanistic understanding can guide the rational development of improved precursors and templates and more robust synthesis strategies for the preparation of mesostructure carbon films.[26, 55]

References

[1] M. Ströck, *GNU Free Documentation License* **2006**.

[2] H. Marsh, *Introduction to Carbon Science* **1989**, Butterworth.

[3] A. Oya, S. Yoshida, J. Alcanizmonge, A. Linaressolano, *Carbon* **1995**, *33*, 1085.

[4] T. Kyotani, *Carbon* **2000**, *38*, 269.

[5] J. Biener, M. Stadermann, M. Suss, M. A. Worsley, M. M. Biener, K. A. Rose, T. F. Baumann, *Energy & Environmental Science* **2011**, *4*, 656.

[6] D. S. Su, S. Perathoner, G. Centi, *Catalysis Today* **2012**, *186*, 1.

[7] R. C. Bansal, J. B. Donnet, F. Stoeckli, *Active Carbon* **1988**, Marcel Dekker.

[8] A. Stein, Z. Y. Wang, M. A. Fierke, *Advanced Materials* **2009**, *21*, 265.

[9] M. Antonietti, G. A. Ozin, *Chemistry – A European Journal* **2004**, *10*, 28.

[10] J. Lee, J. Kim, T. Hyeon, *Advanced Materials* **2006**, *18*, 2073.

[11] A. H. Lu, F. Schuth, *Advanced Materials* **2006**, *18*, 1793.

[12] C. D. Liang, Z. J. Li, S. Dai, *Angewandte Chemie-International Edition* **2008**, *47*, 3696.

[13] Y. Wan, Y. F. Shi, D. Y. Zhao, *Chemistry of Materials* **2008**, *20*, 932.

[14] Y. Meng, D. Gu, F. Q. Zhang, Y. F. Shi, L. Cheng, D. Feng, Z. X. Wu, Z. X. Chen, Y. Wan, A. Stein, D. Y. Zhao, *Chemistry of Materials* **2006**, *18*, 4447.

[15] Y. S. Hu, P. Adelhelm, B. M. Smarsly, S. Hore, M. Antonietti, J. Maier, *Advanced Functional Materials* **2007**, *17*, 1873.

[16] L. Z. Fan, Y. S. Hu, J. Maier, P. Adelhelm, B. Smarsly, M. Antonietti, *Advanced Functional Materials* **2007**, *17*, 3083.

[17] A. Walcarius, *Trac-Trends in Analytical Chemistry* **2012**, *38*, 79.

[18] B. Smarsly, M. Antonietti, *European Journal of Inorganic Chemistry* **2006**, 1111.

[19] C. Sanchez, C. Boissiere, D. Grosso, C. Laberty, L. Nicole, *Chemistry of Materials* **2008**, *20*, 682.

[20] D. Feng, Y. Y. Lv, Z. X. Wu, Y. Q. Dou, L. Han, Z. K. Sun, Y. Y. Xia, G. F. Zheng, D. Y. Zhao, *Journal of the American Chemical Society* **2011**, *133*, 15148.

[21] Z. Qiang, J. Xue, K. A. Cavicchi, B. D. Vogt, *Langmuir* **2013**, *29*, 3428.

[22] A. Labiano, M. Dai, W.-S. Young, G. E. Stein, K. A. Cavicchi, T. H. Epps, B. D. Vogt, *The Journal of Physical Chemistry C* **2012**, *116*, 6038.

[23] L. Song, D. Feng, H.-J. Lee, C. Wang, Q. Wu, D. Zhao, B. D. Vogt, *The Journal of Physical Chemistry C* **2010**, *114*, 9618.

[24] L. Song, D. Feng, C. G. Campbell, D. Gu, A. M. Forster, K. G. Yager, N. Fredin, H.-J. Lee, R. L. Jones, D. Zhao, B. D. Vogt, *Journal of Materials Chemistry* **2010**, *20*, 1691.

[25] L. Y. Song, D. Feng, N. J. Fredin, K. G. Yager, R. L. Jones, Q. Y. Wu, D. Y. Zhao, B. D. Vogt, *Acs Nano* **2010**, *4*, 189.

[26] J. Schuster, R. Kohn, M. Doblinger, A. Keilbach, H. Amenitsch, T. Bein, *Journal of the American Chemical Society* **2012**, *134*, 11136.

[27] J. Schuster, R. Kohn, A. Keilbach, M. Doblinger, H. Amenitsch, T. Bein, *Chemistry of Materials* **2009**, *21*, 5754.
[28] L. Chuenchom, R. Kraehnert, B. M. Smarsly, *Soft Matter* **2012**, *8*, 10801.
[29] J. Ozaki, N. Endo, W. Ohizumi, K. Igarashi, M. Nakahara, A. Oya, S. Yoshida, T. Iizuka, *Carbon* **1997**, *35*, 1031.
[30] R. Ryoo, S. H. Joo, S. Jun, *Journal of Physical Chemistry B* **1999**, *103*, 7743.
[31] R. Ryoo, S. H. Joo, M. Kruk, M. Jaroniec, *Advanced Materials* **2001**, *13*, 677.
[32] J. Lee, S. Han, T. Hyeon, *Journal of Materials Chemistry* **2004**, *14*, 478.
[33] H. F. Yang, D. Y. Zhao, *Journal of Materials Chemistry* **2005**, *15*, 1217.
[34] B. Sakintuna, Y. Yurum, *Industrial & Engineering Chemistry Research* **2005**, *44*, 2893.
[35] F. B. Su, Z. C. Zhou, W. P. Guo, J. J. Liu, X. N. Tian, X. S. Zhao, in *Chemistry and Physics of Carbon, Vol 30, Vol. 30*, Crc Press-Taylor & Francis Group, Boca Raton, **2008**, pp. 63.
[36] Y. D. Xia, Z. X. Yang, R. Mokaya, *Nanoscale* **2010**, *2*, 639.
[37] E. Ortel, A. Fischer, L. Chuenchom, J. Polte, F. Emmerling, B. Smarsly, R. Kraehnert, *Small* **2012**, *8*, 298.
[38] C. D. Liang, K. L. Hong, G. A. Guiochon, J. W. Mays, S. Dai, *Angewandte Chemie-International Edition* **2004**, *43*, 5785.
[39] P. Van der Voort, C. Vercaemst, D. Schaubroeck, F. Verpoort, *Physical Chemistry Chemical Physics* **2008**, *10*, 347.
[40] X. Q. Wang, K. N. Bozhilov, P. Y. Feng, *Chemistry of Materials* **2006**, *18*, 6373.
[41] Y. R. Liang, D. C. Wu, R. W. Fu, *Langmuir* **2009**, *25*, 7783.
[42] Y. H. Deng, C. Liu, T. Yu, F. Liu, F. Q. Zhang, Y. Wan, L. J. Zhang, C. C. Wang, B. Tu, P. A. Webley, H. T. Wang, D. Y. Zhao, *Chemistry of Materials* **2007**, *19*, 3271.
[43] H. J. Liu, W. J. Cui, L. H. Jin, C. X. Wang, Y. Y. Xia, *Journal of Materials Chemistry* **2009**, *19*, 3661.
[44] C. D. Liang, S. Dai, *Journal of the American Chemical Society* **2006**, *128*, 5316.
[45] F. Q. Zhang, Y. Meng, D. Gu, Y. Yan, C. Z. Yu, B. Tu, D. Y. Zhao, *Journal of the American Chemical Society* **2005**, *127*, 13508.
[46] C. Y. Liu, L. X. Li, H. H. Song, X. H. Chen, *Chemical Communications* **2007**, 757.
[47] Y. H. Deng, T. Yu, Y. Wan, Y. F. Shi, Y. Meng, D. Gu, L. J. Zhang, Y. Huang, C. Liu, X. J. Wu, D. Y. Zhao, *Journal of the American Chemical Society* **2007**, *129*, 1690.
[48] Y. Meng, D. Gu, F. Q. Zhang, Y. F. Shi, H. F. Yang, Z. Li, C. Z. Yu, B. Tu, D. Y. Zhao, *Angewandte Chemie-International Edition* **2005**, *44*, 7053.
[49] S. Tanaka, Y. Katayama, M. P. Tate, H. W. Hillhouse, Y. Miyake, *Journal of Materials Chemistry* **2007**, *17*, 3639.
[50] G. J. D. Soler-illia, C. Sanchez, B. Lebeau, J. Patarin, *Chemical Reviews* **2002**, *102*, 4093.
[51] Y. Wan, D. Y. Zhao, *Chemical Reviews* **2007**, *107*, 2821.
[52] Q. S. Huo, D. I. Margolese, U. Ciesla, P. Y. Feng, T. E. Gier, P. Sieger, R. Leon, P. M. Petroff, F. Schuth, G. D. Stucky, *Nature* **1994**, *368*, 317.

[53] G. Soler-Illia, P. Innocenzi, *Chemistry-a European Journal* **2006**, *12*, 4478.
[54] X. Q. Wang, C. D. Liang, S. Dai, *Langmuir* **2008**, *24*, 7500.
[55] M. Florent, C. Xue, D. Zhao, D. Goldfarb, *Chemistry of Materials* **2012**, *24*, 383.
[56] H. Kosonen, J. Ruokolainen, P. Nyholm, O. Ikkala, *Macromolecules* **2001**, *34*, 3046.
[57] S. Valkama, A. Nykanen, H. Kosonen, R. Ramani, F. Tuomisto, P. Engelhardt, G. ten Brinke, O. Ikkala, J. Ruokolainen, *Advanced Functional Materials* **2007**, *17*, 183.
[58] E. Fitzer, K. H. Kochling, H. P. Boehm, H. Marsh, *Pure and Applied Chemistry* **1995**, *67*, 473.
[59] W. Ruland, B. Smarsly, *Journal of Applied Crystallography* **2002**, *35*, 624.
[60] G. A. Zickler, B. Smarsly, N. Gierlinger, H. Peterlik, O. Paris, *Carbon* **2006**, *44*, 3239.
[61] H. Kosonen, S. Valkama, A. Nykanen, M. Toivanen, G. ten Brinke, J. Ruokolainen, O. Ikkala, *Advanced Materials* **2006**, *18*, 201.
[62] S. Tanaka, N. Nishiyama, Y. Egashira, K. Ueyama, *Chemical Communications* **2005**, 2125.
[63] D. H. Long, W. M. Qiao, L. Zhan, X. Y. Liang, L. C. Ling, *Microporous and Mesoporous Materials* **2009**, *121*, 58.
[64] S. Tanaka, A. Doi, N. Nakatani, Y. Katayama, Y. Miyake, *Carbon* **2009**, *47*, 2688.
[65] J. Jin, N. Nishiyama, Y. Egashira, K. Ueyama, *Microporous and Mesoporous Materials* **2009**, *118*, 218.
[66] J. Gorka, C. Fenning, M. Jaroniec, *Colloids and Surfaces a-Physicochemical and Engineering Aspects* **2009**, *352*, 113.
[67] S. Kataoka, T. Yamamoto, Y. Inagi, A. Endo, M. Nakaiwa, T. Ohmori, *Carbon* **2008**, *46*, 1358.
[68] J. Jin, T. Mitome, Y. Egashira, N. Nishiyama, *Colloids and Surfaces a-Physicochemical and Engineering Aspects* **2011**, *384*, 58.
[69] M. J. Xie, H. H. Dong, D. D. Zhang, X. F. Guo, W. P. Ding, *Carbon* **2011**, *49*, 2459.
[70] P. Li, Y. Song, Q. G. Guo, J. L. Shi, L. Liu, *Materials Letters* **2011**, *65*, 2130.
[71] X. F. Qian, H. X. Li, Y. Wan, *Microporous and Mesoporous Materials* **2011**, *141*, 26.
[72] U. B. Suryavanshi, T. Ijima, A. Hayashi, Y. Hayashi, M. Tanemura, *Chemical Communications* **2011**, *47*, 10758.
[73] Y. Huang, J. P. Yang, H. Q. Cai, Y. P. Zhai, D. Feng, Y. H. Deng, B. Tu, D. Y. Zhao, *Journal of Materials Chemistry* **2009**, *19*, 6536.
[74] Y. Huang, H. Q. Cai, T. Yu, F. Q. Zhang, F. Zhang, Y. Meng, D. Gu, Y. Wan, X. L. Sun, B. Tu, D. Y. Zhao, *Angewandte Chemie-International Edition* **2007**, *46*, 1089.
[75] Y. H. Deng, Y. Cai, Z. K. Sun, D. Gu, J. Wei, W. Li, X. H. Guo, J. P. Yang, D. Y. Zhao, *Advanced Functional Materials* **2010**, *20*, 3658.
[76] J. Y. Zhang, Y. H. Deng, J. Wei, Z. K. Sun, D. Gu, H. Bongard, C. Liu, H. H. Wu, B. Tu, F. Schuth, D. Y. Zhao, *Chemistry of Materials* **2009**, *21*, 3996.
[77] Y. H. Deng, J. Liu, C. Liu, D. Gu, Z. K. Sun, J. Wei, J. Y. Zhang, L. J. Zhang, B. Tu, D. Y. Zhao, *Chemistry of Materials* **2008**, *20*, 7281.
[78] X. Y. Liu, B. Z. Tian, C. Z. Yu, F. Gao, S. H. Xie, B. Tu, R. C. Che, L. M. Peng, D. Y. Zhao, *Angewandte Chemie-International Edition* **2002**, *41*, 3876.

[79] J. Fan, C. Z. Yu, J. Lei, Q. Zhang, T. C. Li, B. Tu, W. Z. Zhou, D. Y. Zhao, *Journal of the American Chemical Society* **2005**, *127*, 10794.
[80] S. N. Che, A. E. Garcia-Bennett, X. Y. Liu, R. P. Hodgkins, P. A. Wright, D. Y. Zhao, O. Terasaki, T. Tatsumi, *Angewandte Chemie-International Edition* **2003**, *42*, 3930.
[81] Y. Q. Wang, C. M. Yang, B. Zibrowius, B. Spliethoff, M. Linden, F. Schuth, *Chemistry of Materials* **2003**, *15*, 5029.
[82] Y. Deng, C. Liu, D. Gu, T. Yu, B. Tu, D. Zhao, *Journal of Materials Chemistry* **2008**, *18*, 91.
[83] A. H. Lu, B. Spliethoff, F. Schuth, *Chemistry of Materials* **2008**, *20*, 5314.
[84] G. P. Hao, W. C. Li, D. Qian, G. H. Wang, W. P. Zhang, T. Zhang, A. Q. Wang, F. Schuth, H. J. Bongard, A. H. Lu, *Journal of the American Chemical Society* **2011**, *133*, 11378.
[85] G. P. Hao, W. C. Li, S. A. Wang, G. H. Wang, L. Qi, A. H. Lu, *Carbon* **2011**, *49*, 3762.
[86] S. Kubo, R. J. White, N. Yoshizawa, M. Antonietti, M. M. Titirici, *Chemistry of Materials* **2011**, *23*, 4882.
[87] A. T. Rodriguez, X. F. Li, J. Wang, W. A. Steen, H. Y. Fan, *Advanced Functional Materials* **2007**, *17*, 2710.
[88] C. J. Brinker, Y. F. Lu, A. Sellinger, H. Y. Fan, *Advanced Materials* **1999**, *11*, 579.
[89] D. Grosso, F. Cagnol, G. Soler-Illia, E. L. Crepaldi, H. Amenitsch, A. Brunet-Bruneau, A. Bourgeois, C. Sanchez, *Advanced Functional Materials* **2004**, *14*, 309.
[90] Z. K. Sun, B. Sun, M. H. Qiao, J. Wei, Q. Yue, C. Wang, Y. H. Deng, S. Kaliaguine, D. Y. Zhao, *Journal of the American Chemical Society* **2012**, *134*, 17653.
[91] P. Gao, A. Wang, X. Wang, T. Zhang, *Chemistry of Materials* **2008**, *20*, 1881.
[92] A. H. Lu, W. C. Li, Z. S. Hou, F. Schuth, *Chemical Communications* **2007**, 1038.
[93] L. N. Kong, W. Wei, Q. F. Zhao, J. Q. Wang, Y. Wan, *Acs Catalysis* **2012**, *2*, 2577.
[94] Y. Wan, H. Y. Wang, Q. F. Zhao, M. Klingstedt, O. Terasaki, D. Y. Zhao, *Journal of the American Chemical Society* **2009**, *131*, 4541.
[95] P. Gao, A. W. Wang, X. D. Wang, T. Zhang, *Catalysis Letters* **2008**, *125*, 289.
[96] Y. Chi, L. Zhao, Q. Yuan, X. Yan, Y. J. Li, N. Li, X. T. Li, *Journal of Materials Chemistry* **2012**, *22*, 13571.
[97] Z. X. Wu, Y. Y. Lv, Y. Y. Xia, P. A. Webley, D. Y. Zhao, *Journal of the American Chemical Society* **2012**, *134*, 2236.
[98] Z. X. Wu, P. A. Webley, D. Y. Zhao, *Langmuir* **2010**, *26*, 10277.
[99] Y. P. Zhai, Y. Q. Dou, X. X. Liu, B. Tu, D. Y. Zhao, *Journal of Materials Chemistry* **2009**, *19*, 3292.
[100] L. Sterk, J. Gorka, M. Jaroniec, *Colloids and Surfaces a-Physicochemical and Engineering Aspects* **2010**, *362*, 20.
[101] M. Z. Dai, L. Y. Song, J. T. LaBelle, B. D. Vogt, *Chemistry of Materials* **2011**, *23*, 2869.
[102] J. S. Li, J. Gu, H. J. Li, Y. Liang, Y. X. Hao, X. Y. Sun, L. J. Wang, *Microporous and Mesoporous Materials* **2010**, *128*, 144.
[103] J. Gorka, M. Jaroniec, *Journal of Physical Chemistry C* **2008**, *112*, 11657.

[104] Z. Ji, S. Liang, Y. Jiang, H. Li, Z. Liu, T. Zhao, *Carbon* **2009**, *47*, 2194.
[105] L. She, J. Li, Y. Wan, X. D. Yao, B. Tu, D. Y. Zhao, *Journal of Materials Chemistry* **2011**, *21*, 795.
[106] F. H. Puls, K. D. Ruhnke, *US patent 4* **1981**, *260*, 840.
[107] H. U. Hammershaimb, J. B. Spinner, *US patent 4* **1988**, *774*, 375
[108] K. Flick, C. Herion, H. M. Allmann, *US patent 5* **1999**, *856*, 262.
[109] G. R. Gildert, H. M. Putman, D. Hearn, *US patent 5* **1999**, *877*, 363.
[110] G. Chaput, J. Laurent, J. P. Boitiaux, J. Cosyns, P. Sarrazin, *Hydrocarbon Processing* **1992**, *71*, 51.
[111] J. Silvestre-Albero, G. Rupprechter, H. J. Freund, *Chemical Communications* **2006**, 80.
[112] J. Silvestre-Albero, G. Rupprechter, H. J. Freund, *Journal of Catalysis* **2005**, *235*, 52.
[113] T. Cukic, R. Kraehnert, M. Holena, D. Herein, D. Linke, U. Dingerdissen, *Applied Catalysis a-General* **2007**, *323*, 25.
[114] T. von Graberg, P. Hartmann, A. Rein, S. Gross, B. Seelandt, C. Roger, R. Zieba, A. Traut, M. Wark, J. Janek, B. M. Smarsly, *Science and Technology of Advanced Materials* **2011**, *12*, 12.
[115] S. Sokolov, E. Ortel, J. Radnik, R. Kraehnert, *Thin Solid Films* **2009**, *518*, 27.
[116] R. T. Mayes, C. Tsouris, J. O. Kiggans, S. M. Mahurin, D. W. DePaoli, S. Dai, *Journal of Materials Chemistry* **2010**, *20*, 8674.
[117] B. K. Guo, X. Q. Wang, P. F. Fulvio, M. F. Chi, S. M. Mahurin, X. G. Sun, S. Dai, *Advanced Materials* **2011**, *23*, 4661.
[118] S. Brunauer, P. H. Emmett, E. Teller, *Journal of the American Chemical Society* **1938**, *60*, 309.
[119] E. P. Barrett, L. G. Joyner, P. P. Halenda, *Journal of the American Chemical Society* **1951**, *73*, 373.
[120] M. Thommes, *Chemie Ingenieur Technik* **2010**, *82*, 1059.
[121] K. A. Cychosz, X. Guo, W. Fan, R. Cimino, G. Y. Gor, M. Tsapatsis, A. V. Neimark, M. Thommes, *Langmuir* **2012**, *28*, 12647.
[122] E. Ortel, S. Sokolov, C. Zielke, I. Lauermann, S. Selve, K. Weh, B. Paul, J. Polte, R. Kraehnert, *Chemistry of Materials* **2012**, *24*, 3828.
[123] P. F. Fulvio, R. T. Mayes, X. Q. Wang, S. M. Mahurin, J. C. Bauer, V. Presser, J. McDonough, Y. Gogotsi, S. Dai, *Advanced Functional Materials* **2011**, *21*, 2208.
[124] C. Tsouris, R. Mayes, J. Kiggans, K. Sharma, S. Yiacoumi, D. DePaoli, S. Dai, *Environmental Science & Technology* **2011**, *45*, 10243.
[125] S. A. Al-Muhtaseb, J. A. Ritter, *Advanced Materials* **2003**, *15*, 101.
[126] B. Smarsly, D. Grosso, T. Brezesinski, N. Pinna, C. Boissiere, M. Antonietti, C. Sanchez, *Chemistry of Materials* **2004**, *16*, 2948.
[127] D. Fattakhova-Rohlfing, M. Wark, T. Brezesinski, B. M. Smarsly, J. Rathousky, *Advanced Functional Materials* **2007**, *17*, 123.
[128] W. Ruland, B. M. Smarsly, *Journal of Applied Crystallography* **2007**, *40*, 409.
[129] T. Brezesinski, A. Fischer, K. Iimura, C. Sanchez, D. Grosso, M. Antonietti, B. M. Smarsly, *Advanced Functional Materials* **2006**, *16*, 1433.

[130] Y. P. Zhai, Y. Q. Dou, D. Y. Zhao, P. F. Fulvio, R. T. Mayes, S. Dai, *Advanced Materials* **2011**, *23*, 4828.
[131] B. D. Vogt, V. L. Chavez, M. Z. Dai, M. R. C. Arreola, L. Y. Song, D. Feng, D. Y. Zhao, G. M. Perera, G. E. Stein, *Langmuir* **2011**, *27*, 5607.
[132] D. Fattakhova-Rohfing, T. Brezesinski, J. Rathousky, A. Feldhoff, T. Oekermann, M. Wark, B. Smarsly, *Advanced Materials* **2006**, *18*, 2980.
[133] T. Brezesinski, M. Groenewolt, M. Antonietti, B. Smarsly, *Angewandte Chemie-International Edition* **2006**, *45*, 781.
[134] T. Brezesinski, J. Wang, R. Senter, K. Brezesinski, B. Dunn, S. H. Tolbert, *Acs Nano* **2010**, *4*, 967.
[135] J. M. Szeifert, D. Fattakhova-Rohlfing, D. Georgiadou, V. Kalousek, J. Rathouský, D. Kuang, S. Wenger, S. M. Zakeeruddin, M. Grätzel, T. Bein, *Chemistry of Materials* **2009**, *21*, 1260.
[136] S. Guldin, P. Docampo, M. Stefik, G. Kamita, U. Wiesner, H. J. Snaith, U. Steiner, *Small* **2012**, *8*, 432.
[137] T. Brezesinski, M. Groenewolt, A. Gibaud, N. Pinna, M. Antonietti, B. M. Smarsly, *Advanced Materials* **2006**, *18*, 2260.
[138] C. Weidmann, K. Brezesinski, C. Suchomski, K. Tropp, N. Grosser, J. Haetge, B. M. Smarsly, T. Brezesinski, *Chemistry of Materials* **2012**, *24*, 486.
[139] E. Ortel, T. Reier, P. Strasser, R. Kraehnert, *Chemistry of Materials* **2011**, *23*, 3201.
[140] D. Grosso, C. Boissiere, B. Smarsly, T. Brezesinski, N. Pinna, P. A. Albouy, H. Amenitsch, M. Antonietti, C. Sanchez, *Nature Materials* **2004**, *3*, 787.
[141] B. Eckhardt, E. Ortel, J. Polte, D. Bernsmeier, O. Gorke, P. Strasser, R. Kraehnert, *Advanced Materials* **2012**, *24*, 3115.
[142] S. Sokolov, E. Ortel, R. Kraehnert, *Materials Research Bulletin* **2009**, *44*, 2222.
[143] M. Groenewolt, T. Brezesinski, H. Schlaad, M. Antonietti, P. W. Groh, B. Ivan, *Advanced Materials* **2005**, *17*, 1158.
[144] A. Sidorenko, I. Tokarev, S. Minko, M. Stamm, *Journal of the American Chemical Society* **2003**, *125*, 12211.
[145] W. van Zoelen, G. ten Brinke, *Soft Matter* **2009**, *5*, 1568.
[146] B. Smarsly, C. Göltner, M. Antonietti, W. Ruland, E. Hoinkis, *The Journal of Physical Chemistry B* **2001**, *105*, 831.
[147] F. B. Su, J. H. Zeng, X. Y. Bao, Y. S. Yu, J. Y. Lee, X. S. Zhao, *Chemistry of Materials* **2005**, *17*, 3960.
[148] V. Raghuveer, A. Manthiram, *Journal of the Electrochemical Society* **2005**, *152*, A1504.
[149] R. Ubago-Perez, F. Carrasco-Marin, C. Moreno-Castilla, *Applied Catalysis a-General* **2004**, *275*, 119.
[150] V. Lordi, N. Yao, J. Wei, *Chemistry of Materials* **2001**, *13*, 733.
[151] X. Q. Wang, S. Dai, *Adsorption-Journal of the International Adsorption Society* **2009**, *15*, 138.
[152] L. Sterk, J. Gorka, A. Vinu, M. Jaroniec, *Microporous and Mesoporous Materials* **2012**, *156*, 121.

[153] X. Q. Wang, Q. Zhu, S. M. Mahurin, C. D. Liang, S. Dai, *Carbon* **2010**, *48*, 557.
[154] J. P. Boitiaux, J. Cosyns, E. Robert, *Applied Catalysis* **1987**, *32*, 145.
[155] F. Hasche, T. P. Fellinger, M. Oezaslan, J. P. Paraknowitsch, M. Antonietti, P. Strasser, *Chemcatchem* **2012**, *4*, 479.
[156] D. Seth, A. Sarkar, F. T. T. Ng, G. L. Rempel, *Chemical Engineering Science* **2007**, *62*, 4544.
[157] I. Muylaert, A. Verberckmoes, J. De Decker, P. Van der Voort, *Advances in Colloid and Interface Science* **2012**, *175*, 39.
[158] D. C. Lee, J. H. Kim, W. J. Kim, J. H. Kang, S. H. Moon, *Applied Catalysis a-General* **2003**, *244*, 83.
[159] T. P. Fellinger, F. Hasche, P. Strasser, M. Antonietti, *Journal of the American Chemical Society* **2012**, *134*, 4072.
[160] J. P. Paraknowitsch, Y. J. Zhang, B. Wienert, A. Thomas, *Chemical Communications* **2013**, *49*, 1208.
[161] J. Wei, D. Zhou, Z. Sun, Y. Deng, Y. Xia, D. Zhao, *Advanced Functional Materials* **2013**, ASAP.
[162] M. Zhong, E. K. Kim, J. P. McGann, S. E. Chun, J. F. Whitacre, M. Jaroniec, K. Matyjaszewski, T. Kowalewski, *Journal of the American Chemical Society* **2012**, *134*, 14846.
[163] X. Xu, Y. Li, Y. T. Gong, P. F. Zhang, H. R. Li, Y. Wang, *Journal of the American Chemical Society* **2012**, *134*, 16987.
[164] C. D. Liang, S. Dai, *Chemistry of Materials* **2009**, *21*, 2115.

Appendix

List of abbreviations and symbols

Abbreviations

BET	Brunauer-Emmett-Teller
BJH	Barrett-Joyner-Halenda
EDX	Energy Dispersive X-Ray Analysis
EISA	Evaporation-Induced Self-Assembly
EtOH	Ethanol
FFT	Fast Fourier Transform
FT-IR	Fourier Transform Infrared Spectroscopy
HRTEM	High Resolution Transmission Electron Microscopy
IUPAC	International Union of Pure and Applied Chemistry
NP	Nanoparticles
NL/QS DFT	Non-Local/Quenched-State Density Functional Theory
OMCs	Ordered Mesoporous Carbons
PB	Poly(butadiene)
PEO	Poly(ethyleneoxide)
PIB	Poly(isobutylene)
PPO	Poly(propyleneoxide)
F127	PEO_{106}-*b*-PPO_{70}-*b*-PEO_{106}
PIB-PEO 3000	PIB_{53}-*b*-PEO_{45}
10k-PB	PEO_{213}-*b*-PB_{184}-*b*-PEO_{213}
$Pd(acac)_2$	Palladium(II)acetylacetonate

PF	Phenol-Formaldehyde
PSD	Pore Size Distribution
RF	Resorcinol-Formaldehyde
RH	Relative Humidity
SAED	Selected Area Electron Diffraction
1D-/2D-SAXS	One Dimensional/ Two Dimensional-Small-Angle X-Ray Scattering
SEM	Scanning Electron Microscopy
TEM	Transmission Electron Microscopy
TGA	Thermogravimetric Analysis
THF	Tetrahydrofuran
WAXS	Wide-Angle X-Ray Scattering
WDX	Wavelength Dispersive X-Ray Analysis

Symbols

λ	Wavelength
θ	Bragg Angle
β	Angle between The Film Surface and Incident X-Ray (used in 2D-SAXS)
d	Periodic Distance ($d = 2\pi/q$)
q	Scattering Vector ($q = 2\pi/d$), $q = 4\pi/(\lambda\sin(\theta/2))$
s	Scattering Vector ($s = 2\sin(\theta)/\lambda$)
p/p_0	Relative Pressure
R_a	Average Surface Roughness
D_{NP}	Nanoparticle Size in Diameter
E_a	Activation Energy

List of publications and presentations

Publications

Recent progress in soft-templating of porous carbon materials
L. Chuenchom, R. Kraehnert, B. M. Smarsly, *Soft Matter* **2012**, *8*, 10801.

New Triblock Copolymer Templates, PEO-PB-PEO, for the Synthesis of Titania Films with Controlled Mesopore Size, Wall thickness, and Bimodal Porosity
E. Ortel, A. Fischer, **L. Chuenchom**, J. Polte, F. Emmerling, B. Smarsly, R. Kraehnert, *Small* **2012**, *8*, 298.

Generation of Hierarchical Meso-Macro-Porous Carbon from Mesophase Pitch by Spinodal Decomposition with Polymer Templates
P. Adelhelm, Y. S. Hu, **L. Chuenchom**, M. Antonietti, B. M. Smarsly, M. Maier, *Advanced Materials* **2007**, *19*, 4012.

Presentations

Crack-free mesoporous carbon films with open cubic pores through soft-templating
L. Chuenchom, E. Ortel, B Paul, B. M. Smarsly, R. Kraehnert
22. Deutsche Zeolith-Tagung, Munich, Germany, 3-5 March 2010.

Soft-templating synthesis of mesoporous carbon coatings with pores bigger than 10 nm templated with a novel block-copolymer
L. Chuenchom, E. Ortel, B. M. Smarsly, R. Kraehnert
23. Deutsche Zeolith-Tagung, Erlangen, Germany, 2-4 March 2011.

To protect the personal data from misuse, the curriculum vitae was removed.